SYNTHESIS AND CHARACTERIZATION OF NICKEL-NITRILOTRIACETIC (Ni-NTA) FUNCTIONALIZED DENDRIMERS

by

John Emoche James

A thesis submitted in partial fulfillment
of the requirements for the degree

of

Master of Science

in

Chemistry

MONTANA STATE UNIVERSITY
Bozeman, Montana

August 2025

DEDICATION

To the Almighty, family and friends

ACKNOWLEDGEMENTS

All thanks to NSF and the Tamara Joy Henderson Fund for their financial support through this arduous journey. I am grateful to my great and patient supervisor, Professor Mary Cloninger. I am also thankful to all my past and present lab members for their support. My thanks also go to my committee members, Dr. David Fialho, Dr. Tom Livinghouse, and Dr. Michael Mock. Thank you to Brian Tripet and Don Smith for their analytical skills. I am forever grateful to anyone who has, in one form or another, made me a better chemist and a better human in general, whether knowingly or unknowingly.

TABLE OF CONTENTS

TABLE OF CONTENTS CONTINUED

LIST OF TABLES

Table Page

LIST OF FIGURES

Figure Page

LIST OF FIGURES CONTINUED

LIST OF FIGURES CONTINUED

LIST OF FIGURES CONTINUED

LIST OF FIGURES CONTINUED

NOMENCLATURE

1. PAMAM: Poly(amidoamine)
2. NMR: Nuclear Magnetic Resonance
3. G (2): Generation 2
4. G (3): Generation 3
5. G (4): Generation 4
6. G (6): Generation 6
7. DMSO: Dimethyl sulfoxide
8. DCM: Dichloromethane
9. CRD: Carbohydrate Recognition Domain
10. MWCO: Molecular Weight Cut-Off
11. DI: Deionized
12. HSQC: Heteronuclear Single Quantum Coherence

ABSTRACT

Immobilized metal affinity chromatography (IMAC) is a very popular protein purification technique in biochemistry. Resins are functionalized with nitrilotriacetic acid (NTA), a chelating group often charged before use with a divalent or trivalent metal, usually Ni (II). In IMAC using Ni-NTA, open coordination sites on nickel are bound by two imidazole ring side chains of a histidine tag, which has been added to the protein of interest. In this work, the Ni-NTA ligand commonly used in IMAC was tethered to a poly(amidoamine) (PAMAM) dendrimer. PAMAM dendrimers are hyperbranched macromolecules with a well-defined structure characterized by a central core, repetitive branching, and a doubling of the termini with each successive generation. Because the number of end groups can be readily altered by changing the generation of the dendrimer, dendrimers are ideal frameworks for displaying different numbers of Ni-NTA groups. For this study, NTA derivatives containing an azide were added to propargylated PAMAM dendrimers of generations 2, 3, 4, and 6 (G(2), G(3), G(4), and G(6), respectively) using Cu(I)-mediated triazole formation, or “click” chemistry. Characterization of new compounds was performed using ^{1}H nuclear magnetic resonance (NMR), ^{13}C NMR, infrared (IR) spectroscopy, and mass spectrometry (MS). The Ni-NTA functionalized dendrimers will be used to bind histidine-tagged proteins, allowing for the study of the effect of clustering a protein on its function.

CHAPTER ONE

INTRODUCTION

Galectins

Proteins play diverse roles in human biological processes, with their function closely linked to their structure. One important family of proteins is the galectins. Galectins are extensively distributed throughout the animal kingdom. Their typical expression is found in various organs and tissues, including the central and peripheral nervous systems, lungs, liver, and intestinal system[1]. They are a family of carbohydrate-binding proteins that play critical roles in various biological processes, including cell-cell adhesion, cell signaling, and immune regulation. These versatile proteins are characterized by their ability to recognize and bind to specific glycan structures, often with low monovalent affinities. The galectins can exhibit enhanced avidity through multivalent interactions. [2, 3] Every known galectin contains conserved carbohydrate-recognition domains (CRDs) of about 130 amino acids. These CRDs are the key players in the carbohydrate-binding process[4].

There are three families of carbohydrate-binding galectins. Prototypical galectins have one CRD (galectin-1, -2, -5, -7, -10, -11, -13, -14 and -15) and typically are noncovalent homodimers in solution, while the tandem-repeat-type galectins contain two CRDs in a single polypeptide chain, separated by a linker of up to 70 amino acids (galectin-4, -6, -8, -9 and -12). On the other hand, galectin-3, the only chimera protein, contains a non-lectin N-terminal region of 111 amino acids connected to its CRD. Galectin-3, the most studied galectin, has been identified to have a wide range of physiological and pathological functions, such as cancer, inflammation, and fibrosis[4].

Among all the carbohydrate recognition proteins, galectins were the first family of glycan-binding proteins (GBPs) recognized for their immune regulatory activity[4]. The unusual structure of galectin-3 makes this protein likely to have somewhat different functions than the prototype and the tandem-repeat galectins. The notable characteristics of galectin-3 are its carbohydrate recognition domain and an N-terminal domain essential to galectin-3 oligomerization[2]. Figure 1A schematically shows the structures of the three different families of galectins, and functions of galectins in cancer are shown in Figure 1B.

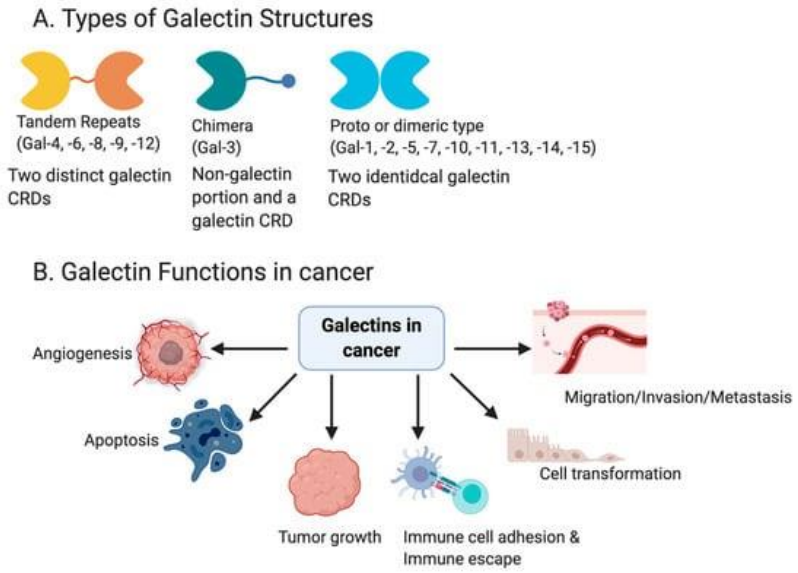

Figure 1: (A) Schematic of Galectins Structures and (B) Their Roles in Cancer Progression[3]

Galectin-3

Galectin-3 is a versatile 26 kDa protein that occurs mainly in the cytosol but can also traverse membranes, reaching the nucleus and mitochondria[2]. Within the galectin family, this protein is the most studied and is used as a biomarker for numerous diseases. Galectin-3 has been observed to undergo oligomerization, primarily implicating the N-terminal domain (Figure 2).[5] Due to the critical role galectin-3 plays in cell adhesion, activation, growth, differentiation, and apoptosis, numerous reports have been published on its presence in cellular compartments, including on the cell surface[3]. Though the role of galectin-3 in cancer progression is not well understood, most published papers agree that its unique function is due to the presence of its N-terminal domain, which enables galectin-3 to stay in circulatory vesicles and also cross the lipid bilayer of a cell.[6] As earlier stated, galectin-3 has both a CRD, which includes the carbohydrate-binding site, and a highly dynamic N-terminal domain, which will have little effect on the CRD regions but contributes to the overall functionality of this protein and makes it different from other members of the galectin family.[2]

This human chimera galectin has 250 amino acid residues, of which 111 belong to the N-terminal domain, with 27 prolines that account for 25% of the N-terminal amino acids. Moreover, the positions of prolines within the N-terminal part of galectin-3 are highly conserved across species, yet their presence and functional value have not been fully explored.[7]

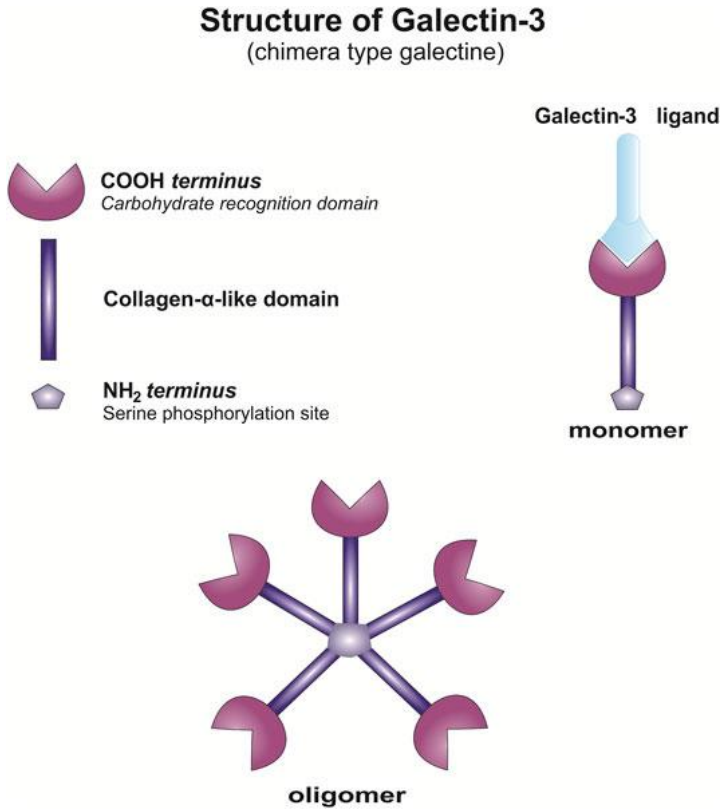

Figure 2: Galectin-3: Chimeric Structure of galectin-3 & Oligomer Formation[2]

Multivalency in Galectin-3

The concept of multivalency was first used in the early 20th century by Paul Ehrlich, referring to therapeutic agents that bind selectively to pathogens without losing affinity for host cells.[8] When multivalent interactions occur, relatively weak noncovalent interactions between an individual receptor and its ligand are synergistically magnified when multiple receptors bind multiple ligands. Multivalent interactions play an essential role in cellular recognition processes.[9] Two important modes of multivalent interactions are entropically enhanced binding and steric stabilization. Entropically enhanced binding refers to the increased binding strength due to the simultaneous interaction of multiple connected ligands and receptors, which reduces the overall entropic cost

relative to individual binding events. Steric stabilization involves the formation of a loose, water-swollen, gel-like layer on the surface of the target, preventing close approach and interaction with other surfaces[10]. Additional modes of multivalent binding include the chelate effect and receptor clustering.

To synthesize a multivalent polymer or macromolecule, scientists must choose a scaffold such as a linear polymer, a protein, a star polymer, or a dendrimer. Flexible linkages or rigid structures could be used, each with advantages and challenges. Figure 3 highlights a divalent protein-protein interaction and a possible pentavalent multimerization upon carbohydrate binding for galectin-3.

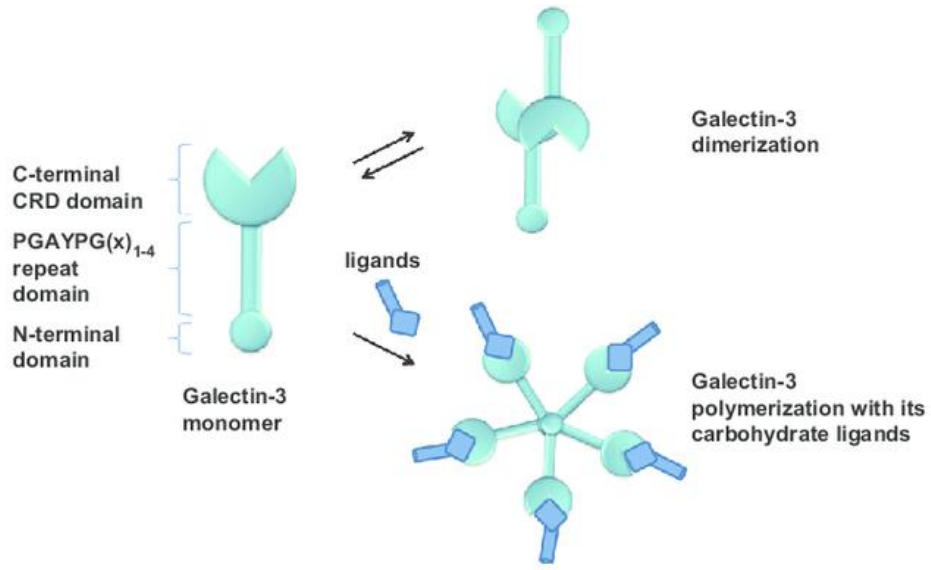

Figure 3: Schematic of multivalent interaction in the presence of a sugar[11]

Poly(amidoamine) (PAMAM) Dendrimers

Nanomedicine is a branch of science that uses 100 nm or smaller materials to address health-related problems. Several nanostructures have been prepared, including nanoparticles, nanotubes, nanoporous membranes, etc. A dendrimer is one of the unique nanoparticles that has played an essential role in nanomedicine[12]. The word "dendrimer" comes from the Greek words dendron, which translates to "tree" or "branch," and meros, which means "part." Dendrimers have also been called "arborols" and "cascade polymers." These compounds are three-dimensional, hyper-branched, monodisperse structures. Dendrimers often have a central core surrounded by peripheral groups, as shown in Figure 4.

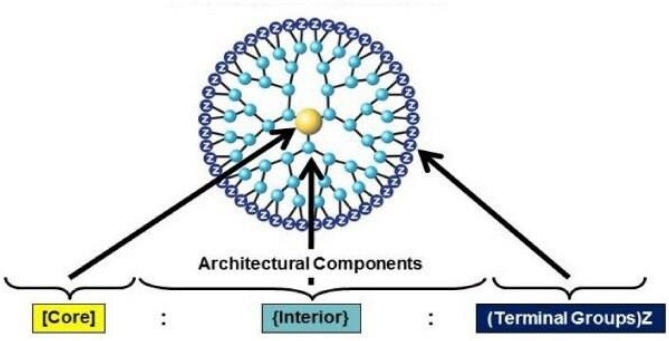

Figure 4: Architectural components and Structure of PAMAM dendrimer[13]

Dendrimers can efficiently transport active pharmaceutical ingredients across cellular barriers, often bypassing efflux transporters[14]. Furthermore, the exterior of these nanoparticles can be functionalized with targeting moieties, such as antibodies or ligands, to enhance their specificity and selectivity for specific cell types or tissues. This targeted delivery approach has shown promise in addressing various healthcare challenges, including cancer, AIDS, and Alzheimer's disease, where there is a need for improved therapies[15]. The unique properties of dendrimers, such as their

well-defined structure and multivalent surface, have also been explored for enzyme immobilization. The ability to engineer dendrimers with specific functional groups has enabled nano-biocatalysts to develop with enhanced catalytic activity and stability.

Poly(amidoamine) (PAMAM) dendrimers are the most well-known and extensively studied dendrimer frameworks. Each increasing generation, i.e., G(1)-, G(2)-, G(3)-PAMAM, and so on, has twice as many endgroups as the previous generation[12]. The size of the dendrimer and the included functionality can be tailored to meet the specific requirements of the intended application, optimizing the dendrimer's properties to suit a wide range of uses, from drug delivery to enzyme immobilization and beyond. For example, the G(2)-PAMAM framework has 16 surface amino groups (Figure 5), while the G(3)-PAMAM has 32 endgroups, allowing for greater targeting or prodrug-loading capacity in the latter.[16] Specifically, many scientists have reported carbohydrate-functionalized PAMAM dendrimers for studying and mediating protein-carbohydrate interactions.

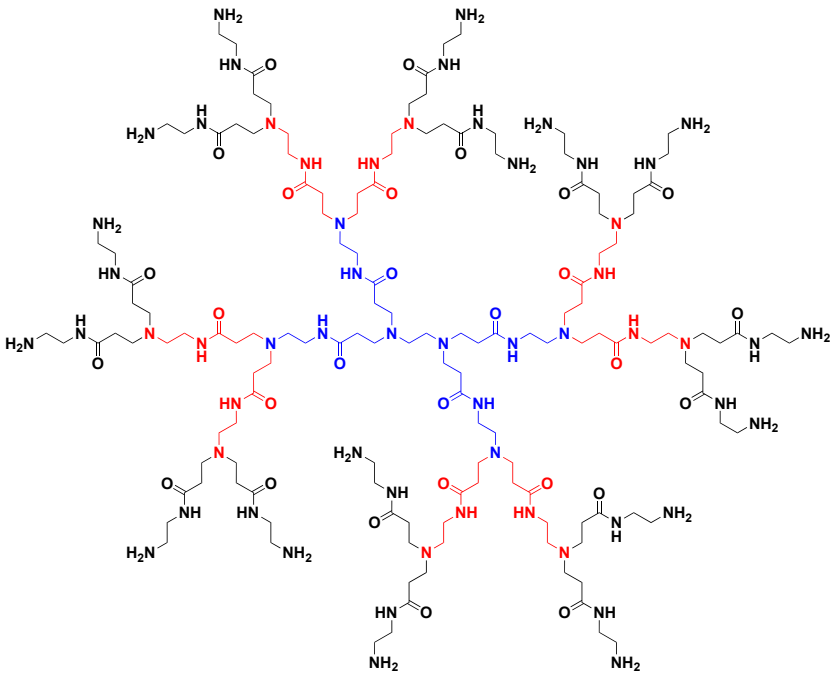

Figure 5: A G (2)-PAMAM dendrimer structure. The blue, red, and black stand for generations 0, 1, and 2, respectively

Nickel-Nitrilotriacetic Acid for Immobilizations

Protein immobilization involves attaching proteins to solid supports. Immobilization of enzymes in their native structure allows them to retain their catalytic activity while allowing for repeated and continuous use.[17] Additionally, immobilization typically enhances the enzyme's stability, making it more resilient to changes in temperature, pH, and solvents, which might otherwise hinder its activity. Moreover, the ease with which immobilized enzymes can be separated from the reaction mixture simplifies product purification. Finally, using immobilized enzymes in continuous fixed-bed reactors allows for more efficient and streamlined processes.[15]

There are several techniques for immobilizing a protein. One common technique is adsorption (Figure 6a), where enzymes are physically adsorbed onto the surface of a support material. This method relies on weak interactions between the enzyme and the support, such as van der Waals forces, hydrogen bonds, and hydrophobic interactions. Adsorption is a relatively simple and cost-effective method, and it often preserves the enzyme's activity because it does not involve chemical modification of the enzyme. However, the weak binding forces can lead to enzyme leaching from the support, especially under harsh conditions like high temperatures or extreme pH.[18] Another widely used technique is entrapment (Figure 6b), where enzymes are physically confined within a porous matrix. This matrix can be a gel, a membrane, or a fiber. The pores of the matrix are large enough to allow substrates and products to diffuse through but small enough to prevent the enzyme from escaping. Entrapment is a gentle method that often preserves enzyme activity and can be used to immobilize enzymes in their native conformation. However, mass transfer limitations can be

problematic, especially for high-molecular-weight substrates.[19] Covalent binding (not shown in Figure 6) is a more robust method of enzyme immobilization, where enzymes are chemically linked to the support material through covalent bonds. This method typically involves functional groups on the enzyme's surface, such as amino, carboxyl, or hydroxyl groups, reacting with complementary groups on the support material.

Covalent binding offers high stability and prevents enzyme leaching, making it suitable for applications requiring harsh conditions. However, the chemical modification upon covalent binding may decrease enzyme activity.[20] Immobilized metal affinity chromatography (IMAC, Figure 6c) utilizes metal coordination to anchor the protein to a solid support. IMAC is a powerful technique that is frequently employed for enzyme immobilization. IMAC leverages the affinity of specific amino acid residues, typically histidine, for metal ions like nickel (Ni^{2+}). In this method, a support material is functionalized with a chelating agent, such as nitrilotriacetic acid, which can tightly bind to the metal ion. The enzyme of interest is engineered to have a histidine tag, a sequence of histidine residues typically added to the N- or C-terminus of the protein.

When the His-tagged protein is passed through the support, the histidine residues in the tag bind to open coordination sites on the immobilized metal ions, effectively anchoring the enzyme to the support matrix.[21] NTA's ability to chelate metal ions enables its incorporation into polymer-based systems, facilitating the attachment of targeting ligands and expanding the potential of these materials for targeted therapies.[22]

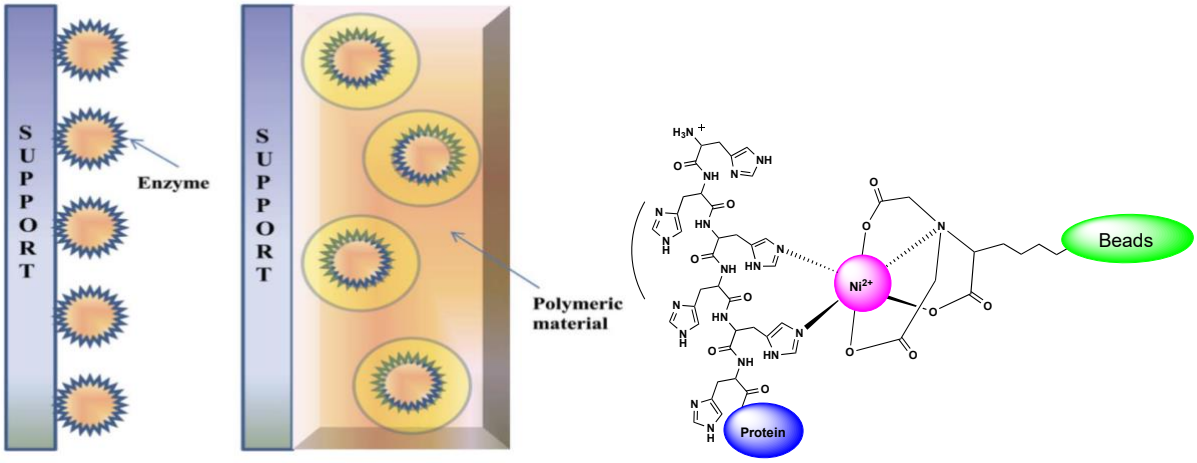

6a. Adsorption.[18] 6b. Entrapment[18] 6c. IMAC[21]

Figure 6: Schematic for the techniques mentioned above.

Hypothesis and Goals

Hypothesis for this research:

The hypothesis governing this research is that using different generations of Ni-NTA functionalized dendrimers will allow for the control and fine-tuning of the arrangement galectin-3 around the dendrimer. Altering the presentation of galectin-3 will influence its properties in cellular aggregation assays and could change the quaternary structure of the galectin-3 N-terminal domain.

Project goals:

Four generations of Ni-NTA-modified dendrimers will be synthesized, purified, and characterized using nuclear magnetic resonance and infrared spectroscopy. Then, the Ni-NTA functionalized dendrimers will be used to bind histidine-tagged galectin-3, and the dendrimer/galectin-3

aggregates will be rigorously investigated using circular dichroism, electron microscopy, and cellular aggregation assays.

The Ni-NTA functionalized PAMAM/galectin-3 clusters, the goal of this project, are summarized in Figure 7. The number of Ni-NTA functional groups on each dendrimer depends on the generation number, sterics, and the number of alkyne groups available for the click reaction.

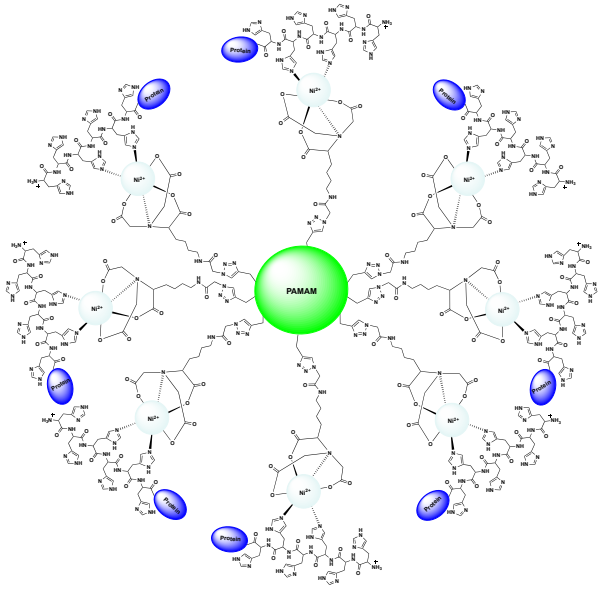

Figure 7: Schematic for Polyamidoamine (PAMAM)

The hypothesis of this research is focused on understanding the effects of protein clustering caused by the introduction of the newly synthesized molecule on protein function. Each chapter will focus on a distinct aspect of this project. Chapter 2 of the thesis will be focused on the synthesis of each of the desired ligands and their addition to four generations of PAMAM dendrimers (G(2), G(3), G (4), and G (6)). Each of the synthesized ligands will be full characterized. Chapter 3 will study each synthesized molecule with galectin-3 using different techniques, beginning with

transmission electron microscopy (TEM). Circular dichroism will also be developed to understand how clustering of galectin-3 by the reported Ni-NTA functionalized dendrimers impacts the structure and function of the protein. Cell-based assays, although beyond the scope of this thesis, will also be performed using the Ni-NTA functionalized dendrimers. The discussion and conclusion of this project will be presented in chapter 4.

CHAPTER TWO

SYNTHESIS AND CHARACTERIZATION OF NI-NTA FUNCTIONALIZED DENDRIMERS

INTRODUCTION

This chapter will provide the step-by-step details of the synthesis and characterization of each molecule. Some procedures have been previously carried out, while others were developed and optimized as described herein. These procedures begin with synthesizing the simplest molecule of azidoacetic acid (1) to the last nickel-complexed macromolecule ready for protein binding studies. A complete synthetic scheme is shown in Scheme 1.

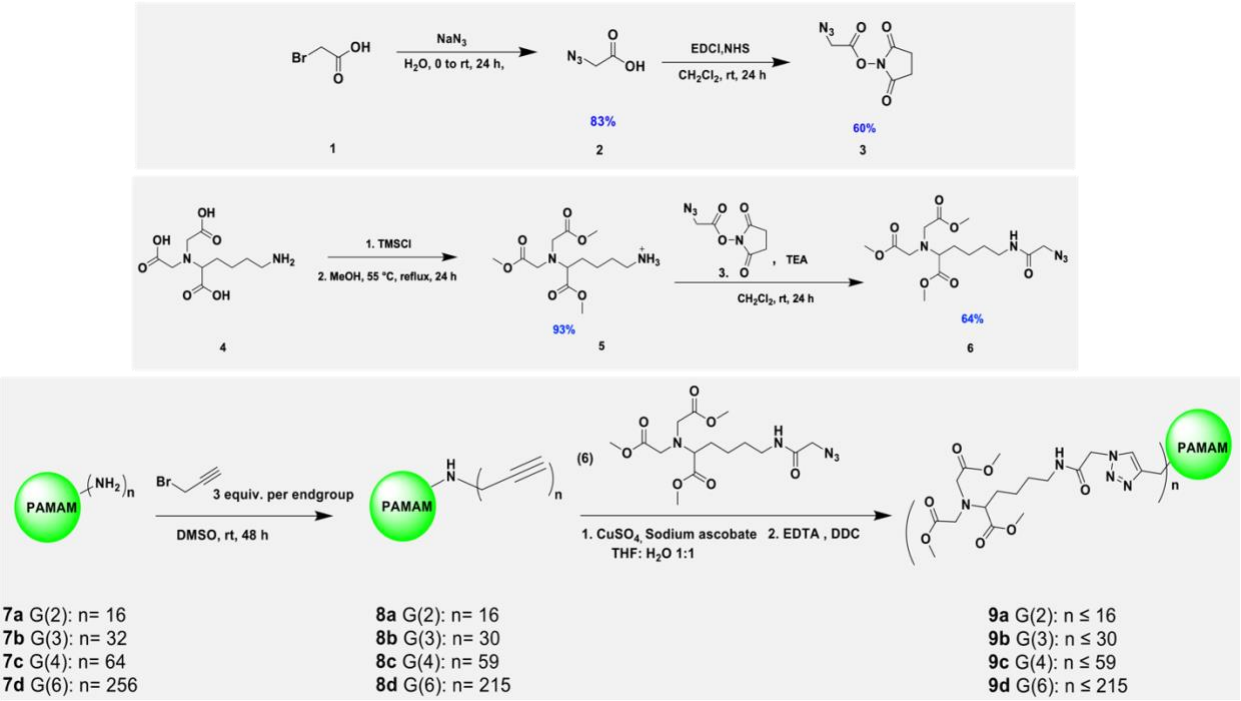

Scheme 1: Synthesis of Ni-NTA functionalized poly(amidoamine) (PAMAM) dendrimers.

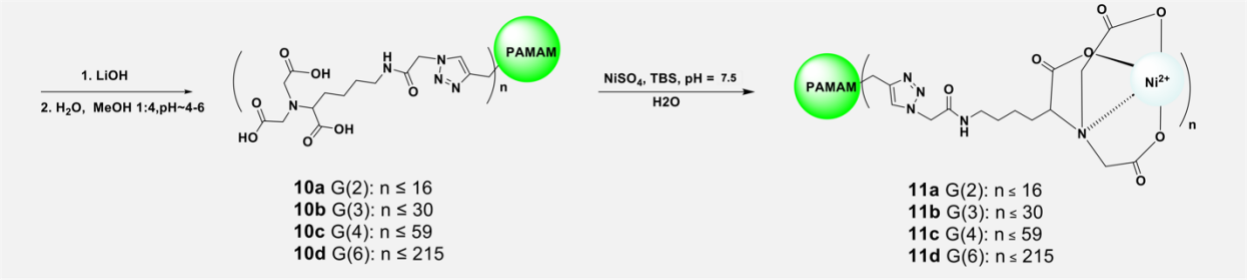

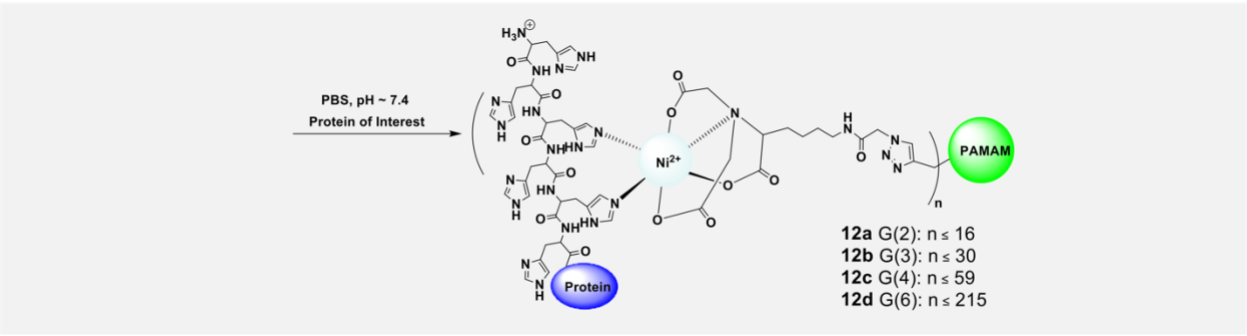

Results

As shown above, the synthesis begins with the S_N2 reaction of bromoacetic acid (1) with sodium azide at room temperature in water, leading to the formation of the azidoacetic acid[23] (2) in 83% yield. Conversion of 2 to its NHS ester was performed using 1-(3-dimethylaminopropyl)-3-ethylcarbodiimide hydrochloride (EDCI) and N-hydroxysuccimamide, which act as coupling and activating reagents. Dry dichloromethane was used as the solvent to prevent hydrolysis of the product due to the NHS ester's sensitivity to water[24]. To synthesize dimethyl 2,2'-((6-amino-1-methoxy-1-oxohexan-2-yl) azanediyl)triacetate (5), N,N-Bis(carboxymethyl)-L-lysine was reacted in methanol with trimethylsilyl chloride to form methyl esters via the trimethylsilyl intermediate[25]. The methyl ester-protected amine 5 was reacted with NHS ester 3 with triethylamine in dichloromethane for 24 hours at room temperature to form azide 6. Aqueous

workup was followed by column chromatography in $CHCl_3$: MeOH (90:10) to afford 64% yield of purified product 6[26]. The propargylation reaction to form 8a-d was performed in the polar aprotic solvent of DMSO to promote S_N2 reactions between propargyl bromide and the primary amine endgroups of the PAMAM[27]. As the reaction was optimized, the number of equivalents of propargyl bromide used in the response per amino endgroup was increased from 1.1 to 3, and the solvent volume was reduced to improve reaction kinetics and promote reactivity. ^1H NMR was used to calculate the average number of propargylations for each generation. For each propargylation, as shown in Table 1, the number of propargyl groups (alkynes added per generation) per amino endgroup continues to decrease as the dendrimer generation increases. The increase in steric hindrance is the cause of this.

Table 1: propargylated generations with three equivalents per end-group (8a-8d)

Generations	Actual number of end groups	Average functionalized end groups (from ^1H NMR)	Actual mass of dendrimer (before functionalization)	Mass of dendrimer after propargylation (Based on data from ^1H NMR in g/mol)
G2	16	16	3,256	3,868
G3	32	30	6,909	8,126
G4	64	59	14,215	16,457
G6	256	215	58,048	66,196

The synthesis of 9a-d was optimized to reduce the amount of copper ion contamination in the product that could cause broadening in the ^{1}H NMR spectrum. Removal of copper ions was done using ethylenediaminetetraacetic acid (EDTA) and dicyclohexylcarbodiimide (DDC)[28], both of which were able to remove residual Cu (II), and Cu(I) left after the reaction. EDTA and DDC were used under pH 7 before the dialysis. Synthesis of the triazole product 9a-d occurred when propargylated PAMAMs 8a-d, G (2), G(3), G (4), or G (6) were reacted with azide 6 in a Cu(I) mediated click reaction. To synthesize 10a-d (G(2), G(3), G(4), and G(6)), the deprotected form of 9a-d, lithium hydroxide, a strong base, was used in the presence of a mixture of water and tetrahydrofuran at a ratio of 1:1 This resulted in the shift of the carbonyl IR peak to a lower frequency as compared to the IR spectrum of the methylated starting material. Although peaks still show the presence of a few methyl esters in the HSQC for higher generations G(4) and G(6), there was an overall reduction in the peak size and intensity in the ^{1}H NMR. A DEPT-135 was carried out to corroborate the deprotection compared with the protected molecules(10a-10d), and there were no prominent CH_3 positive peaks (as expected).

Discussion

The figure below shows the ^{1}H NMR spectrum of the propargylated compound (with the respective generations having a 1:2 ratio for the alkyne signals).

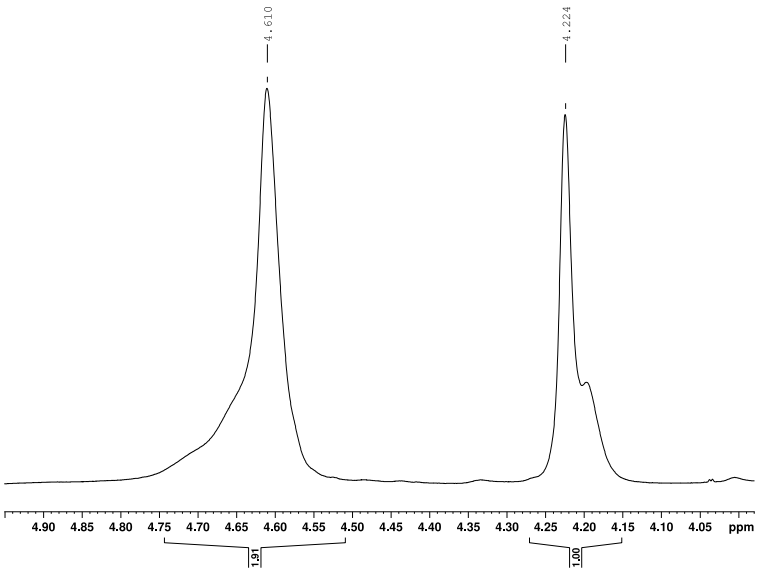

Figure 8: The relevant portion of the ^{1}H NMR spectrum of propargylated dendrimer 8a.

All four generations (G (2), G (3), G (4), and G (6)) showed similar trends in their ^{13}C NMR spectra for compounds 8a-d, where alkyne peaks occurred between 65-85 ppm (specifically 70.33 and 84.07 ppm for compound 8a) but were not present in the spectra of 9a-d after the click reaction was performed.

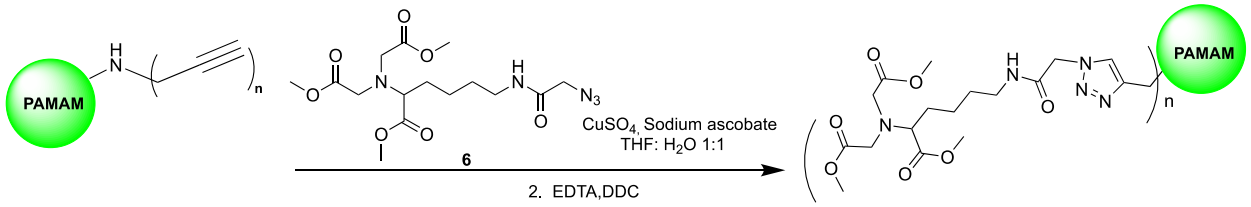

8a G(2):n=16
8b G(3):n=32
8c G(4):n=59
8d G(6):n=215

9a G(2):n≤16
9b G(3):n≤32
9c G(4):n≤64
9d G(6):n≤256

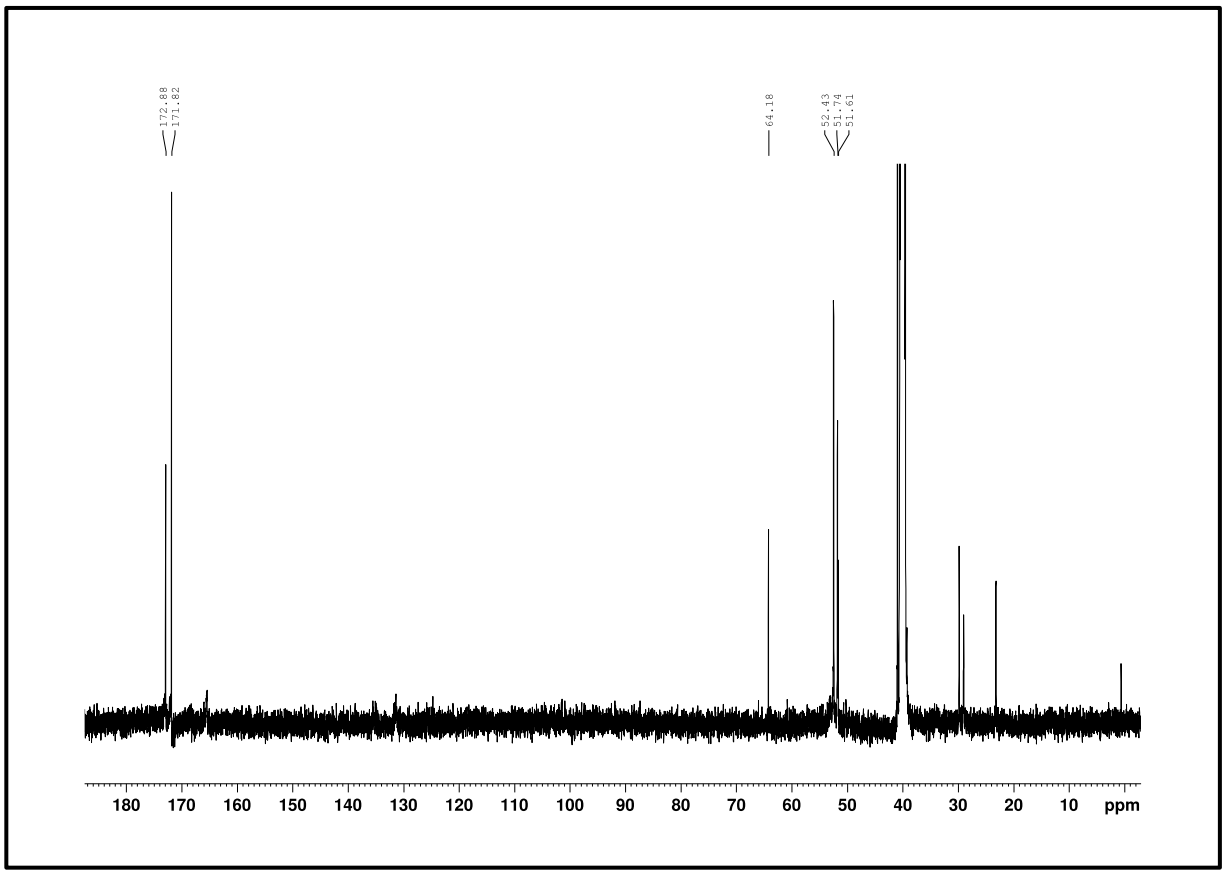

Figure 9: ^{13}C NMR spectrum of propargylated 8a and protected 9a (PAMAM-G (2)).

In addition to the ^{13}C NMR spectrum, an IR spectrum was obtained on the clicked compound 9 and was compared to the propargylated dendrimer 8. For every generation, there is a clear peak due to the alkyne at 2100 cm^{-1} before the click reaction, but this peak is not present after the click reaction.

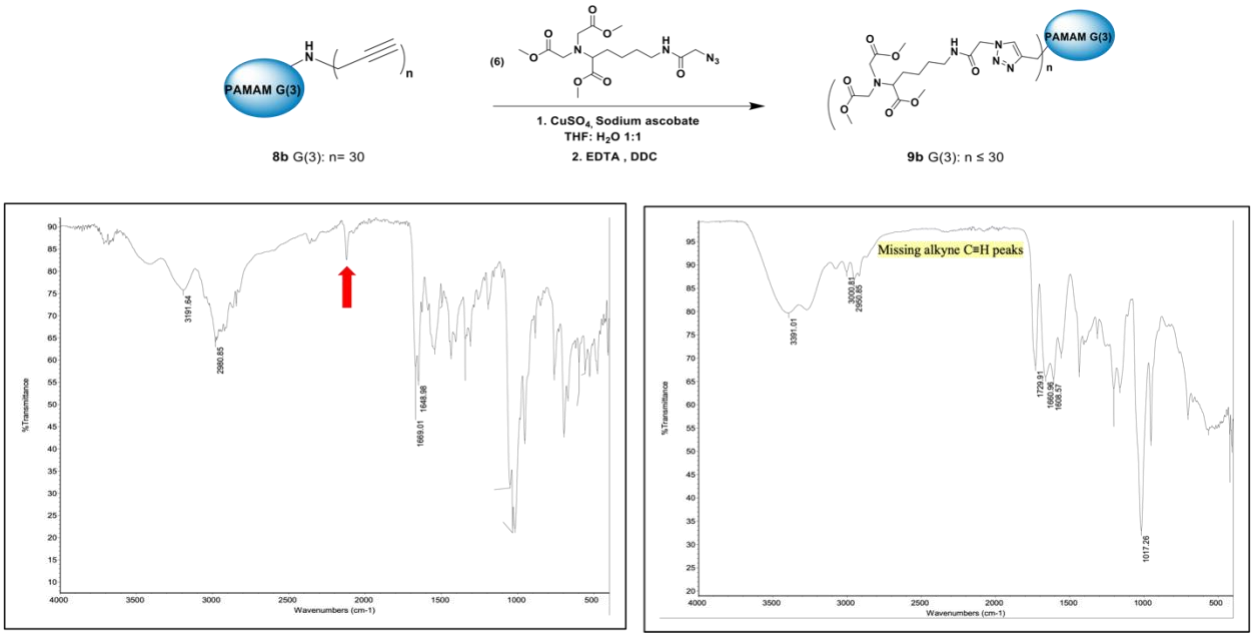

Figure 10: IR of propargylated 8b and protected PAMAM-G (3) 9b

To further corroborate the synthesis of product 8a, a 2D NMR was carried out to confirm the presence of a CH_3. Using HSQC and one of the generations shown below, we notice the presence of a new peak at 3.58,52.22ppm for the CH_3, a signal that is absent in the propargylated compound as shown in the figure below:

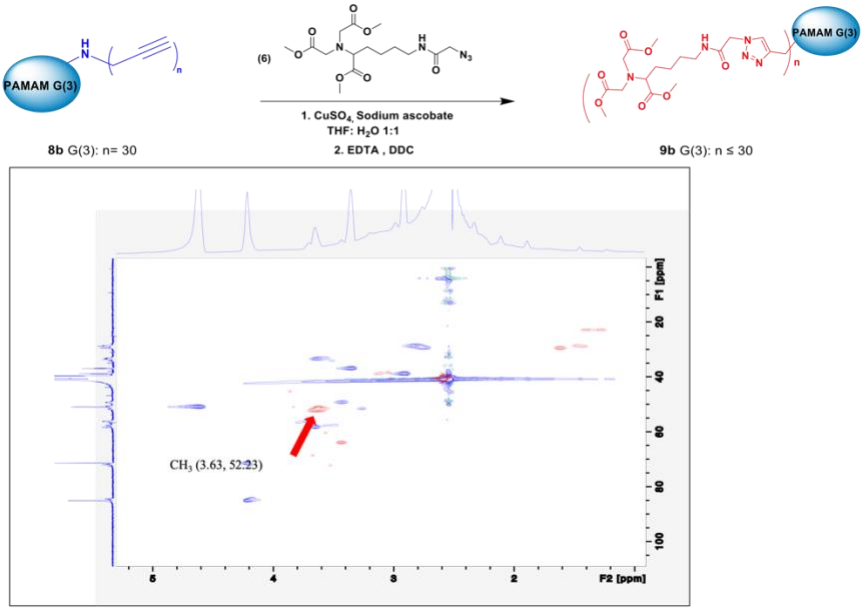

Figure 11: HSQC of propargylated 8b and protected 9b (PAMAM-G (3)).

The results of the DEPT-135 and HSQC experiments on the clicked compound and the deprotected compound are significant. For every generation, the absence of the CH_3 peaks (3.61 and 51.39 ppm for G (3)) compared to the initial protected compound that had those peaks provides crucial insights into the effectiveness of the deprotection.

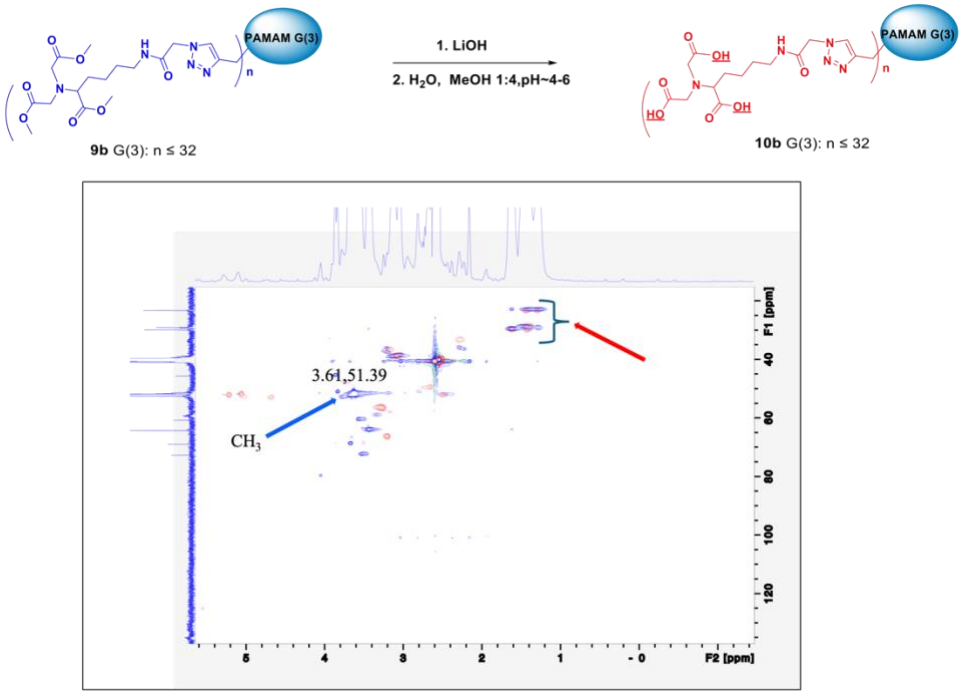

Figure 12: HSQC of protected 9b and deprotected 10b (PAMAM-G(3)).

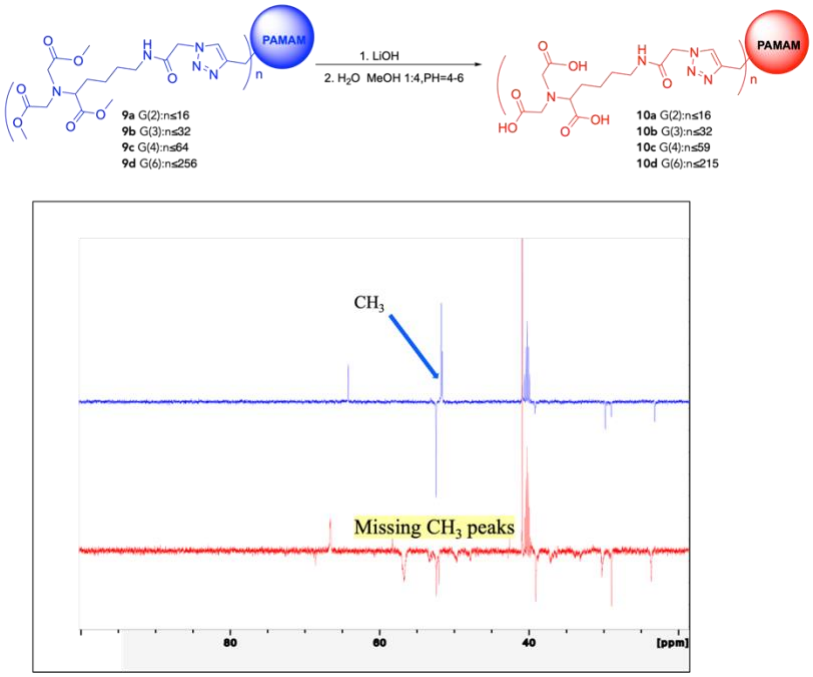

Figure 13: DEPT-135 of protected 9b and deprotected 10b (PAMAM G(3)).

Experimental Methods

General Methods

Solvents such as dichloromethane, diethyl ether, ethyl acetate, dimethylsulfoxide, methanol, tetrahydrofuran, and chloroform were purchased from Fischer. Distilled water was purchased from Rocky Mountain Waters. Chemicals such as propargyl bromide, L-ascorbic acid Sodium salt, and Copper sulfate were purchased from Acros Organics. Dendrimers were obtained from Dendritech, and Bromoacetic acid was sourced from Alfa Aesar. Sodium Azide and bromoacetic acid were also purchased from Sigma-Aldrich and TCI. All dendrimers used were purchased. All synthesized compounds were stored at -20 °C. Glassware for synthesis was cleaned in a base bath (33% 2 M KOH in isopropanol, 66% water), rinsed with water and acetone, and dried at room temperature. ^{1}H NMR spectra were recorded on a Bruker Avance III 400-600 MHz

with a 5 mm broadband auto-tunable probe with Z-gradients at 293 K. Chemical shifts are reported as δ in parts per million (ppm) and referenced to the chemical shift of the residual solvent resonances ($CDCl_3$ δ = 7.26 ppm, DMSO δ=2.50 ppm, MeOD δ=4.89 ppm), couplings are shown as d: doublet, t: triplet, m: multiplet and bs: broad singlet. In most spectra, traces of water appear as a broad singlet at 1.56 ppm ($CDCl_3$) or 3.3 ppm (MeOD). For the ^{1}H, ^{13}C, and 2-D NMR experiments, the 400, 500, and 600 MHz Bruker instruments were used. NMR spectra were processed using Bruker Topspin software. Infrared Spectroscopy was carried out using Diffuse Reflectance Infrared Fourier Transform Spectroscopy (DRIFTS), where IR light reflects diffusely from a powder or liquid sample; scattered light is analyzed.

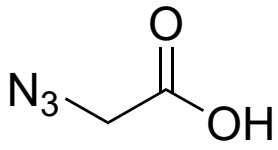

54%

2

Figure 14: Azidoacetic acid (2)

This compound was prepared using a literature procedure[23]. Sodium Azide (1.879 g, 28.9 mmol) was added to a 100 mL round-bottom flask with a stir bar and 10 mL distilled water. The solution was carefully cooled to 0 ^{0}C for 5 minutes. Bromoacetic acid (2.008 g, 14.4 mmoles) was then introduced to the same round bottom flask and left stirring in an ice bath that was allowed to come to room temperature and let stir for 24 h. 10 mL of 10% 12M HCl was added to the reaction

mixture while maintaining the pH between 2 and 3 (pH paper). The solution was extracted using dietyether (50 mL x 3). The organic phase was washed with 10 mL of brine, dried with sodium sulfate, and concentrated in vacuo, giving a colorless solution of azidoacetic acid 0.839 g (54%). The spectral characterization data match previously published spectra. ^{1}H NMR ($CDCl_3$, 400MHz,): δ 3.99 (s, 2H), 11.2 (s, 1H) ppm.^{13}C-NMR: ($CDCl_3$, 400 MHz) 174, 50 ppm. IR: COOH (2914), N_3 (2104), C=O (1717) cm^{-1}.

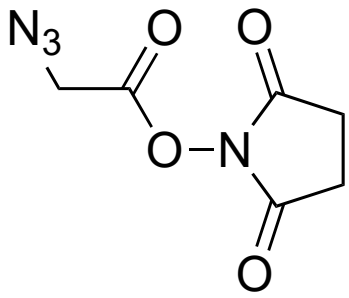

60%

3

Figure 15: Azidoacetic Acid NHS Ester (3).

This compound was prepared using a literature procedure[24].Azidoacetic acid (2, 0.536 g, 5.303 mmol) was added to a 100 mL round-bottom flask with a stir bar and 15 mL dry dichloromethane. The solution was cooled to 0 ^{0}C. N-Hydroxysuccinimide (NHS, 0.732 g, 6.36 mmol) was introduced to the same round-bottom flask. EDCI (1.22 g, 6.36 mmol) was added to the solution, stirring for 24 h. The organic layer was washed with 10 mL of DI water, washed with 10 mL of brine, dried with sodium sulfate, and concentrated in vacuo to give 0.625 g of product as a white solid (60%). ^{1}H NMR: ($CDCl_3$, 400MHz) δ 2.90 (s, 4H), 4.26 (s, 2H),^{13}C-NMR: ($CDCl_3$,400 MHz) 174, 50 ppm. IR: C=O (2104), N_3 (1717), C-H (2996) cm^{-1}.

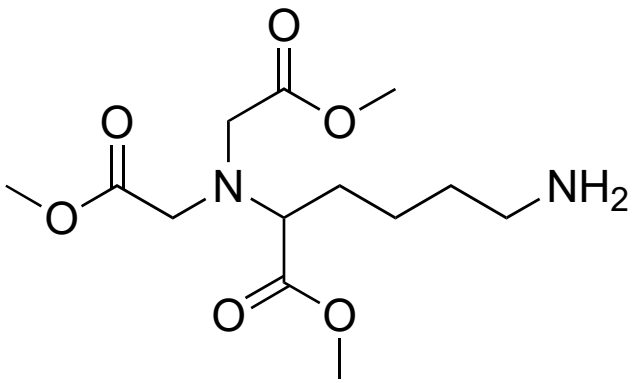

93%

5

JJ.

Figure 16: Dimethyl 2,2'-((6-amino-1-methoxy-1-oxohexan-2-yl) azanediyl) triacetate (5)

This compound was prepared using a literature procedure[29]. To a 200 mL round bottom flask containing N, N-bis(carboxymethyl)-L-lysine (0.501 g, 1.91 mmoles) was added TMSCl (1.45 mL, 11.44 mmoles). This was stirred at room temperature for 5 minutes. To the reaction mixture, 100 mL of methanol was added, and to the reaction was refluxed for 24 h. The reaction mixture was concentrated in vacuo to give a colorless crystalline solid (0.583 g, 99%) ^{1}H NMR:(MeOD,400 MHz) δ 2.189-2.560 (br. s, 6H), 3.565 (s, 2H), 4.381 (s, 9H), 4.800-4.829 (m, 5H) ppm.^{13}C-NMR: (MeOD, 400 MHz)

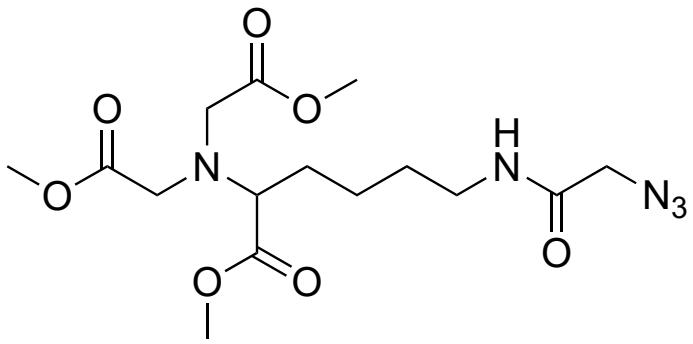

64%

6

Figure 17: Synthesis of Azido-trimethyl ester-protected Lysine-N-Carboxamide Ligand (6).

This compound was prepared using a literature procedure[30] In a 100 mL round-bottom flask, N-tricarboxymethyl lysine trimethyl ester (5) (0.102 g, 0.335 mmol, 1 equiv) was dissolved in 20 mL of dry dichloromethane. Triethylamine (3.6 equiv) was added to this solution, and the reaction was stirred at room temperature for 1 min. Azidoacetic acid NHS ester (3, 1 equiv, 0.335 mmol, 0.0663 g) was added, and the solution was stirred for 24 h at room temperature. The solution was concentrated in vacuo and redissolved in chloroform. This was then washed with brine (3 × 10 mL) and dried over anhydrous sodium sulfate. It was then concentrated and purified using column chromatography ($CHCl_3$: MeOH, 90:10) to afford the product as a light-yellow liquid (0.122 g, 95%,).^{1}H NMR: ($CDCl_3$, 400 MHz) δ 1.516-1.640 (m, 6H), 3.25 (s, 2H), 3.390 (s,1H), 3.56 (s, 4H) 3.58 (s, 9H), 3.91 (s,2H) ppm. IR: N≡N (2951), C-H (3298), C=O (1730) cm^{-1}.

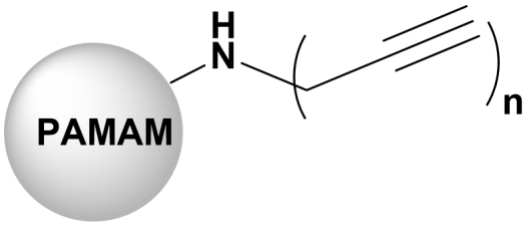

8a G(2): n= 16
8b G(3): n= 30
8c G(4): n= 59
8d G(6): n= 215

Figure 18: General synthesis of Propargylated PAMAM 8a: G (2), 8b: G(3), 8c: G(4), and 8d: G (6).

Dendrimer G (2) (67 mg, 2.074xa0^{-4}, one equiv.) was added to a 10 mL vial, after which 1 mL of dimethylsulfoxide and propargyl bromide (9.943 mL, 3 equiv.) were added to the vial. The reaction was left stirring for approximately 48 hours and then dialyzed in 1 kDa MWCO dialysis tubing for G (2) and 2 kDa MWCO for other generations for 48 hours, with the solutions changed every 12 hours. After dialysis, each solution was lyophilized to dryness, producing a light yellow to orange liquid. ^{1}H NMR in (DMSO-d_6, 600 MHz): δ 4.223 (s, 14H), 4.612 (s, 28H),7.73-8.80 (m, 28H), 2.29-3.89 (m, dendrimer peaks) IR: C≡C (2123.56), N-H (3202.21) CH (3058.00), C=O (1665.66).^{13}C (600MHz, DMSO_d_6) δ168.93, 167.82, 83.52, 7.24, 54.46, 49.76, 37.76, 36.86, 32.23, 27.60.

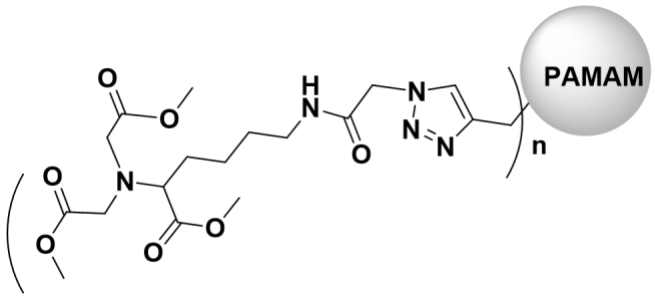

9a G(2): n ≤ 16
9b G(3): n ≤ 30
9c G(4): n ≤ 59
9d G(6): n ≤ 215

Figure 19: General synthesis of protected clicked compound 9 for G (2), G(3), G (4), and G (6).

In a 10 mL vial, 8a G (2) (0.103 g, 2.65×10^{-5} moles, 1 equiv.) was dissolved in 600 µL of a THF: water mixture at a ratio of 1:1. Compound 6 (0.164 g, 4.23×10^{-4} mol) was added. From a 100 mg/mL aqueous stock solution of sodium ascorbate, 251 µL was added to the reaction vial (0.127 mmol, 25 mg, 0.3 equiv. per 6). From a 10 mg/mL aqueous stock solution, copper sulfate pentahydrate (1057.8 uL 4.2 x 10^{-5} mmol, 10.57 mg) was added to the reaction vial. The reaction was stirred at a high velocity for 48 h before adding EDTA and DDC[28] (20 mg/mL stock solution, at 600 µL each) and left stirring for another hour. Dialysis was performed in DMSO using 1 kDa MWCO dialysis tubing, with the solution changed every 12 h for 2 days.

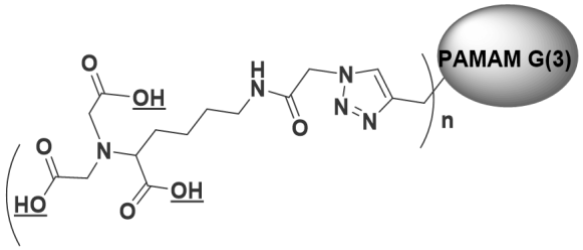

10b G(3): n ≤ 32

Figure 20: General synthesis of protected clicked compound 10 for G(2), G(3), G(4), and G(6).

To a solution of compound 9a (33.38 mg, 3.2011×10^{-5} mol) in MeOH: H_2O mixture, LiOH (36.8 mg, 1.53×10^{-3} mol) was added. An additional 1 mL of deionized water was added to the reaction and stirred for several hours. The reaction mixture was then neutralized using Amberlite resin at a pH of 4-6 for about an hour. Dialysis was performed in DMSO using 1 kDa MWCO dialysis tubing, with the solution changed every 12 h for 2 days. The product was lyophilized to yield a gray, powdery substance. Characterization was performed, with an emphasis on the new peaks formed using ^{13}C, DEPT-135, and HSQC.

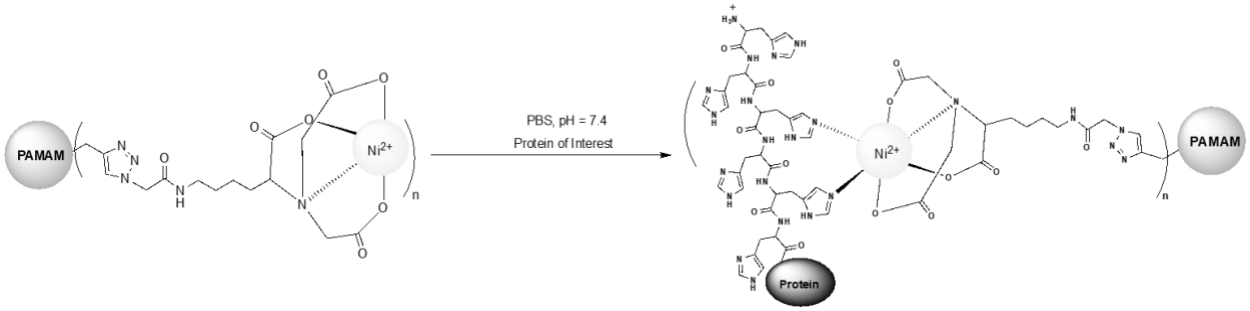

Figure 21: General synthesis of metal complexed 11 and protein binding.

To a solution of deprotected compound 10d (1 mg) in 1 mL TBS buffer, 23.7 µL from a 10 mg/mL stock solution of $NiSO_4$ was added, and the solution was stirred for 24 h to form 11d.

For TEM and CD experiments, 10 uL (1 mg/mL) of this solution of 11d was combined with 91 uL of a 23.7 uM solution of galectin-3 (30 equiv) in PBS to form 12d. This solution mixture was incubated at –20 ^{0}C for an hour before being diluted in TBS and analyzed by TEM as described in chapter 3. TEM was carried out to confirm that the nucleation of oligomerization of galectin-3 by 11d forms 12d. Characterization of 12 is described in Chapter 3.

CHAPTER THREE

PROTEIN BINDING

INTRODUCTION

Protein binding is a crucial phenomenon in biological processes, governing many cellular functions from enzymatic catalysis to molecular transport.[31] Proteins participate in signal transduction, gene transcription, cell death, immune function, structural support, and catalysis of chemical reactions vital for life [32]. Virtually every aspect of the biology of living things involves proteins [33]. Proteins are constructed primarily from diverse combinations of 20 amino acids, resulting in varied structures and functions[34]. Although proteins are often studied individually, developments in molecular biology, analytical technologies, and computing since the 1990s have enabled the study of protein clusters and complexes, leading to a surge of information in this area. A typical example is the modification of the N- or C-protein terminus. Scientists have regularly introduced different bulky chemical groups, or peptide sequences, to proteins to study their binding affinity[35]. Other aspects of the proteins that can be explored include the biophysical properties and the four levels of structure before and after binding[36]. The overall role of protein function and its understanding extends beyond basic biology. It offers critical insights for medicine and pharmacy, facilitating the identification of targets for genetic manipulation and the rational design of novel proteins[37]. Several research articles have studied different methods for manipulating the function of a protein, and one common approach is to bind the protein to a Ni-complexed nitrilotriacetic acid[38].

Amongst many drugs that have been developed, most aim to bind to a protein target. Protein binding of molecules alters the protein's behavior and influences biochemical pathways that control cellular processes such as proliferation and apoptosis[39]. Additionally, therapeutic proteins can compensate for deficiencies or inhibit specific biological processes, making them valuable treatments for various diseases.[37]

For this research, transmission electron microscopy (TEM) and circular dichroism (CD) will be used to study the binding of histidine-labeled proteins to the Ni-NTA functionalized dendrimers reported in chapter 2. Transmission electron micrographs for the sixth-generation Ni-NTA functionalized dendrimer complexed to both the full-length galectin-3 and the galectin-3 carbohydrate recognition domain are described in this chapter. In addition, circular dichroism traces are provided for all four generations of Ni-NTA functionalized dendrimers reported in Chapter 2. The CD traces for protein complexes formed upon the addition of galectins to the dendrimers are also reported in this chapter.

Transmission electron microscopy (TEM)

Transmission electron microscopy (TEM) is a valuable tool in modern materials science, biology, and nanotechnology. Through this technique, visualization of specimens at the atomic level has been made possible[40]. Unlike optical microscopy, which is limited by the diffraction of light, TEM employs a beam of high-energy electrons to interact with the sample, producing significantly higher-resolution images. The fundamental principle of TEM involves transmitting electrons through an ultra-thin specimen and then evaluating the resulting diffraction pattern to obtain information about the structure of the specimen[41]. This allows for the detailed study of internal structures and morphologies that are otherwise impossible to resolve with conventional light-based techniques[4243]. The versatility of TEM extends beyond simple

imaging, encompassing a range of advanced techniques that provide detailed structural and chemical information. Most TEM images, including those reported here, use stains that include heavy metals, but some sophisticated computer programs can analyze unstained samples[44] [45]. Many protein samples are negatively stained with uranyl acetate, and neutral stains like phosphotungstic acid are used for proteins assembled via Ni (II)-complexation. These stains work by embedding electron-dense heavy metals around the macromolecule of interest, enhancing contrast[46].

Circular Dichroism (CD)

Circular dichroism (CD) spectroscopy is a pivotal spectroscopic technique in structural biology and biochemistry. Since its emergence in the 1960s, CD has found extensive applications in examining the structures of proteins, polypeptides, and peptides[47]. CD spectroscopy is particularly valuable for deducing the secondary structure of proteins and peptides in solution, offering a rapid and relatively straightforward approach to assess the conformational states of these macromolecules[48]. The resulting CD spectra reveal characteristic features of different secondary structure elements such as alpha-helices, beta sheets, and random coils.[49] In a CD spectrum, each type of secondary structure, ranging from the alpha helix to anti-parallel and parallel beta-sheets, beta-turns, and random coil, gives rise to a distinctive pattern of circular dichroism.[50] The alpha helix exhibits a strong positive CD band at 193 nm and two negative bands at 208 and 222 nm. The beta sheet, on the other hand, gives rise to a positive band near 195 nm and a negative band near 218 nm. A typical image of these CD traces is shown in Figure 20 below.[51]

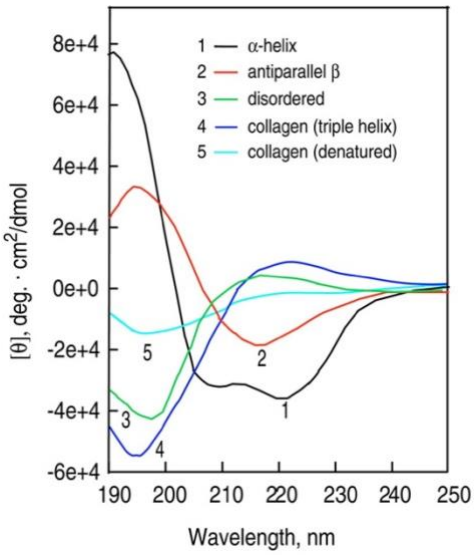

Figure 22: Representative CD traces for the different secondary protein structural elements[42].

This chapter reports the CD spectra for the four generations of Ni-NTA functionalized dendrimers reported in Chapter 2. It also presents their complexation to galectins and analyzes the abundance of each type of secondary structure before and after binding the galectins to the dendrimers.

Experimental Methods

Transmission electron microscopy

For electron microscopy sample preparation, C-flat 300 mesh carbon-coated grids were plasma cleaned in a Pelco EasiGlo instrument for 15s. 4 µL of a 10-20 µg/mL protein solution was applied to grids for 2 minutes, blotted, washed in Milli-Q water, and stained for an additional 2 minutes in 0.5% uranyl acetate. After blotting lightly, the grids were air-dried to allow a stain gradient to form. Grids were imaged at 30,000x magnification in a Tecnai Spirit 120keV electron microscope.

Results and Discussion

In Figure 23a, the unstained transmission electron micrograph of Nickel-NTA polyamidoamine generation G (6) compound 11d shows particles that are approximately 5 nm in diameter. The dendrimers appear as black dot-like particles that are distinguishable from the background. The image in Figure 23a reveals the presence of a nickel-based complex, which affords the black spots visible in the panel. In Figure 24a-b, two TEM images of a sample containing galectin-3 are shown. Glutaraldehyde (0.01% in PBS) was added to a 60 μg/mL solution of galectin-3 in PBS. As expected, the galectin-3 solution is too dilute for protein crosslinking to occur, and the individual proteins are too small to be visible in the micrographs. In Figure 25a-c, the TEM images were obtained for solutions of galectin-3 at the same concentration as in Figure 24 (60 μg/mL), but compound 12d was added. A 20:1 ratio of galectin-3 to 12d was used, and 0.01% glutaraldehyde solution was added. When both the polyamidoamine dendrimer 12d and galectin-3 are present, white dots that are approximately 20 nm in diameter are visible.The images in 25a-c confirm the presence of many Ni-NTA functionalized dendrimers complexed with Galectin-3.

Figure 23a: G6 Only; 10ug/mL, no stain

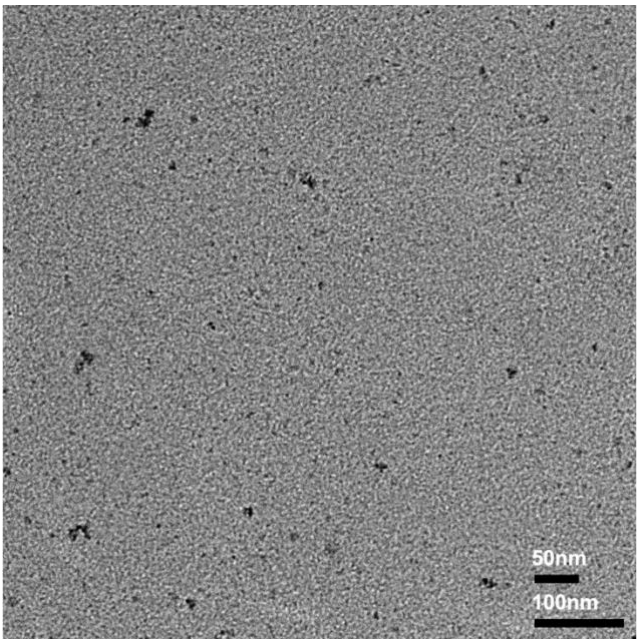

Figure 24a-b: Galectin-3 stained with 0.5% uranyl acetate

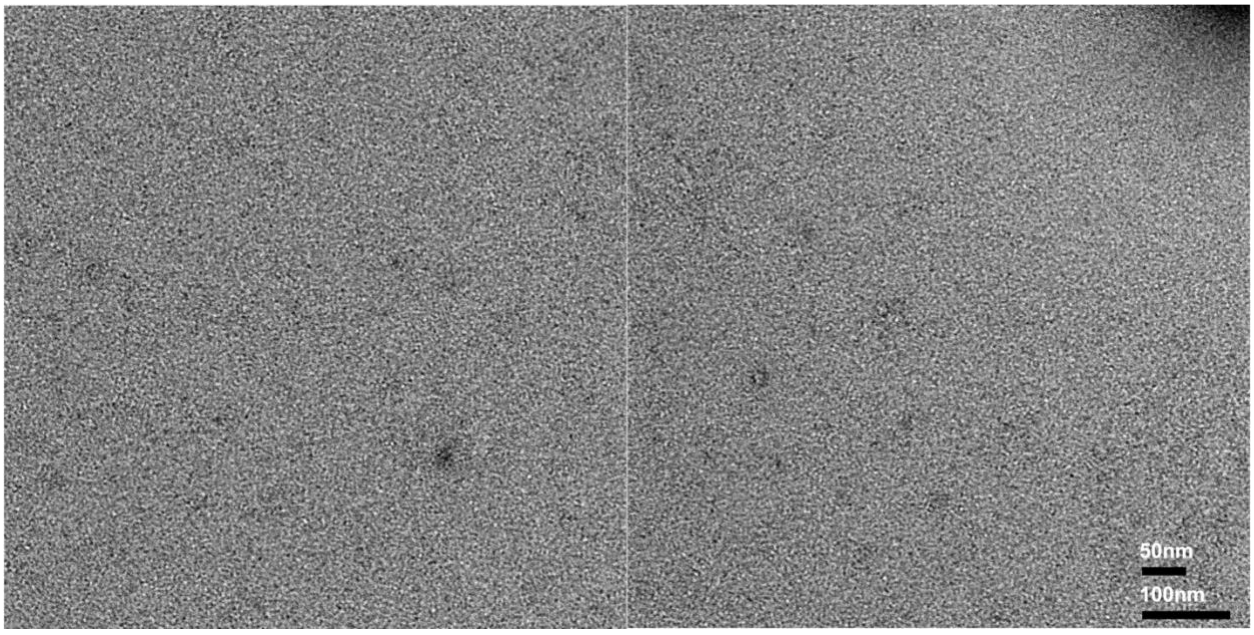

Figure 25a-c: Galectin-3/G6-Ni-NTA Structures: Synthesized and Combined Complexes across three different data collections and stained with 0.5% UA

a b c

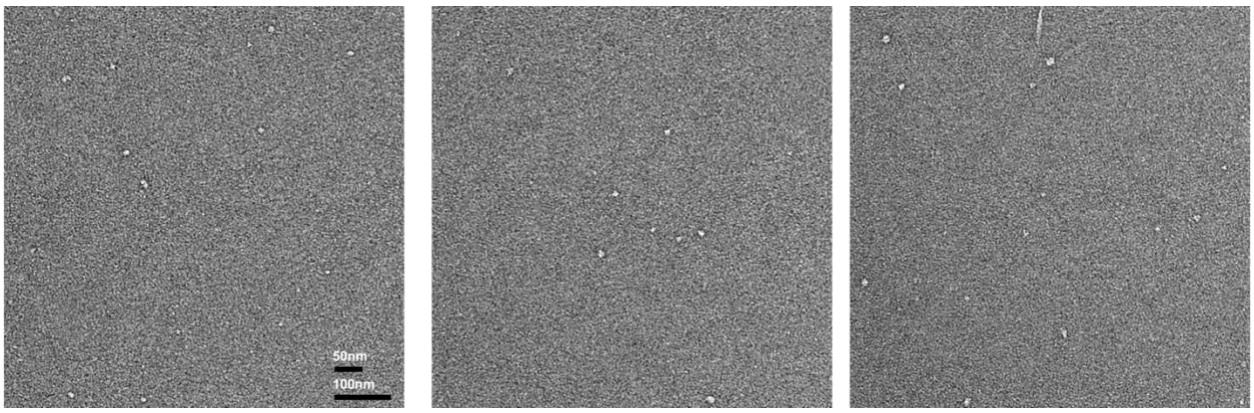

Circular Dichroism (CD) Spectroscopy (Experimental Methods)

CD spectra were acquired using an OLIS DSM 20 UV/VIS Circular Dichroism Spectrophotometer with a bandwidth of 2 nm (slit width 0.5 nm). Three spectra were collected from 190 to 260 nm in 1 nm increments and subsequently averaged. Data were averaged at each wavelength for a time that varied as a function of the voltage applied to the photomultiplier tube. The protein concentration per sample was 10-35 μM in phosphate-buffered saline (PBS). The concentration of 12 in samples without protein was 7 μM in PBS. For mixed samples, final concentrations were 35 μM of protein and 3.5 μM of 12a and 12d (10:1 protein:12) in PBS. In all cases, three spectra of PBS were collected from 190-260 nm in 1 nm increments and subsequently averaged for the baseline. Spectral data were normalized to the most negative signal in the spectrum for stackplots and summations.

Results and Discussion

Figure 26a, shown below, provides the spectra for the synthesized molecules complexed with nickel ions specifically for generation G (2) and G (6) (compounds 11a and 11d, respectively). Comparison to the traces in Figure 22 indicates that the spectra of these molecules are entirely different from the spectra of protein secondary structure motifs that have been known and published in many papers. Although the CDs of both dendrimers are similar to each other, we observe an increase in peaks at approximately 206 nm to 215 nm, and a further overall increase across 224 nm to 257 nm.

After obtaining the CDs of the nickel-complexed dendrimers 11a and 11d, galectin-3 was added in different ratios (10:1 and 8:1) to generations G (6) and G (2) to form 12d and 12a. The CD traces for 12a and 12d are shown in Figure 26b and suggest that there is not a significant difference between complexed and free galectin-3. The CD traces for 12a, 12d, and galectin-3 in the absence of Ni-NTA functionalized dendrimers are all the same.

Figure 26a: Circular dichroism complex of G (2) and G (6)
all three samples.

Figure 26a: Circular dichroism complex of G (2) and G (6)

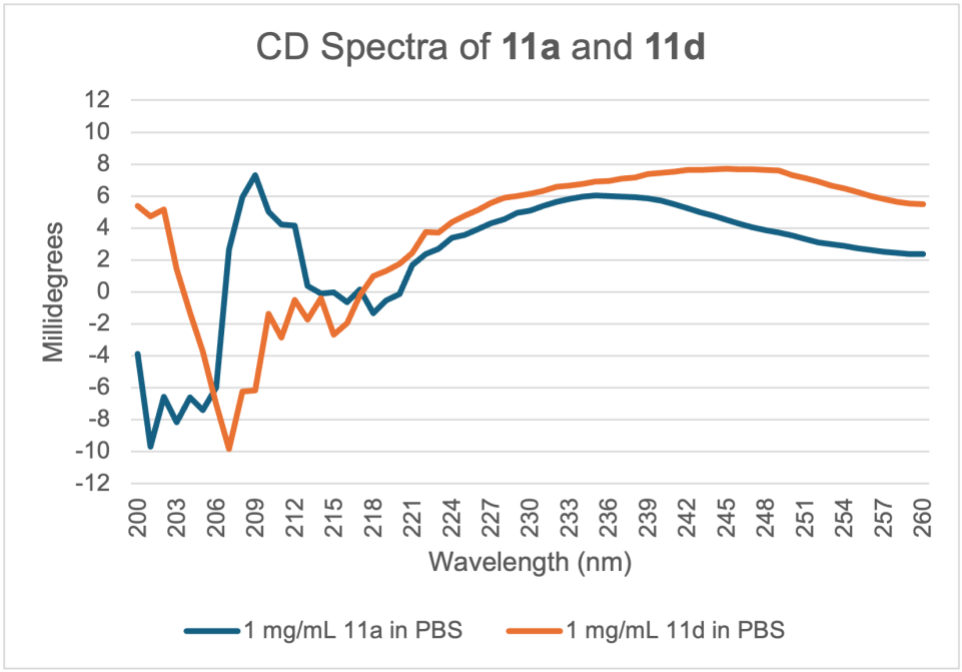

Figure 26b: Circular dichroism for Galectin-3, and complex with Galectin-3

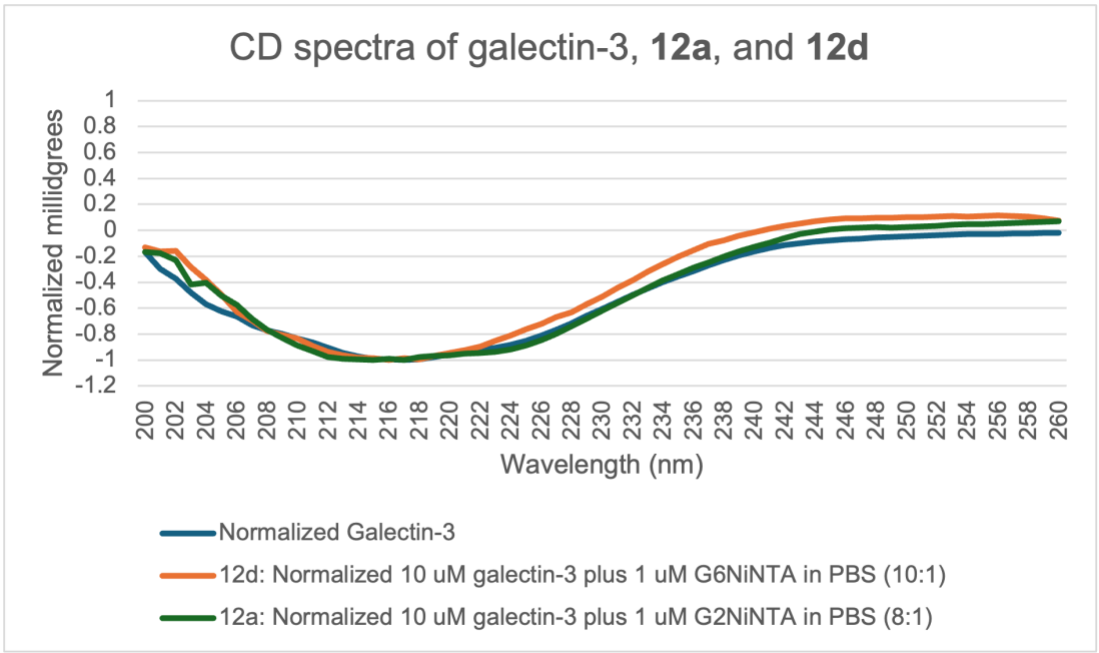

CHAPTER FOUR

CONCLUSION AND FUTURE DIRECTIONS FOR THE PROJECT

The synthetic techniques employed in this project, ranging from substitution nucleophilic reactions (S_N2) to the use of protective agents like TMSCl and Nobel Prize-winning click chemistry, show the scientific approach of our research. This pathway has demonstrated the feasibility of forming the targeted molecule and the ability to select appropriate characterization techniques, including the use of 2D NMR, when conventional mass spectrometric techniques are insufficient for analysis.

To test the efficacy of this synthesized molecule and its ability to form a cluster or complex with galectin 3, a carbohydrate recognition protein, we employed it in transmission electron microscopy and circular dichroism, as shown in various studies. In the images in Figure 25, we observe a large cluster or complex that forms when the protein interacts with the Ni-NTA functionalized dendrimer. Before the complex-protein combination, we see that the unstained synthesized G (6) molecule 12d forms black dots on the TEM micrograph that are approximately 5 nm in diameter (Figure 23). The Ni-NTA functionalized dendrimer is much smaller than the dendrimer/galectin-3 complex. Galectin-3, on its own, in TEM images, is too small to be visible (Figure 24). Overall, the compound, as observed using transmission electron microscopy (TEM), demonstrates its ability to promote protein clustering. Thus, the goals of this project, as described in the final section of Chapter 1, were accomplished.

To further explore the effect of cluster formation (as shown from the transmission electron microscopy) on the structure of the protein, the circular dichroism data were collected and have been reported in chapter three.

Although we hypothesized that binding to the synthesized molecules would cause structural changes to a protein upon the formation of clusters, the circular dichroism data do not show an evident structural change after the molecules 11a and 11d were added to galectin-3. Now that characterization of 12a and 12d using TEM and CD has been completed, the functional effect of complexation of galectin-3 with 11a and 11d to form 12a and 12d on cellular behaviors such as cancer cellular aggregation will be determined.

REFERENCES CITED

(1) Zhao, Z.; Xu, X.; Cheng, H.; Miller, M. C.; He, Z.; Gu, H.; Zhang, Z.; Raz, A.; Mayo, K. H.; Tai, G.; et al. Galectin-3 N-terminal tail prolines modulate cell activity and glycan-mediated oligomerization/phase separation. In Proc Natl Acad Sci U S A, 2021.

(2) Fortuna-Costa, A.; Gomes, A. M.; Kozlowski, E. O.; Stelling, M. P.; Pavao, M. S. G. Extracellular galectin-3 in tumor progression and metastasis. *Front Oncol* 2014, *4*. DOI: ARTN 138 10.3389/fonc.2014.00138.

(3) Nangia-Makker, P.; Balan, V.; Raz, A. Regulation of Tumor Progression by Extracellular Galectin-3. *Cancer Microenviron* 2008, *1* (1), 43-51. DOI: 10.1007/s12307-008-0003-6.

(4) Dumic, J.; Dabelic, S.; Flögel, M. Galectin-3:: An open-ended story. *Bba-Gen Subjects* 2006, *1760* (4), 616-635. DOI: 10.1016/j.bbagen.2005.12.020.

(5) Zhao, Z. H.; Xu, X. J.; Cheng, H. R.; Miller, M. C.; He, Z.; Gu, H. M.; Zhang, Z. Y.; Raz, A.; Mayo, K. H.; Tai, G. H.; et al. Galectin-3 N-terminal tail prolines modulate cell activity and glycan-mediated oligomerization/ phase separation. *P Natl Acad Sci USA* 2021, *118* (19). DOI: ARTN e202107411810.1073/pnas.2021074118.

(6) Thijssen, V. L.; Poirier, F.; Baum, L. G.; Griffioen, A. W. Galectins in the tumor endothelium: opportunities for combined cancer therapy. *Blood* 2007, *110* (8), 2819-2827. DOI: 10.1182/blood-2007-03-077792 From NLM Medline.

(7) Velickovic, M.; Arsenijevic, A.; Acovic, A.; Arsenijevic, D.; Milovanovic, J.; Dimitrijevic, J.; Todorovic, Z.; Milovanovic, M.; Kanjevac, T.; Arsenijevic, N. Galectin-3, Possible Role in Pathogenesis of Periodontal Diseases and Potential Therapeutic Target. *Front Pharmacol* 2021, *12*, 638258. DOI: 10.3389/fphar.2021.638258 From NLM PubMed-not-MEDLINE.

(8) Strebhardt, K.; Ullrich, A. Paul Ehrlich's magic bullet concept: 100 years of progress. *Nat Rev Cancer* 2008, *8* (6), 473-480. DOI: 10.1038/nrc2394 From NLM Medline.

(9) Whitesides, G. M.; Grzybowski, B. Self-assembly at all scales. *Science* 2002, *295* (5564), 2418-2421. DOI: 10.1126/science.1070821 From NLM Medline.

(10) Mammen, M.; Choi, S. K.; Whitesides, G. M. Polyvalent Interactions in Biological Systems: Implications for Design and Use of Multivalent Ligands and Inhibitors. *Angew Chem Int Ed Engl* 1998, *37* (20), 2754-2794. DOI: 10.1002/(SICI)1521-3773(19981102)37:20<2754::AID-ANIE2754>3.0.CO;2-3 From NLM PubMed-not-MEDLINE.

(11) Newlaczyl, A. U.; Yu, L. G. Galectin-3-A jack-of-all-trades in cancer. *Cancer Lett* 2011, *313* (2), 123-128. DOI: 10.1016/j.canlet.2011.09.003.

(12) Sharma, A.; Madhunapantula, S. V.; Robertson, G. P. Toxicological considerations when creating nanoparticle-based drugs and drug delivery systems. *Expert Opin Drug Metab Toxicol* 2012, *8* (1), 47-69. DOI: 10.1517/17425255.2012.637916 From NLM Medline.

(13) Shaikh*, M. A.; Mahima, J. M.; Agnihotri, S. J. A Systematic Review of Nano-Formulations in Breast Cancer Oncology. *Human Journals* 2023, *26* (2), 20.

(14) Demetzos, C. Dendrimers as drug carriers. A new approach to increase the potential of bioactive natural products. *Nat Prod Commun* 2006, *1* (7), 593-600.

(15) Samad, A.; Alam, M. I.; Saxena, K. Dendrimers: A Class of Polymers in the Nanotechnology for the Delivery of Active Pharmaceuticals. *Curr Pharm Design* 2009, *15* (25), 2958-2969. DOI: Doi 10.2174/138161209789058200.

(16) Gonzaga, R. V.; Santos, S. D.; da Silva, J. V.; Prieto, D. C.; Savino, D. F.; Giarolla, J.; Ferreira, E. I. Targeting Groups Employed in Selective Dendrons and Dendrimers. *Pharmaceutics* 2018, *10* (4). DOI: ARTN 219 10.3390/pharmaceutics10040219.

(17) Cao, L. Immobilised enzymes: science or art? *Curr Opin Chem Biol* 2005, *9* (2), 217-226. DOI: 10.1016/j.cbpa.2005.02.014 From NLM Medline.

(18) Guisan, J. M. *Immobilization of enzymes and cells*; Humana Press, 2013.

(19) Klotzbach, T. L.; Watt, M.; Ansari, Y.; Minteer, S. D. Improving the microenvironment for enzyme immobilization at electrodes by hydrophobically modifying chitosan and Nafion® polymers. *J Membrane Sci* 2008, *311* (1-2), 81-88. DOI: 10.1016/j.memsci.2007.11.043.

(20) Sheldon, R. A. Enzyme immobilization: the quest for optimum performance. *Adv Synth Catal* 2007, *349* (8-9), 1289-1307.

(21) Block, H.; Maertens, B.; Spriestersbach, A.; Brinker, N.; Kubicek, J.; Fabis, R.; Labahn, J.; Schäfer, F. Immobilized-Metal Affinity Chromatography (Imac): A Review. *Method Enzymol* 2009, *463*, 439-473. DOI: 10.1016/S0076-6879(09)63027-5.

(22) Hauptmann, N.; Pion, M.; Muñoz-Fernández, M. A.; Komber, H.; Werner, C.; Voit, B.; Appelhans, D. Ni(II)-NTA Modified Poly(ethylene imine) Glycopolymers: Physicochemical Properties and First In Vitro Study of Polyplexes Formed with HIV-Derived Peptides. *Macromol Biosci* 2013, *13* (5), 531-538. DOI: 10.1002/mabi.201200449.

(23) Haridas, V.; Sharma, Y. K.; Sahu, S.; Verma, R. P.; Sadanandan, S.; Kacheshwar, B. G. Designer peptide dendrimers using click reaction. *Tetrahedron* 2011, *67* (10), 1873-1884. DOI: 10.1016/j.tet.2011.01.023.

(24) Munneke, S.; Kodar, K.; Painter, G. F.; Stocker, B. L.; Timmer, M. S. M. The modular synthesis of multivalent functionalised glycodendrons for the detection of lectins including DC-SIGN. *Rsc Adv* 2017, *7* (72), 45260-45268. DOI: 10.1039/c7ra08872h.

(26) Nishimura, T.; Sanada, Y.; Matsuo, T.; Okobira, T.; Mylonas, E.; Yagi, N.; Sakurai, K. A bimolecular micelle constructed from amphiphilic pillar[5]arene molecules. *Chem Commun* 2013, *49* (29), 3052-3054. DOI: 10.1039/c3cc41186a.

(27) Morris, R.; Black, K. A.; Stollar, E. J. Uncovering protein function: from classification to complexes. *Essays Biochem* 2022, *66* (3), 255-285. DOI: 10.1042/Ebc20200108.

(28) Tahmasebi, S.; Sonenberg, N.; Hershey, J. W. B.; Mathews, M. B. Protein Synthesis and Translational Control: A Historical Perspective. *Cold Spring Harb Perspect Biol* 2019, *11* (9). DOI: 10.1101/cshperspect.a035584 From NLM Medline.

(29) In *The Role of Protein and Amino Acids in Sustaining and Enhancing Performance*, 1999.

(30) Jiang, R.; Zhang, M. Q.; Zhang, X. *Basics of Bioinformatics : Lecture Notes of the Graduate Summer School on Bioinformatics of China*, 1st ed.; Springer Berlin Heidelberg : Imprint: Springer,, 2013. DOI: 10.1007/978-3-642-38951-1.

(31) Cloninger, M. J., Bilgiçer, B., Li, L., Mangold, S. L., Phillips, S. T., & Wolfenden, M. L. Multivalency. Supramolecular Chemistry. doi:10.1002/9780470661345. 2012.

(32) Walsh, G. a. W., G. Proteins and Proteomics. 2015. DOI: https://doi.org/10.1002/9781119117599.ch1.

(33) Cai, Y.; Wang, J.; Deng, L. SDN2GO: An Integrated Deep Learning Model for Protein Function Prediction. *Front Bioeng Biotechnol* 2020, *8*, 391. DOI: 10.3389/fbioe.2020.00391 From NLM PubMed-not-MEDLINE.

(34) Keller, D.; Beloqui, A.; Martínez-Martínez, M.; Ferrer, M.; Delaittre, G. Nitrilotriacetic Amine-Functionalized Polymeric Core-Shell Nanoparticles as Enzyme Immobilization Supports. *Biomacromolecules* 2017, *18* (9), 2777-2788. DOI: 10.1021/acs.biomac.7b00677.

(35) Kaliaperumal, J.; Hari, N.; Pavankumar, P.; Elangovan, N. pACC1 peptide loaded chitosan nanoparticles induces apoptosis via reduced fatty acid synthesis in MDA-MB-231 cells. *Appl Nanosci* 2016, *6* (5), 615-627. DOI: 10.1007/s13204-015-0470-2.

(36) Williams, D. B.; Carter, C. B. *Transmission Electron Microscopy*; Springer, 2009.

(37) Kaminskyj, S. G.; Dahms, T. E. High spatial resolution surface imaging and analysis of fungal cells using SEM and AFM. *Micron* 2008, *39* (4), 349-361. DOI: 10.1016/j.micron.2007.10.023 From NLM Medline.

(38) Pennycook, S. J.; Lupini, A. R.; Borisevich, A.; Varela, M.; Peng, Y.; Nellist, P. D.; Duscher, G.; Buczko, R.; Pantelides, S. T. Transmission electron microscopy: Overview and challenges. *Aip Conf Proc* 2003, *683*, 627-633.

(39) Hyo-jin Kang, J. H. K., Jang won Oh, Tae Sun Back, and Ho Joung Kim Ultra-Thin TEM Sample Preparation with Advanced Backside FIB Milling Method. *Microscopy Society of America 2* 2010. DOI: doi:10.1017/S1431927610054474.

(40) Campbell, I. D. The croonian lecture 2006 structure of the living cell. *Philos T R Soc B* 2008, *363* (1502), 2379-2391. DOI: 10.1098/rstb.2006.1960.

(41) Castro-Hinojosa, C.; Del Sol-Fernández, S.; Moreno-Antolín, E.; Martín-Gracia, B.; Ovejero, J. G.; de la Fuente, J. M.; Grazú, V.; Fratila, R. M.; Maria, M. A Simple and Versatile Strategy for Oriented Immobilization of His-Tagged Proteins on Magnetic Nanoparticles. *Bioconjugate Chem* 2023, *34* (12), 2275-2292. DOI: 10.1021/acs.bioconjchem.3c00417.

(42) Winey, M.; Meehl, J. B.; O'Toole, E. T.; Giddings, T. H. Conventional transmission electron microscopy. *Mol Biol Cell* 2014, *25* (3), 319-323. DOI: 10.1091/mbc.E12-12-0863.

(43) Mohamad, N. R.; Marzuki, N. H. C.; Buang, N. A.; Huyop, F.; Wahab, R. A. An overview of technologies for immobilization of enzymes and surface analysis techniques for immobilized enzymes. *Biotechnol Biotec Eq* 2015, *29* (2), 205-220. DOI: 10.1080/13102818.2015.1008192.

(44) Andreeva, N. S.; Iveronova, V. I. Some Diffractional Principles of Fibrous Proteins Structure Classification. *Acta Crystallogr* 1960, *13* (12), 1141-1142.

(45) Mohamad, N. R.; Marzuki, N. H.; Buang, N. A.; Huyop, F.; Wahab, R. A. An overview of technologies for immobilization of enzymes and surface analysis techniques for immobilized enzymes. *Biotechnol Biotechnol Equip* 2015, *29* (2), 205-220. DOI: 10.1080/13102818.2015.1008192 From NLM PubMed-not-MEDLINE.

(46) Greenfield, N. J. Using circular dichroism spectra to estimate protein secondary structure.

Nat Protoc 2006, *1* (6), 2876-2890. DOI: 10.1038/nprot.2006.202 From NLM Medline

(47) Mohamad, N. R.; Marzuki, N. H. C.; Buang, N. A.; Huyop, F.; Wahab, R. A. An overview of technologies for immobilization of enzymes and surface analysis techniques for immobilized enzymes. *Biotechnol Biotec Eq* 2015, *29* (2), 205-220. DOI: 10.1080/13102818.2015.1008192.

(48) Andreeva, N. S.; Iveronova, V. I. Some Diffractional Principles of Fibrous Proteins Structure Classification. *Acta Crystallogr* 1960, *13* (12), 1141-1142.

(49) Mohamad, N. R.; Marzuki, N. H.; Buang, N. A.; Huyop, F.; Wahab, R. A. An overview of technologies for immobilization of enzymes and surface analysis techniques for immobilized

enzymes. *Biotechnol Biotechnol Equip* 2015, *29* (2), 205-220. DOI: 10.1080/13102818.2015.1008192 From NLM PubMed-not-MEDLINE.

(50) Yao, H.; Wynendaele, E.; Xu, X.; Kosgei, A.; De Spiegeleer, B. Circular dichroism in functional quality evaluation of medicines. *J Pharm Biomed Anal* 2018, *147*, 50-64. DOI: 10.1016/j.jpba.2017.08.031 From NLM Medline.

(51) Greenfield, N. J. Using circular dichroism spectra to estimate protein secondary structure. *Nat Protoc* 2006, *1* (6), 2876-2890. DOI: 10.1038/nprot.2006.202 From NLM Medline.

APPENDICES

APPENDIX A

SPECTRA OF SYNTHESIZED MOLECULES

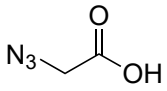

54%

2

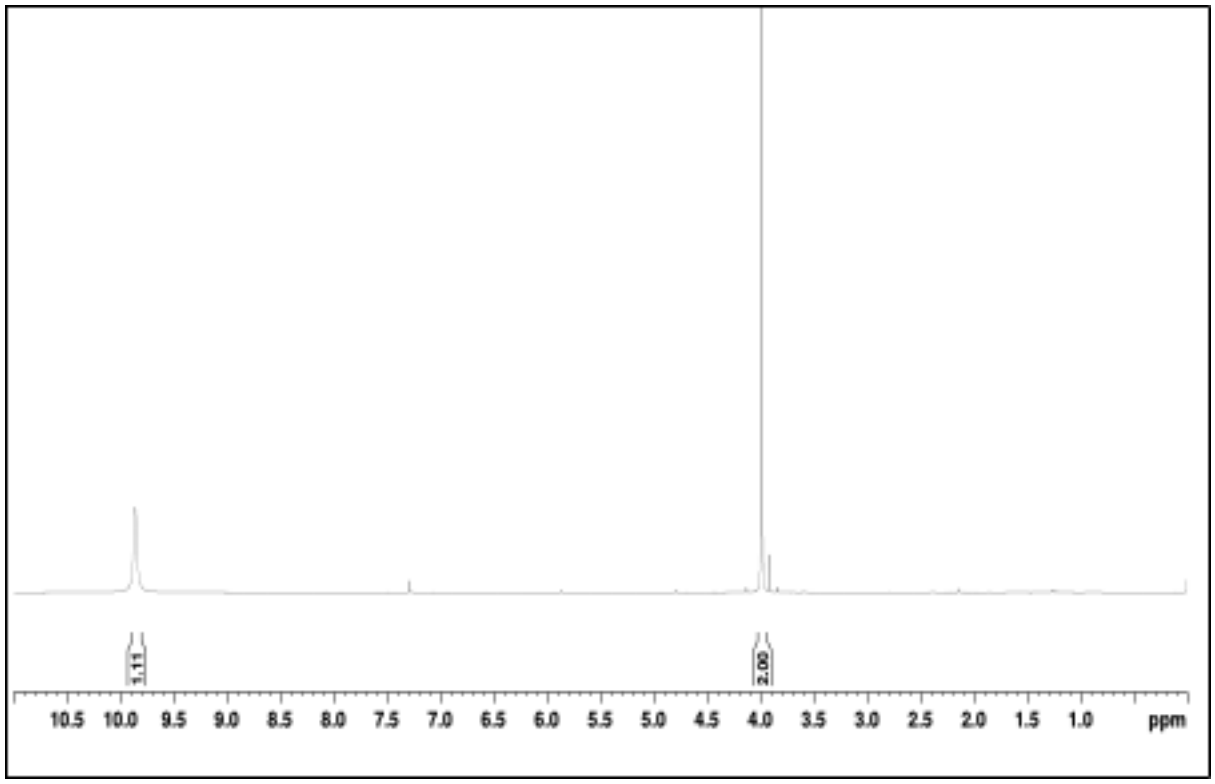

Figure S1: ^{1}H NMR in $CDCl_3$: δ 3.994 (s, 2H), 9.98 (s, 1H),^{13}C-NMR:174ppm, 50.33ppm

IR Spectrum

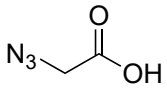

54%

2

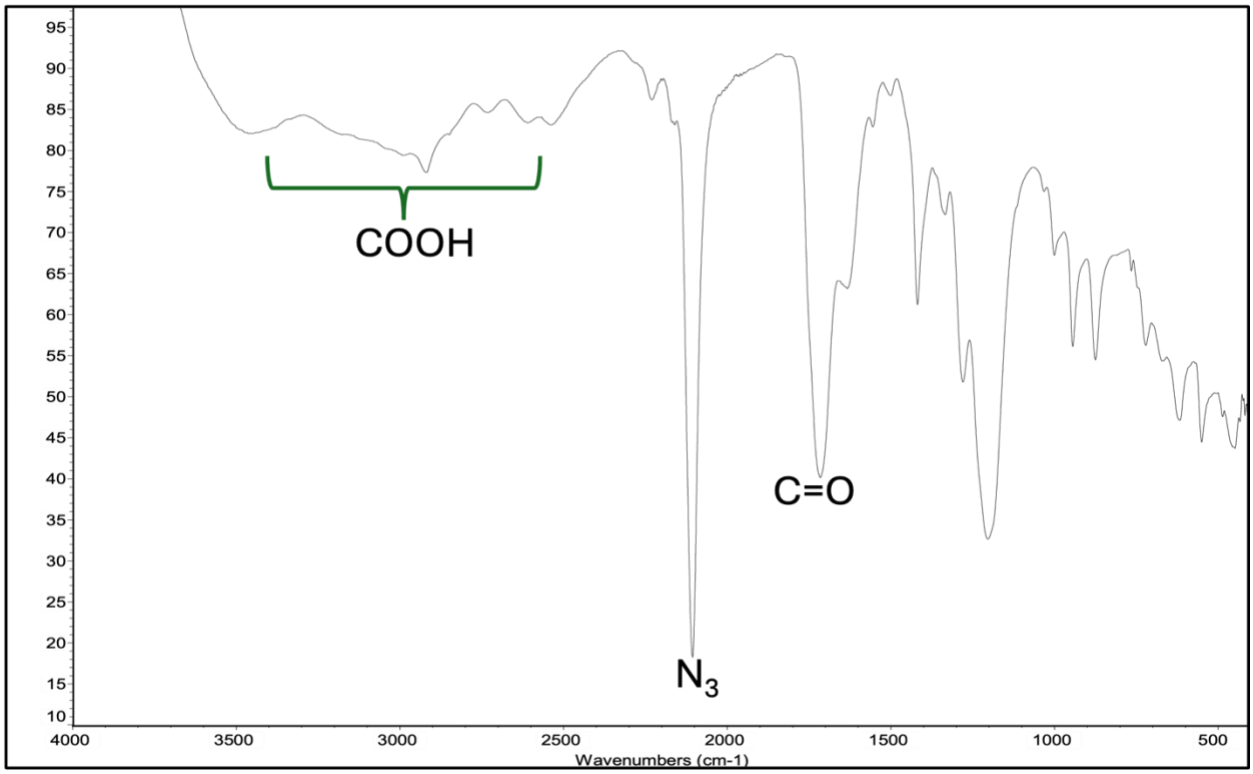

Figure S2 IR: COOH (2914 cm-1), N3 (2104), C=O (1717)

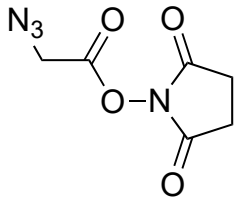

60%

3

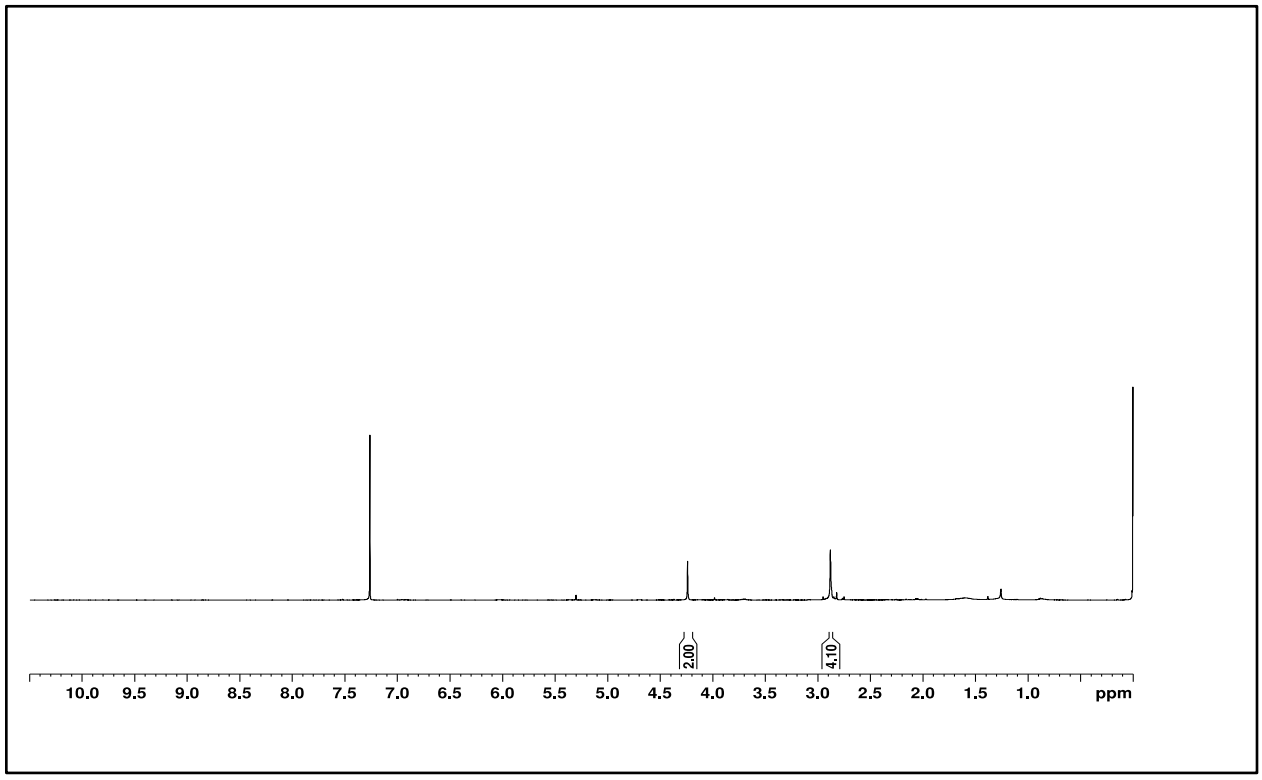

Figure S3 ^{1}HNMR in $CDCl_3$: δ 2.897 (s, 4H), 4.260 (s, 2H),^{13}C-NMR:174ppm, 50.33ppm

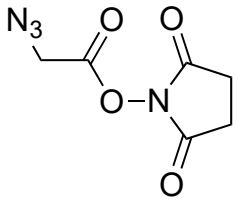

60%

3

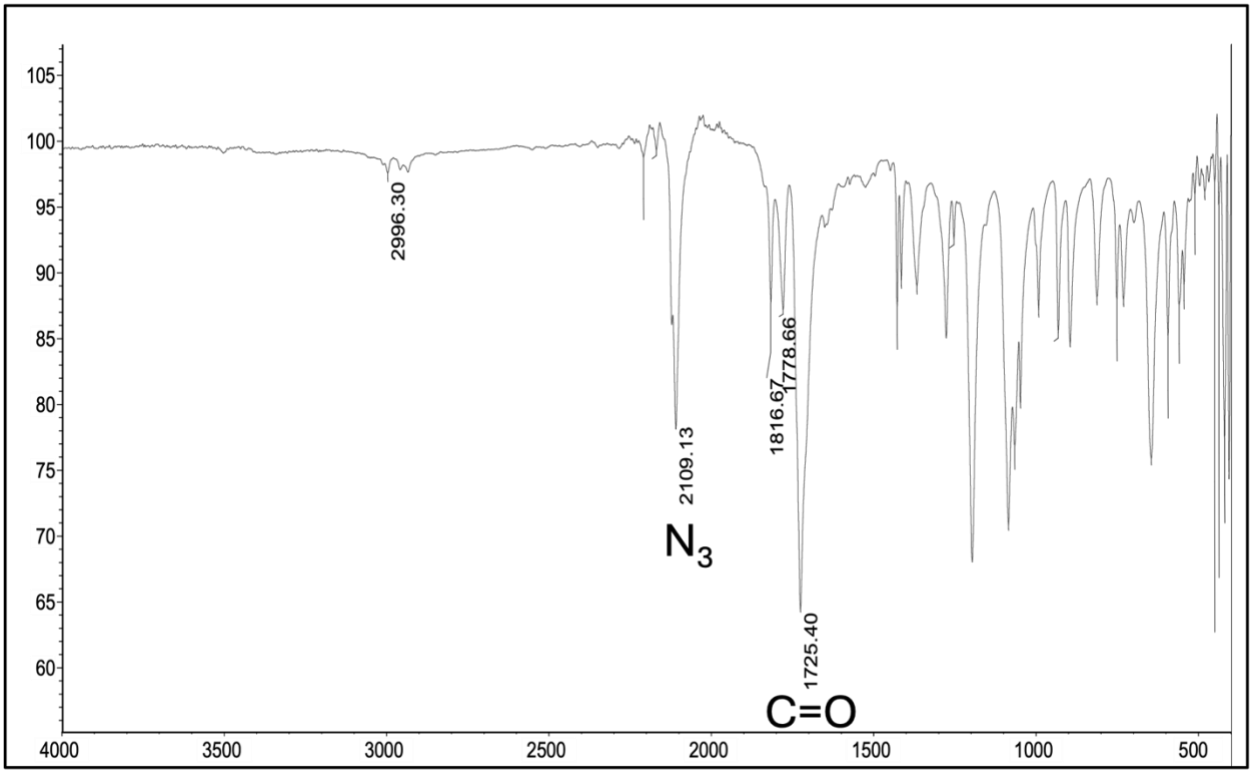

Figure S4 IR: C=O (2104), N_3 (1717), C-H (2996).

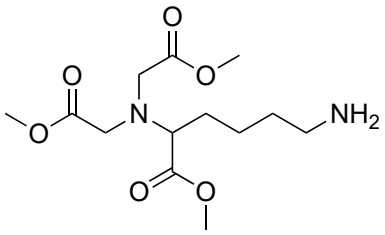

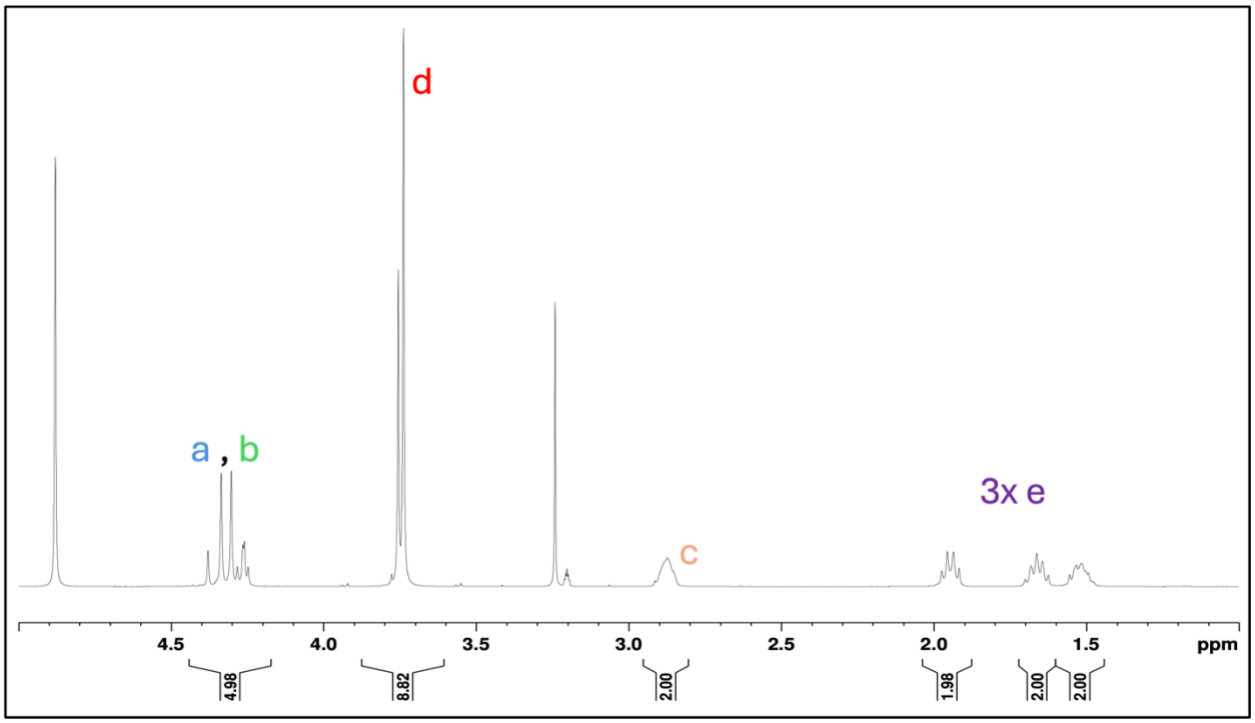

Figure S5: [1]HNMR in MeOD: δ 2.189-2.560(s,6H), 3.565 (s,2H),4.381(9H), 4.800-4.829(5H)),[13]C-NMR in:174ppm, 50.33ppm

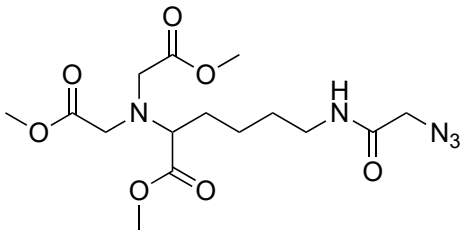

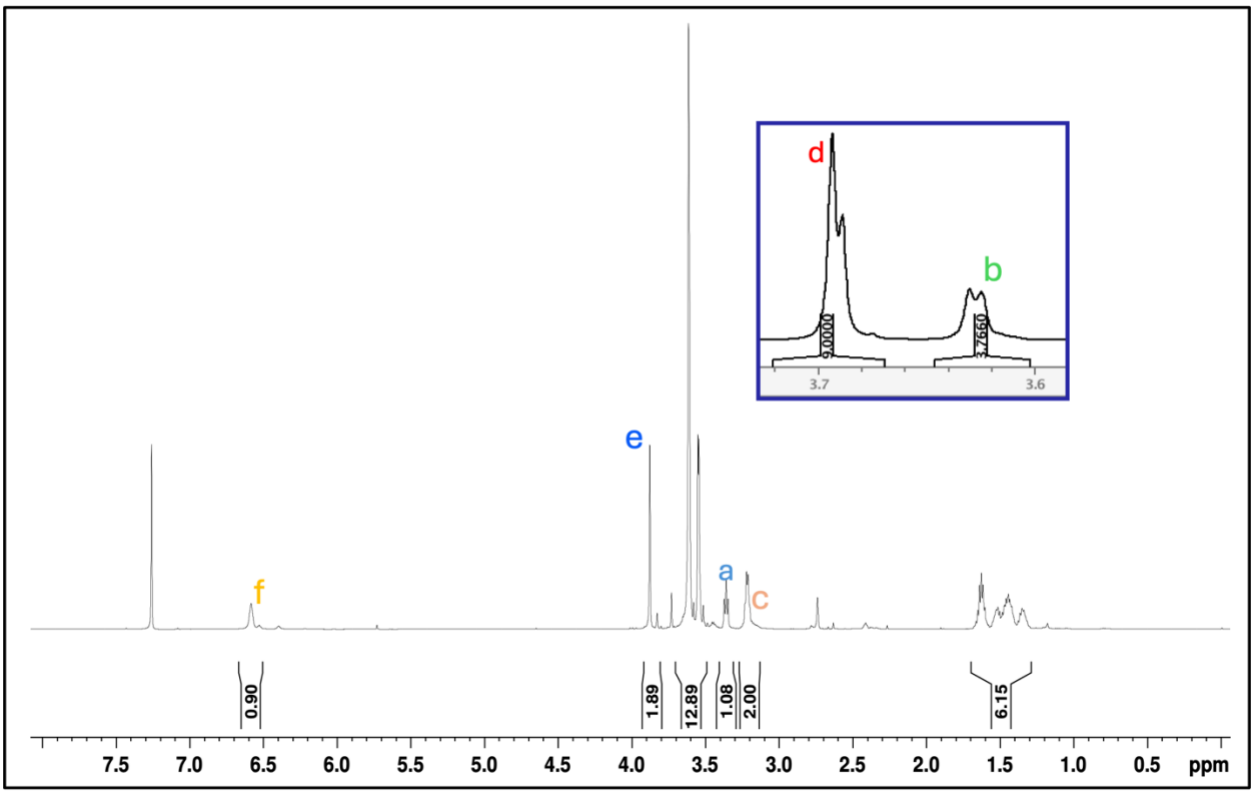

Figure S6: ^{1}HNMR in $CDCl_3$: δ 1.516-1.640 (s, 6H), 3.25 (s, 2H),3.390 (1H), 3.56 (s,4H), 3.580 (s, 9H),3.9140 (2H).

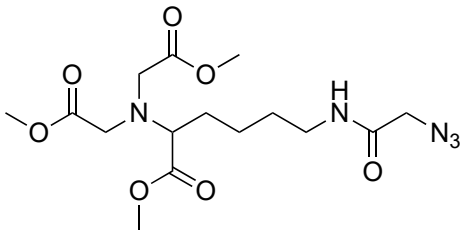

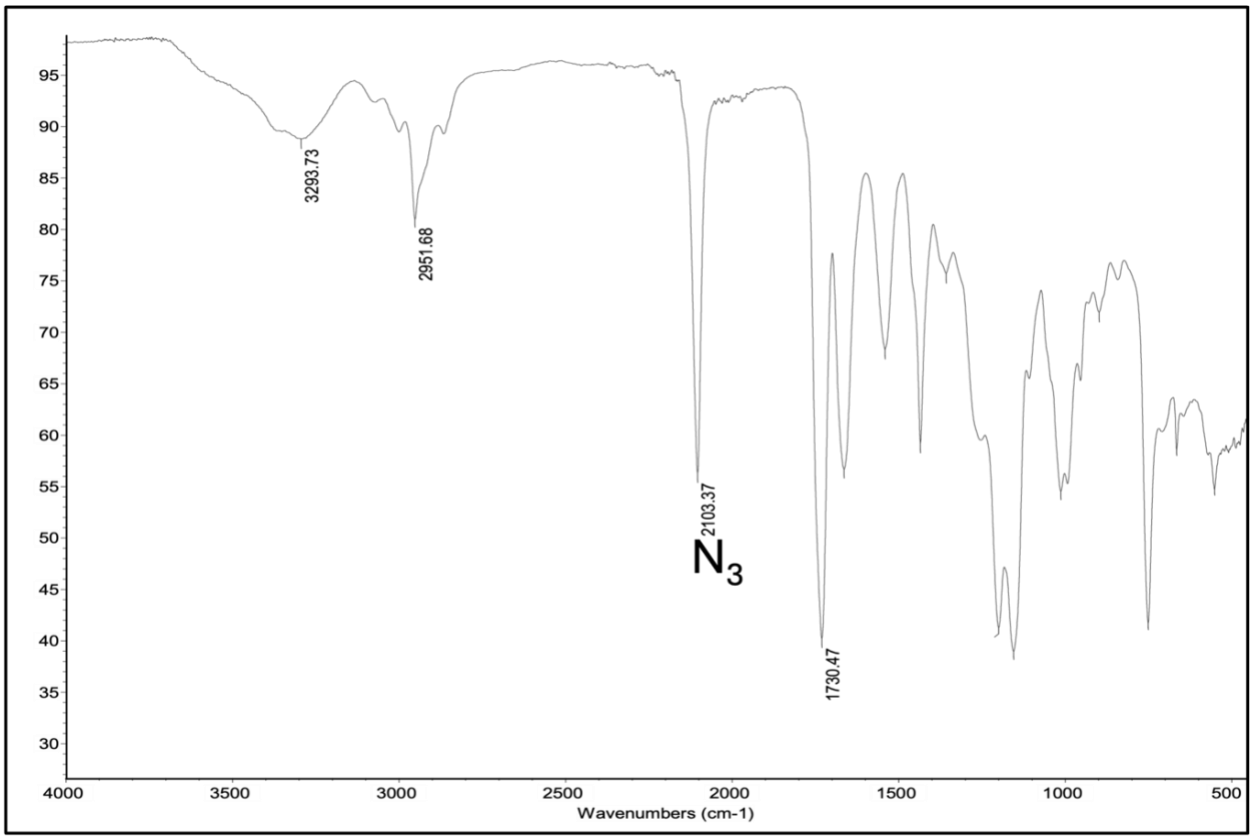

Figure S7 IR: N≡N (2103.37), C-H (3298), C=O (1730.47).

8a

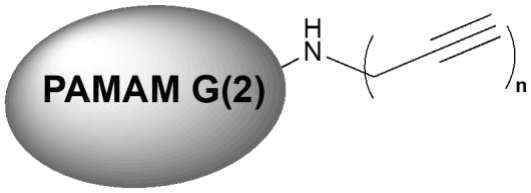

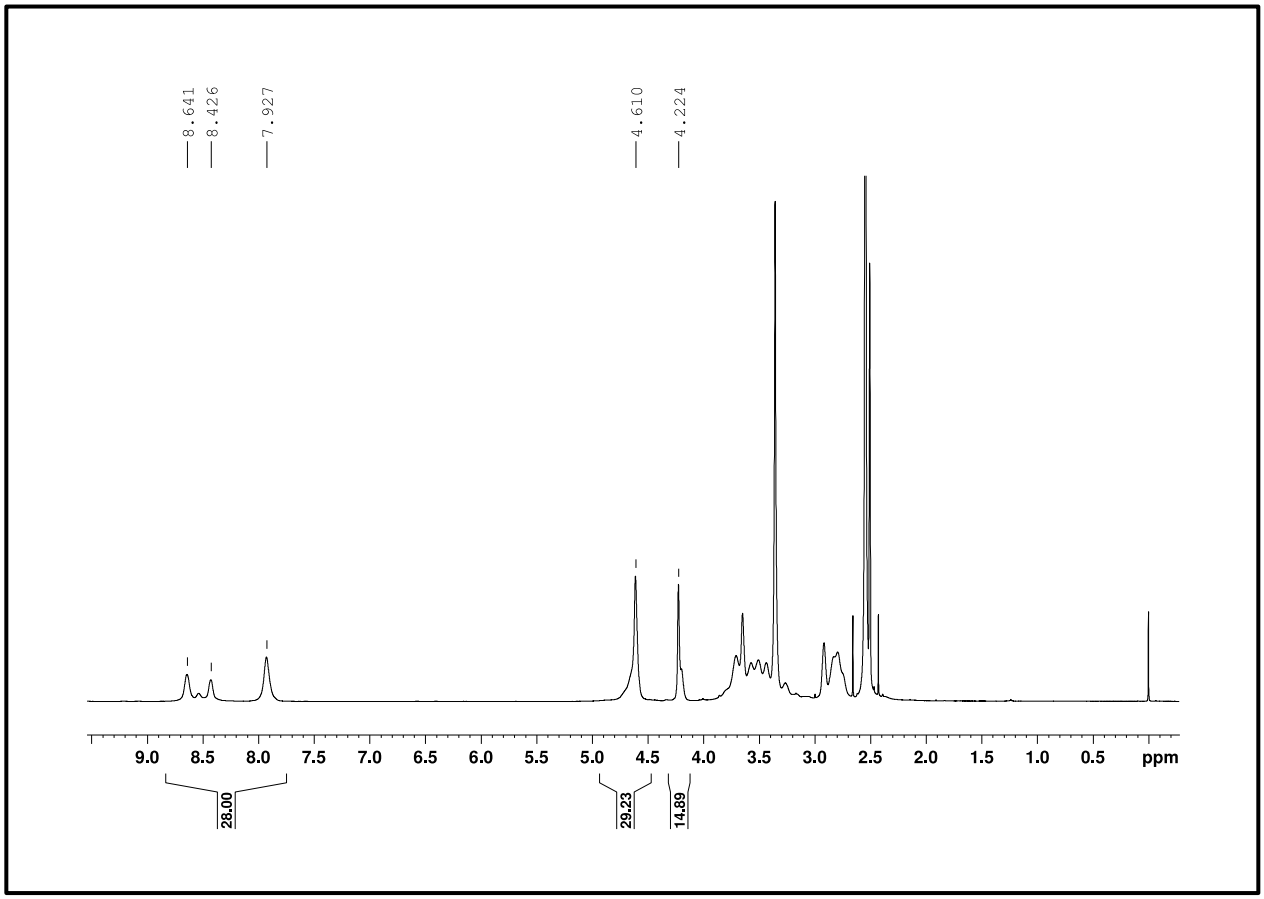

Figure S8: G (2)-PROPARGYLATED: H NMR of 8a

G (2)-PROPARGYLATED-C13

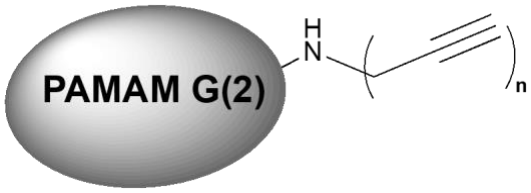

8a

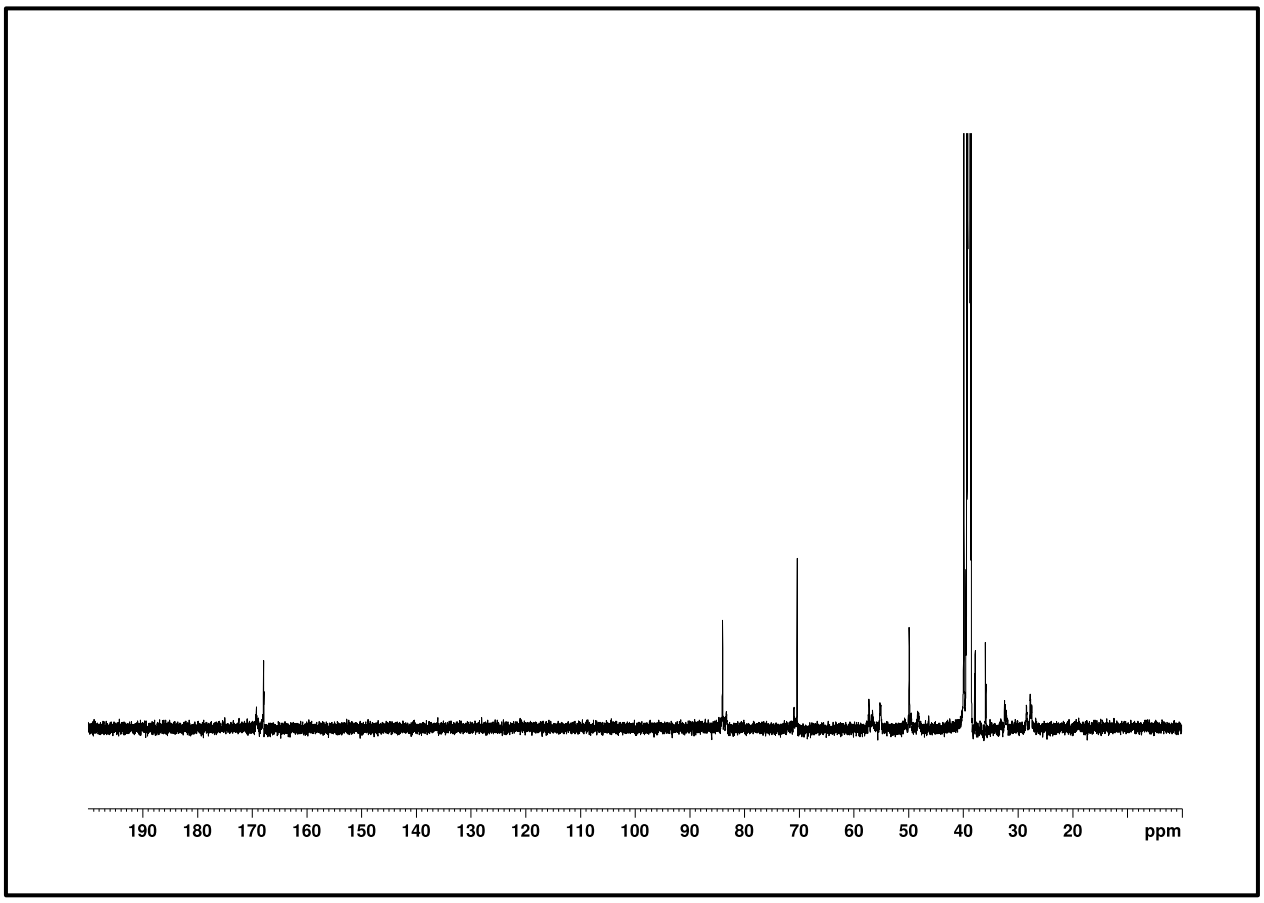

Figure S9: G (2)-PROPARGYLATED: C NMR of 8a

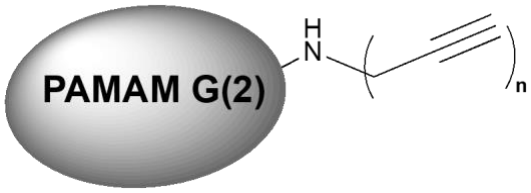

8a

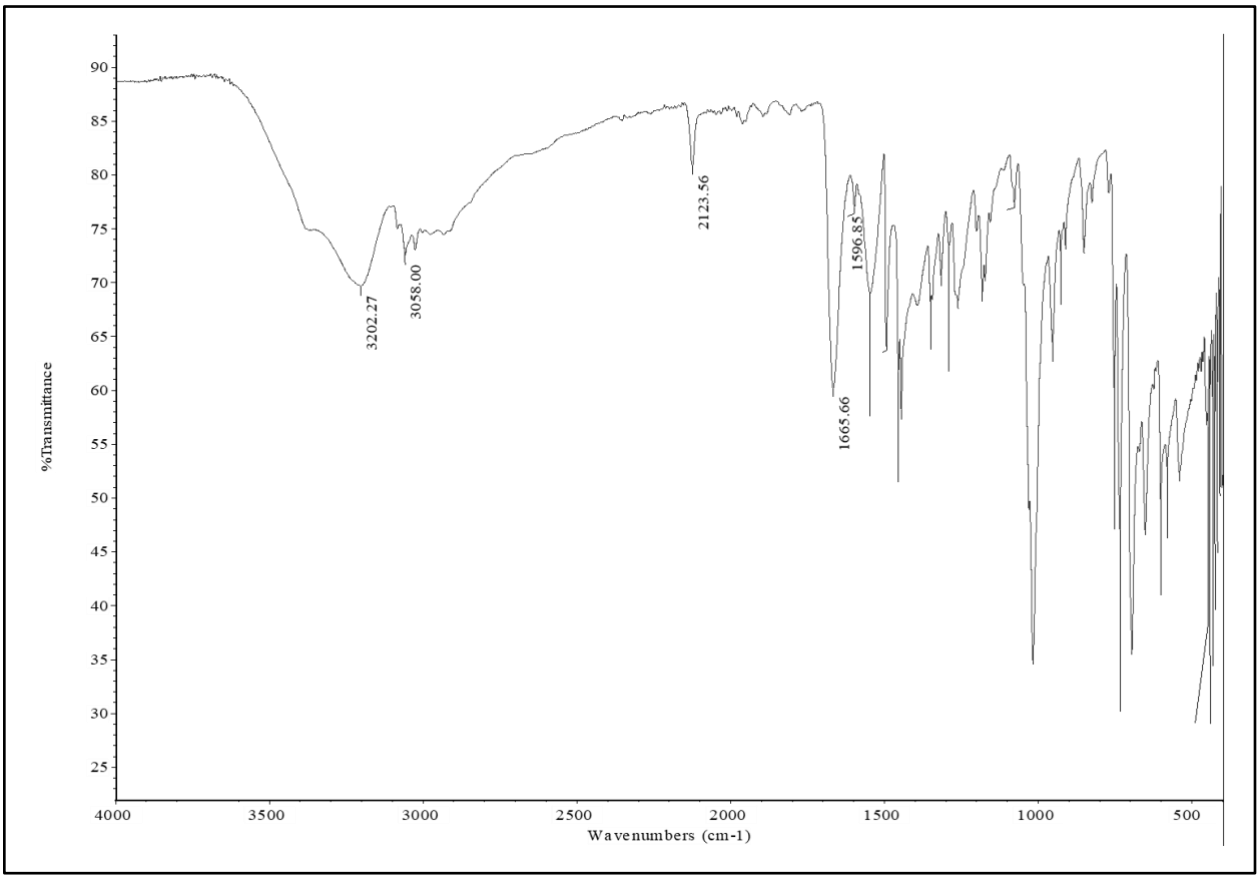

Figure S10: G (2)-PROPARGYLATED-IR of 8a

`G (3)-PROPARGYLATED-HNMR

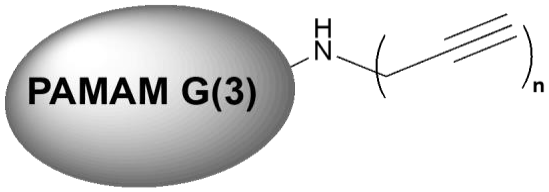

8b

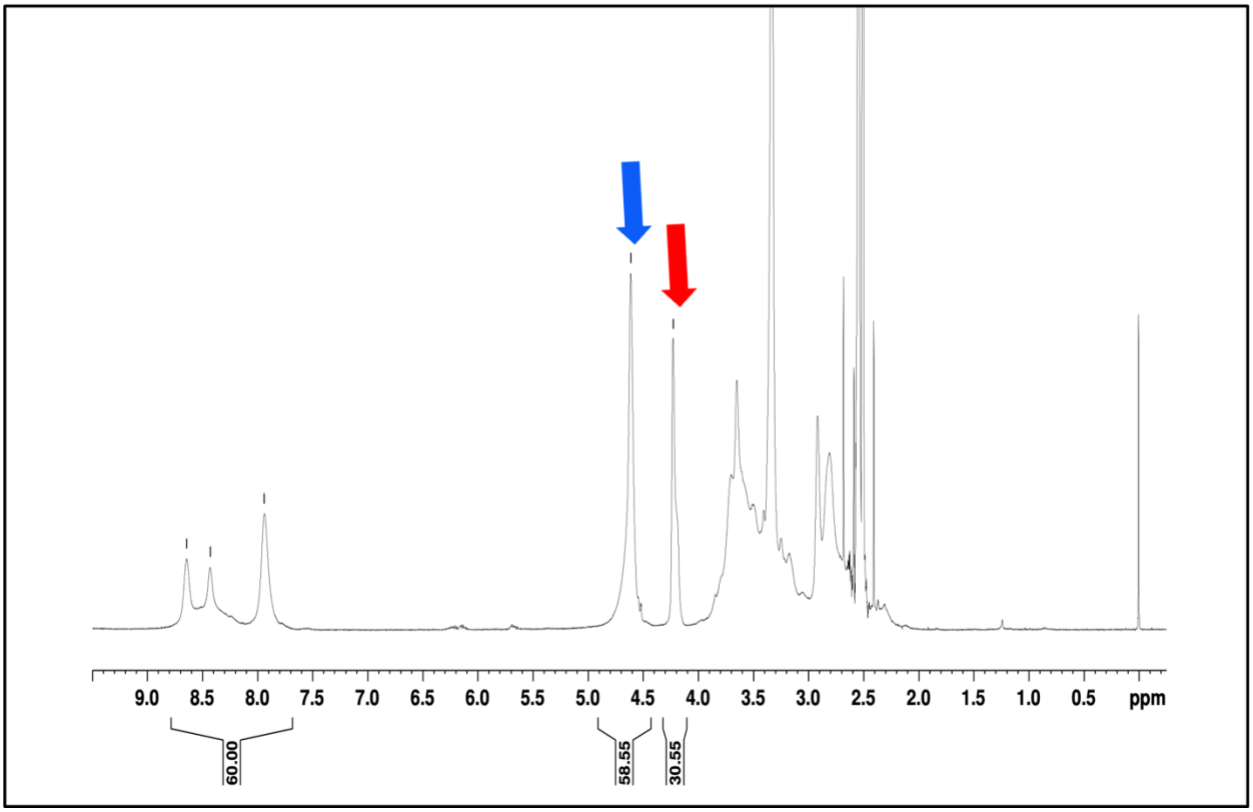

Figure S11: G (3) [1]HNMR of 8b

G (3)-PROPARGYLATED-C13

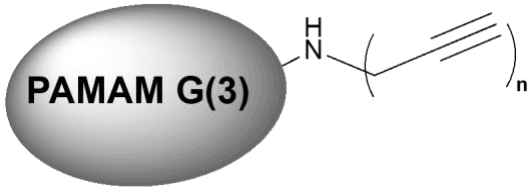

8b

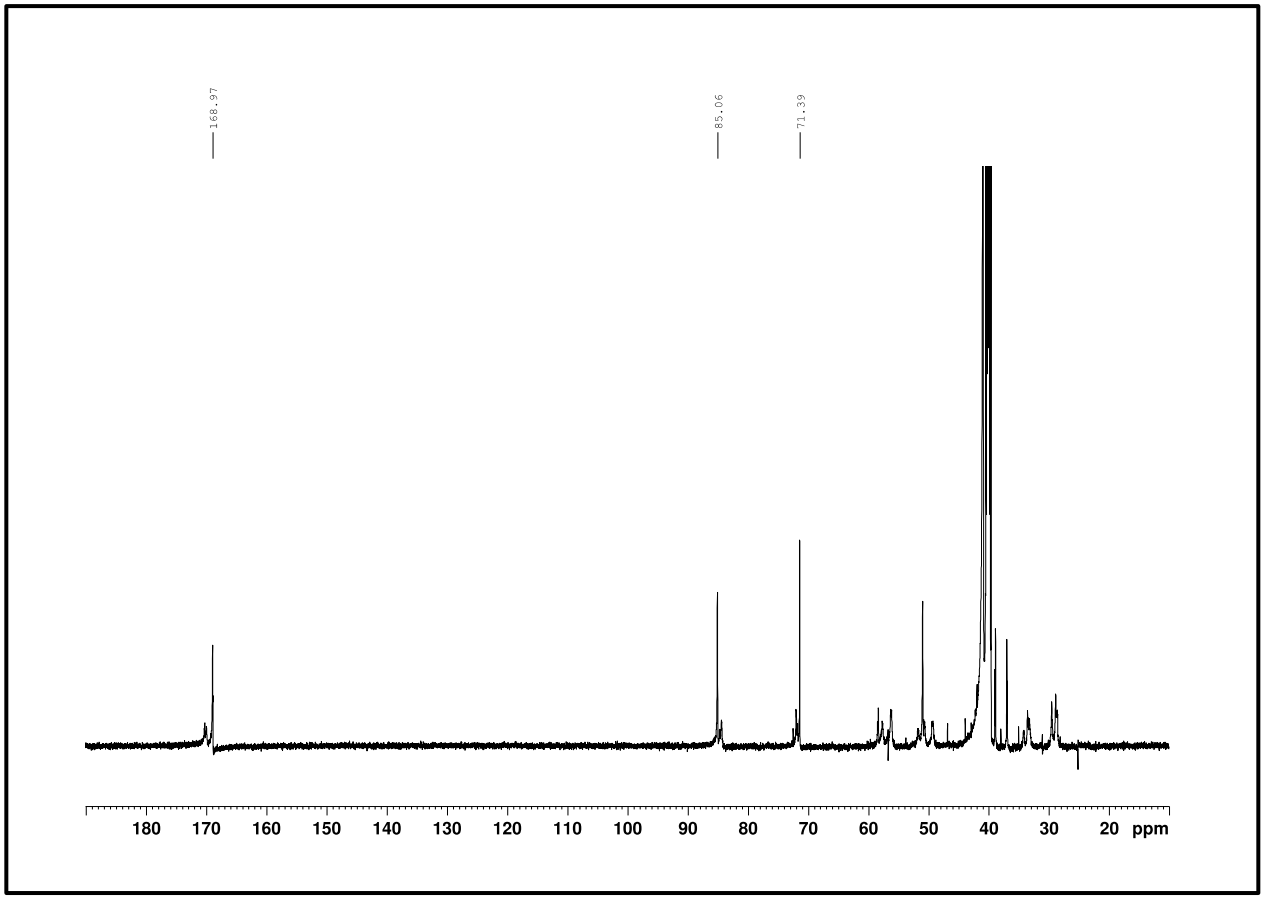

Figure S12: G (3) C NMR of 8b

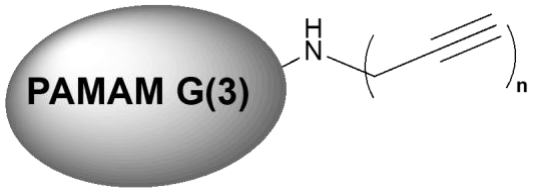

8b

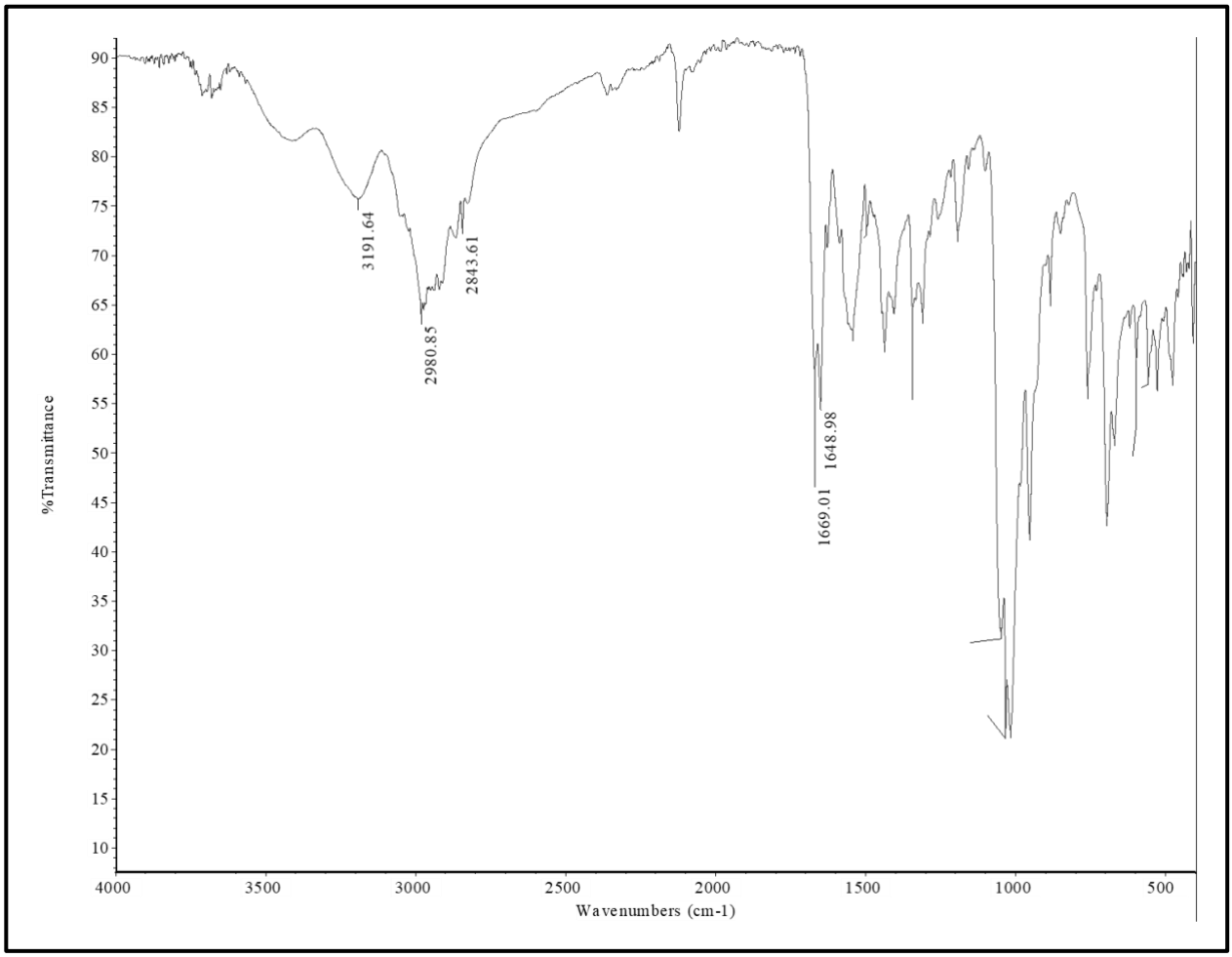

Figure S13: G (3)-PROPARGYLATED-IR of 8b

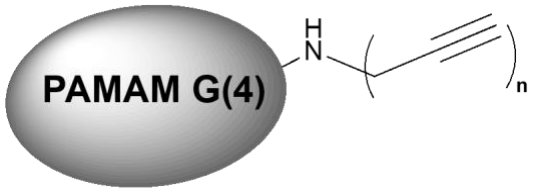

8c

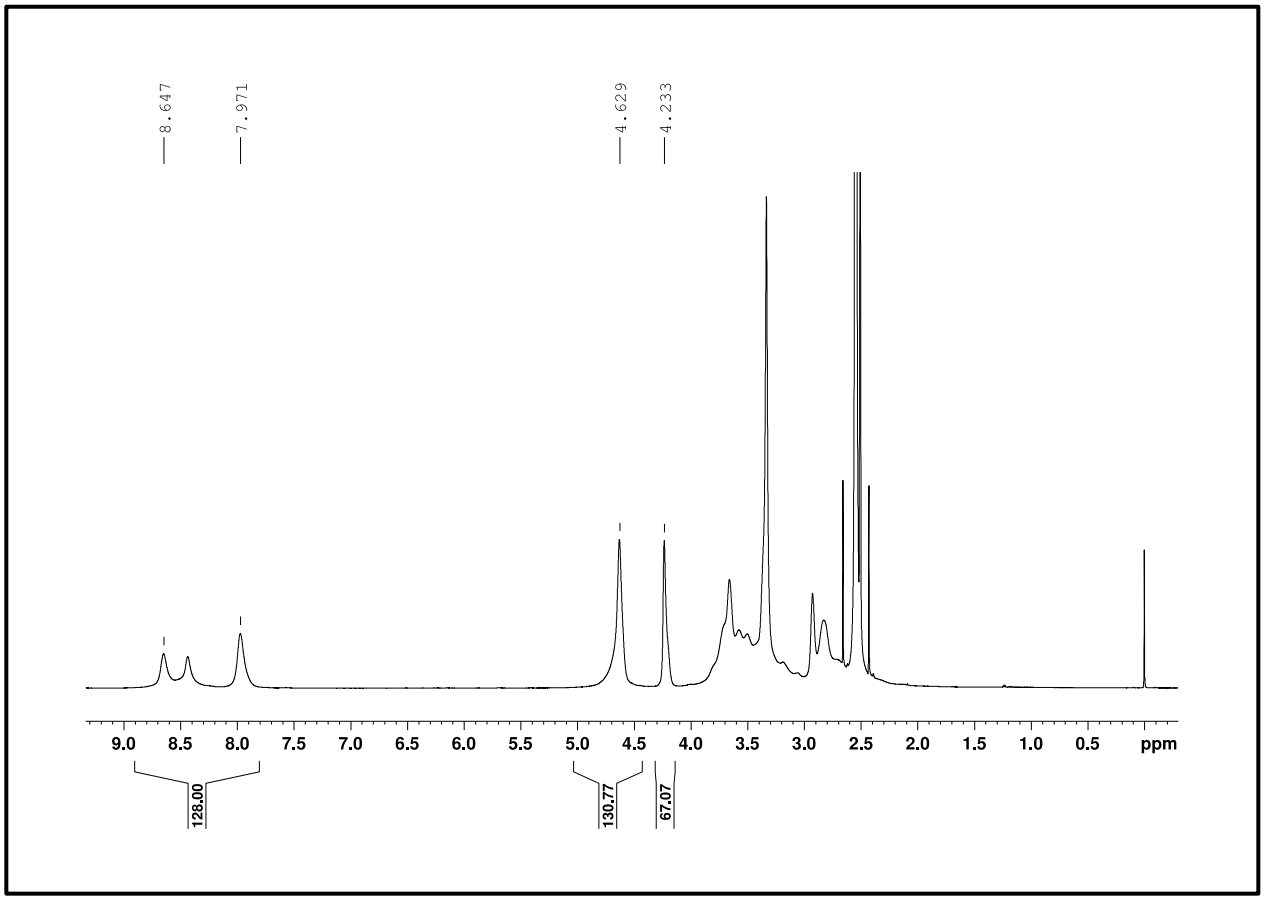

Figure S14: G (4)-PROPARGYLATED- ^{1}H NMR of 8c

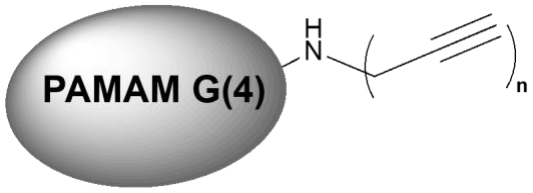

8c

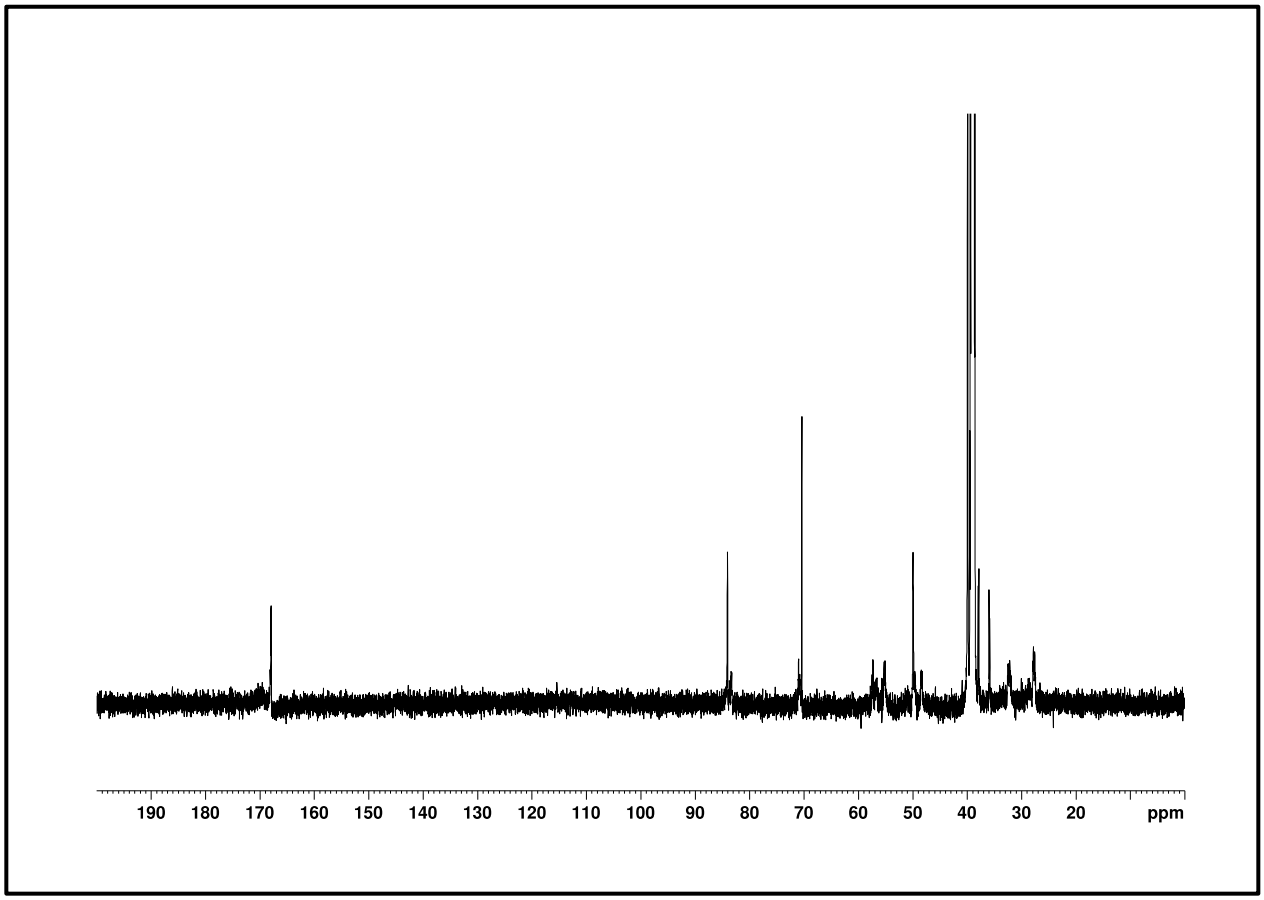

Figure S15: G (4) C NMR of 8c

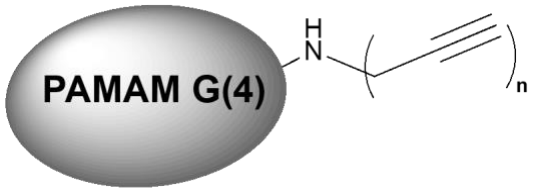

8c

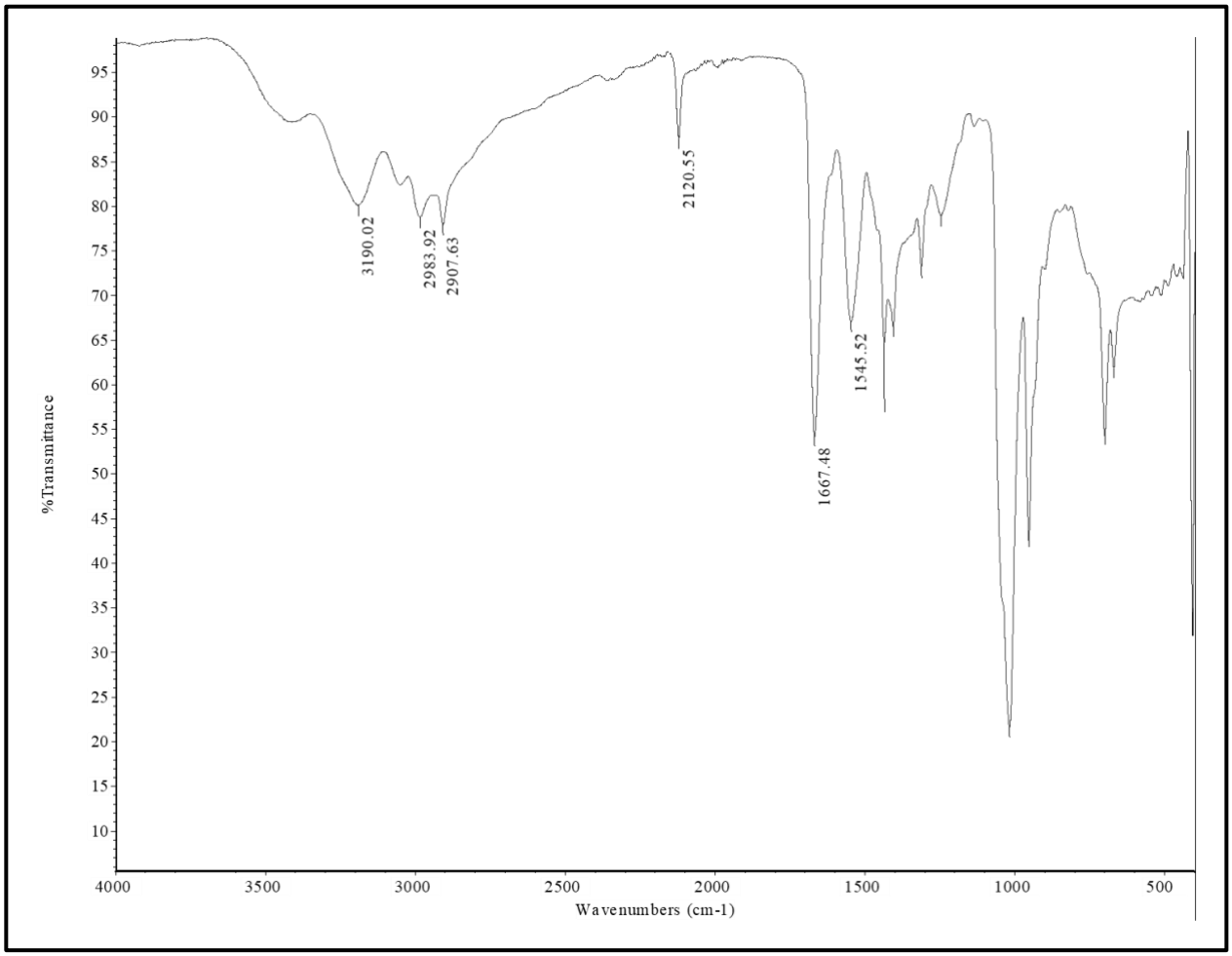

Figure S16: G (4) IR of 8c

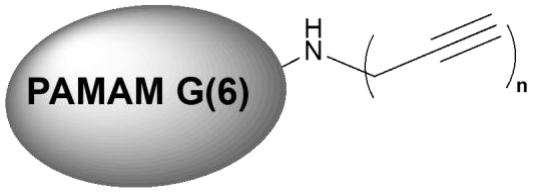

8d

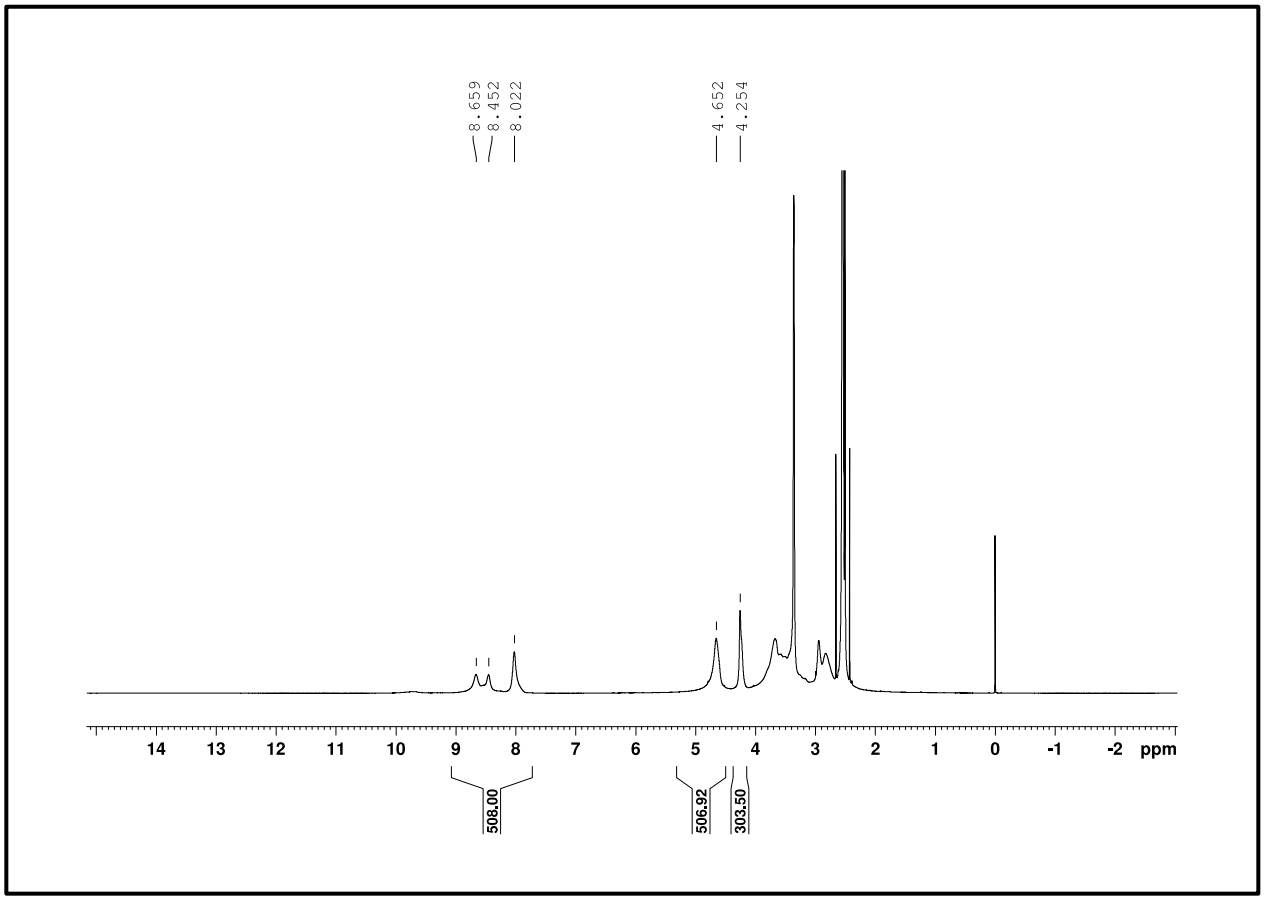

Figure S17: G (6) ^{1}H NMR of 8d

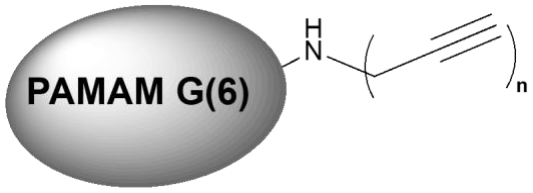

8d

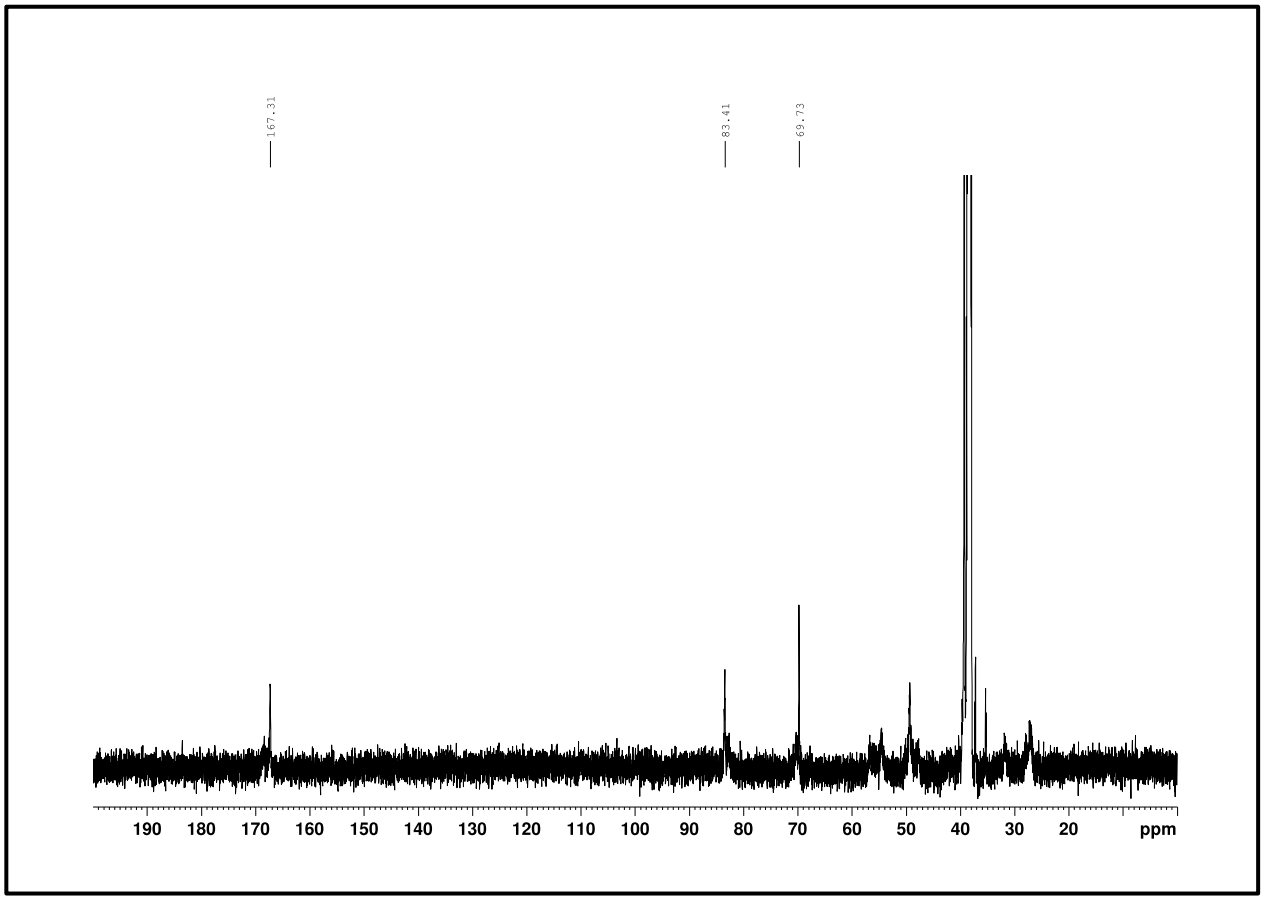

Figure S18: G (6) ^{13}C NMR of 8d

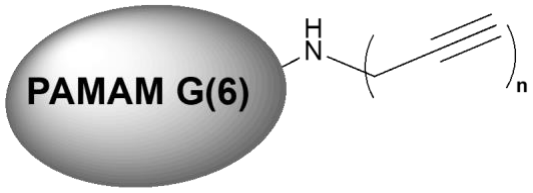

8d

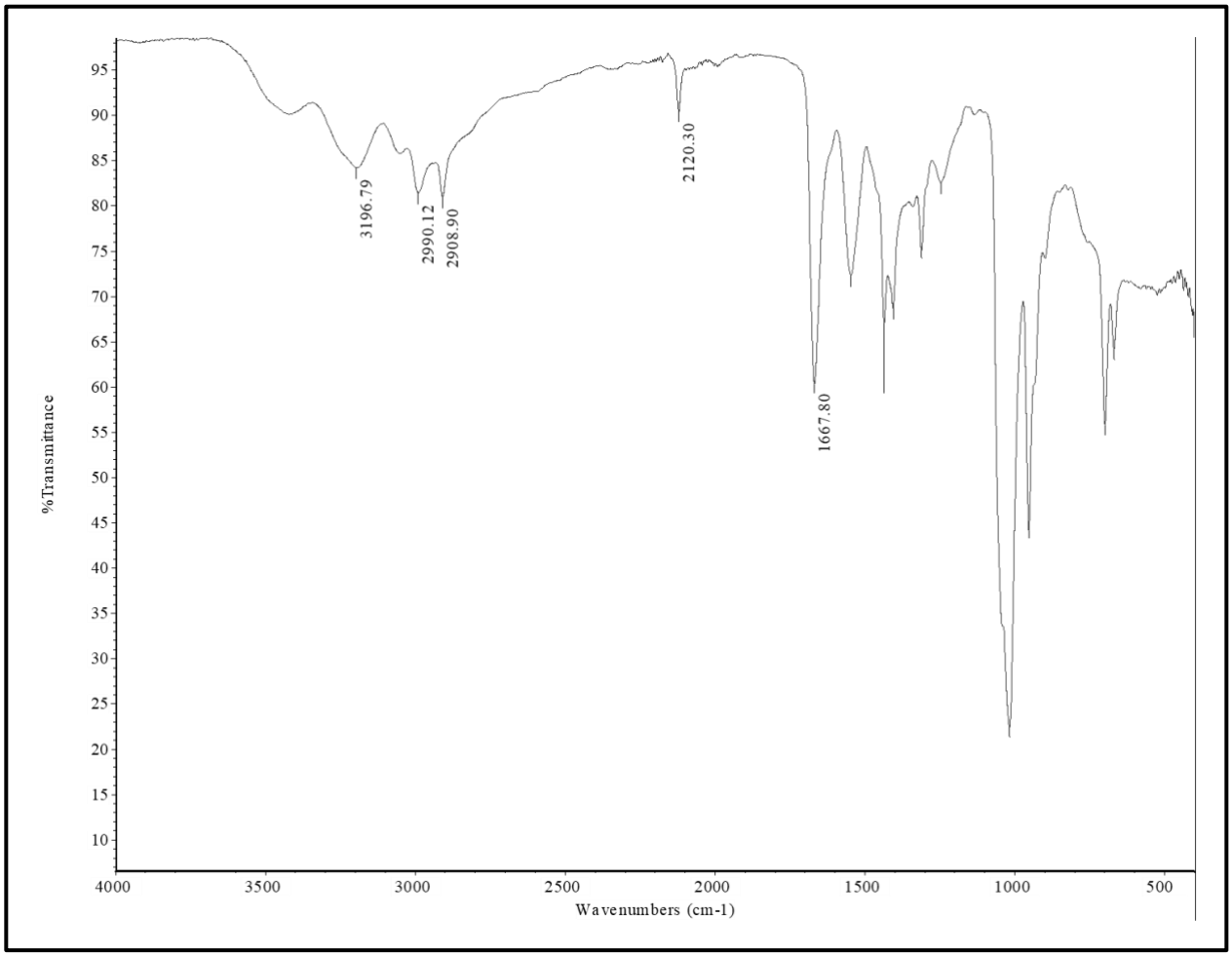

Figure S19: G (6) IR of 8d

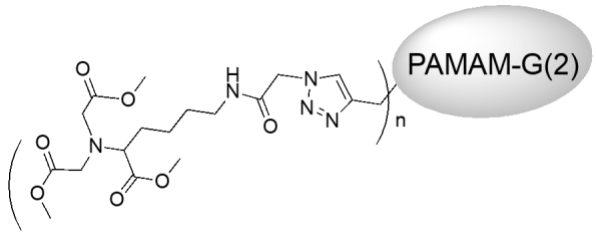

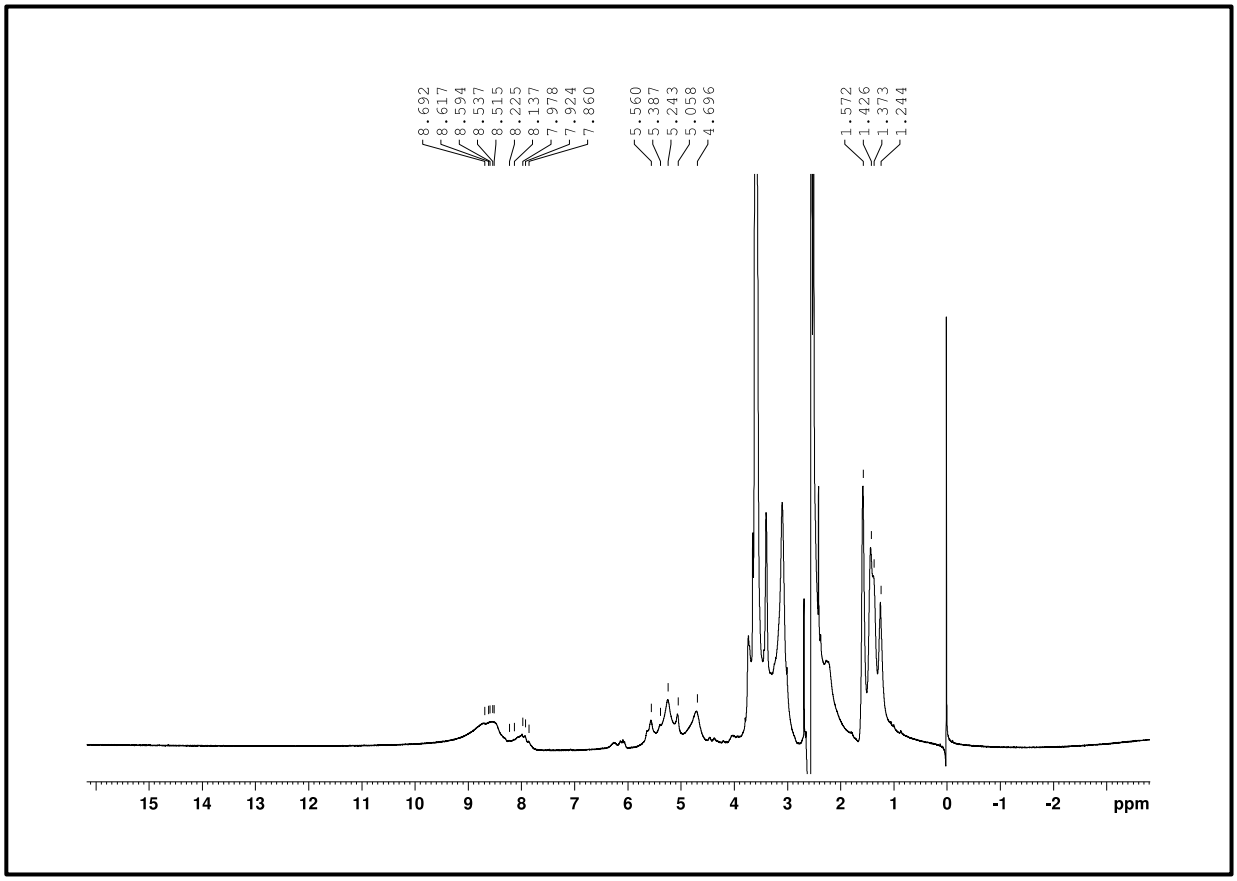

Figure S20: G (2)-clicked: H NMR of 9a

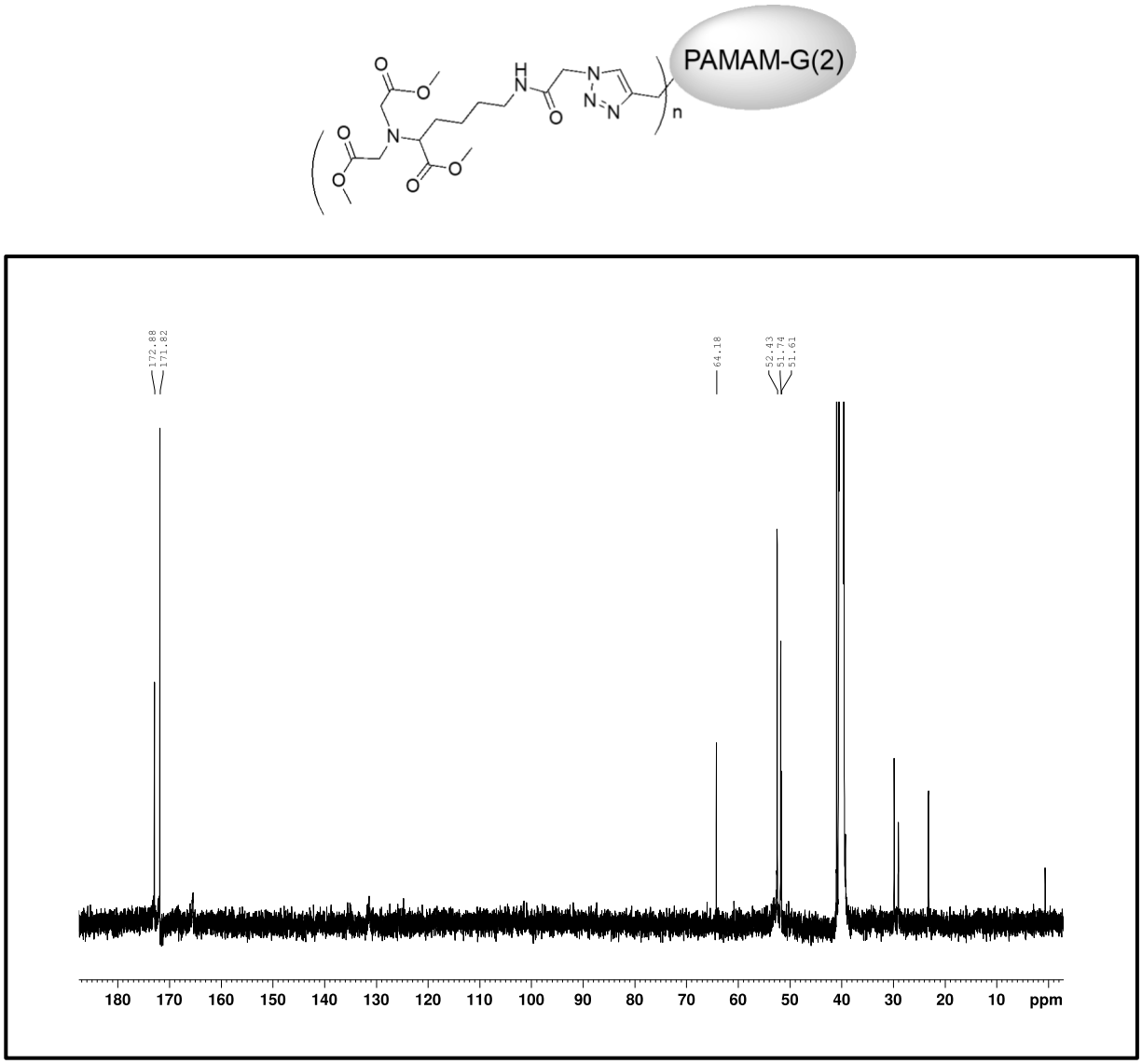

Figure S21: G (2)-clicked: C-13 of 9a

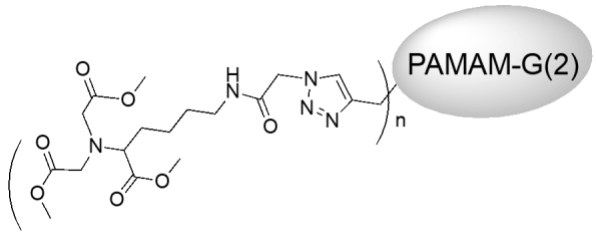

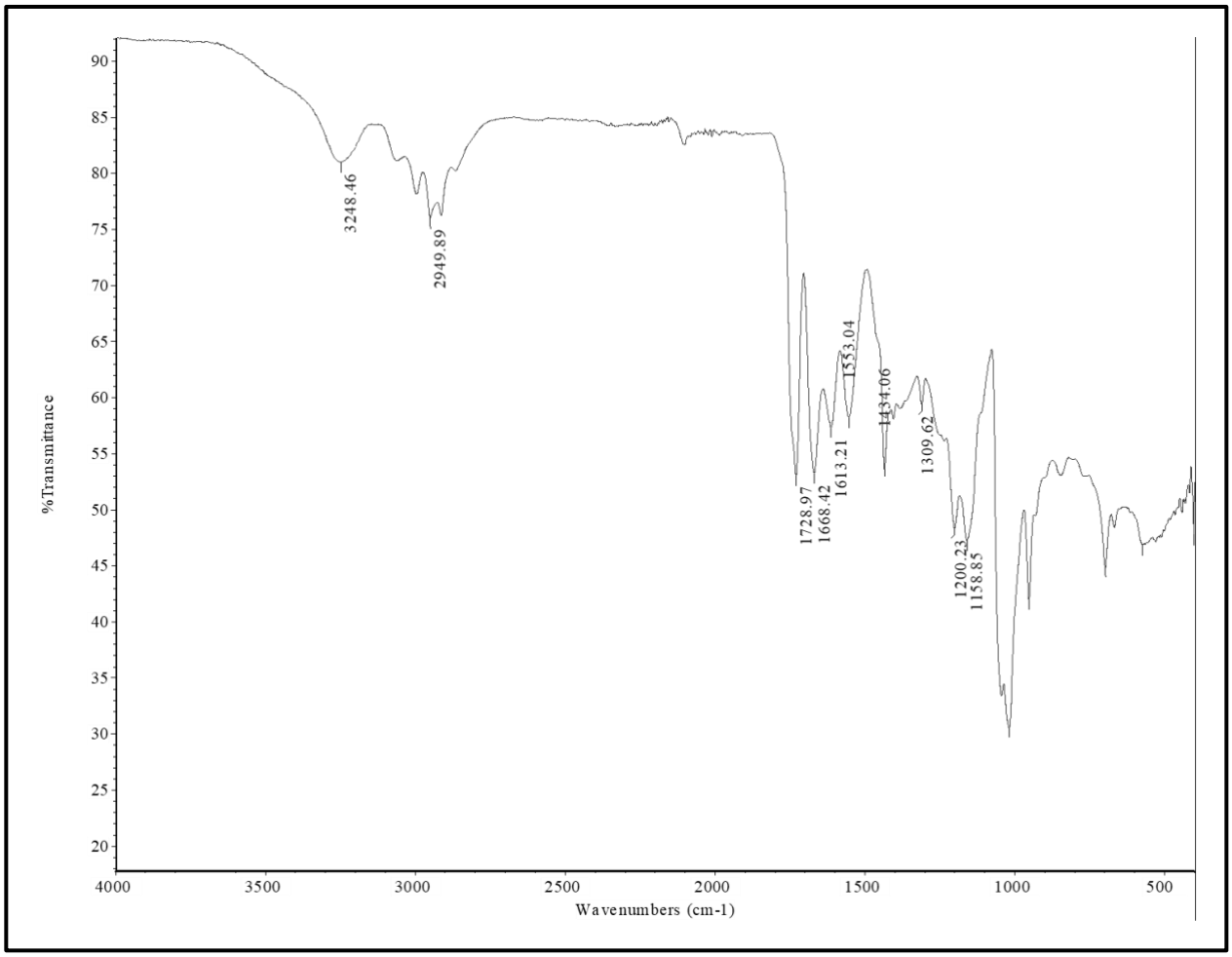

Figure S22: G (2) clicked IR of 9a

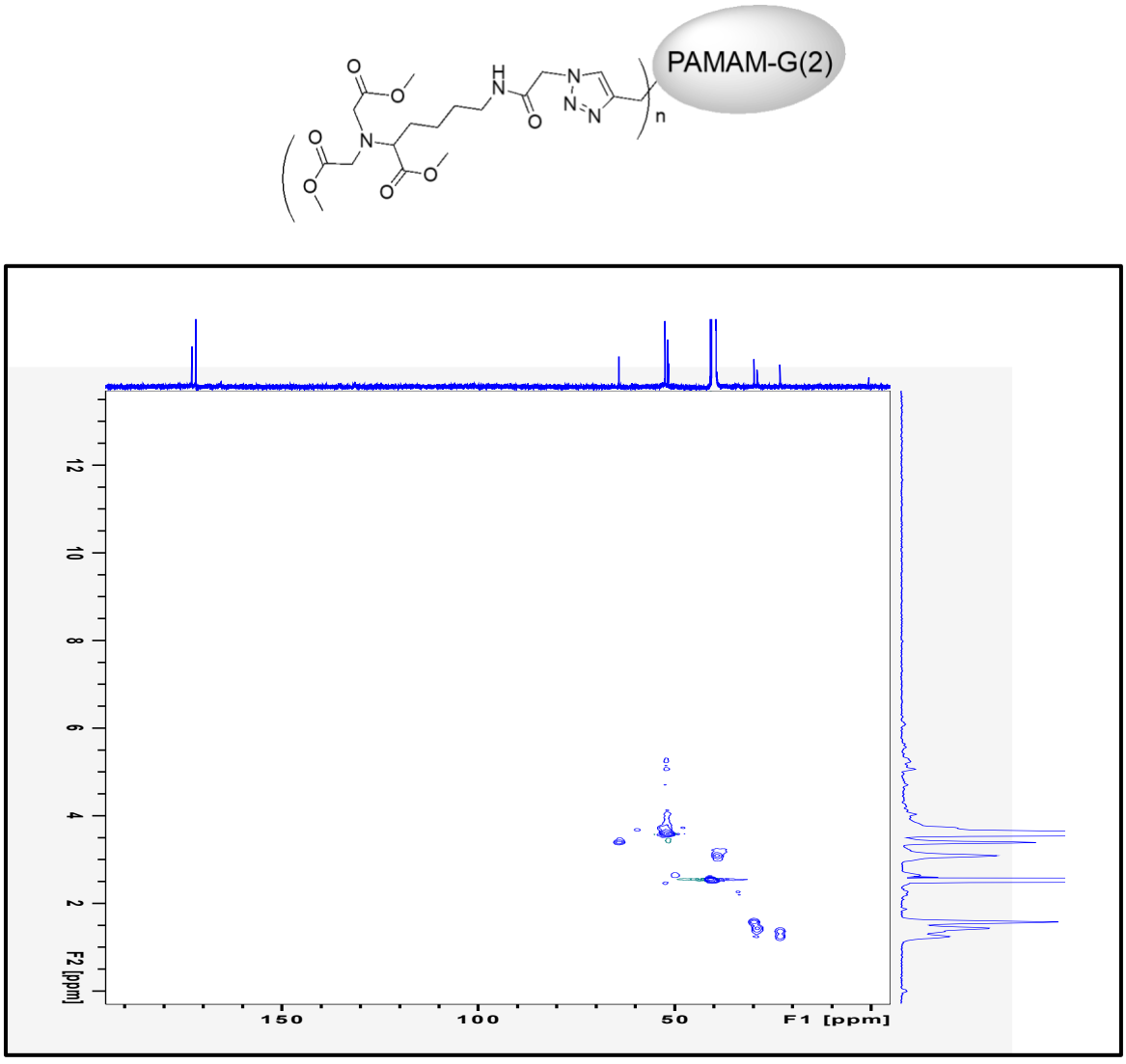

Figure S23: G (2) clicked HSQC of 9a

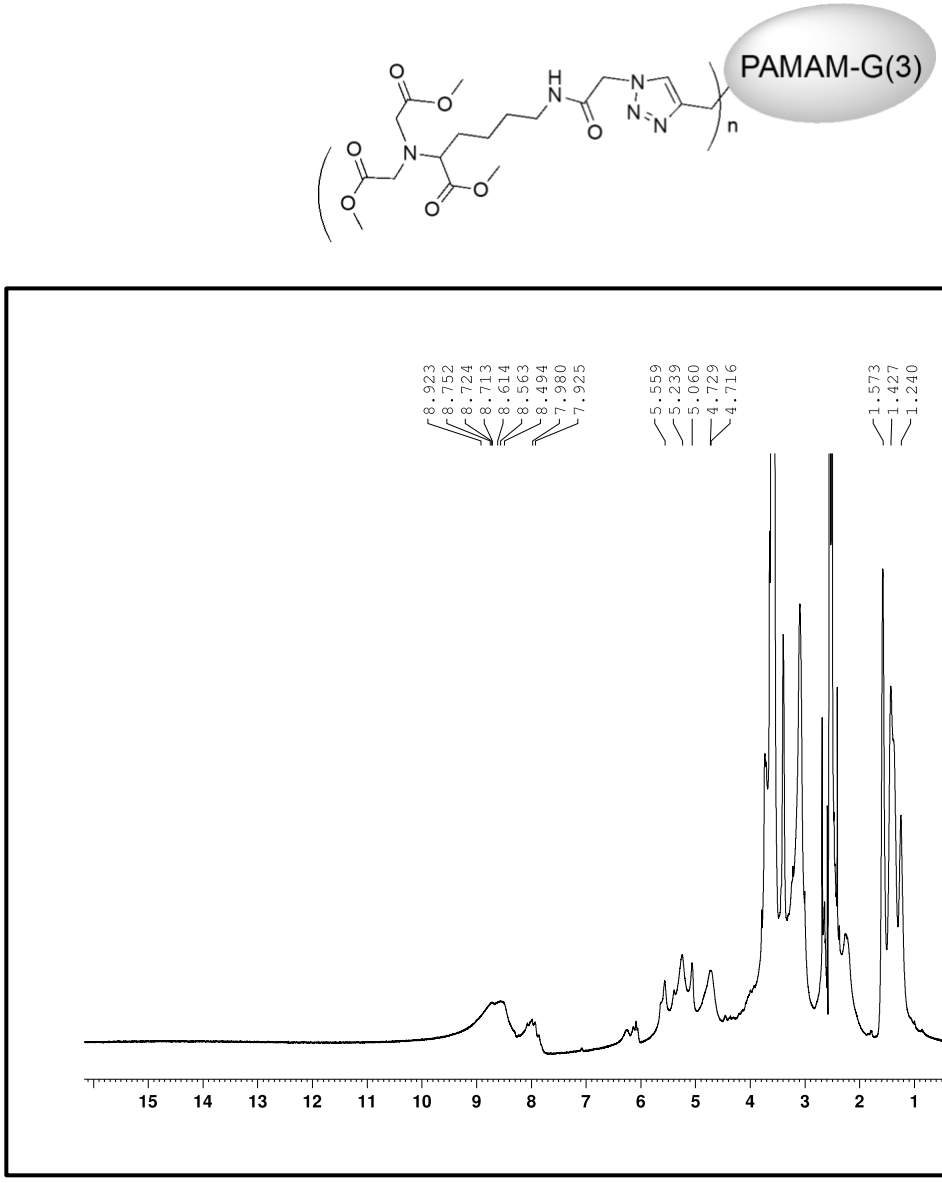

Figure S24: G (3)-clicked: H NMR of 9b

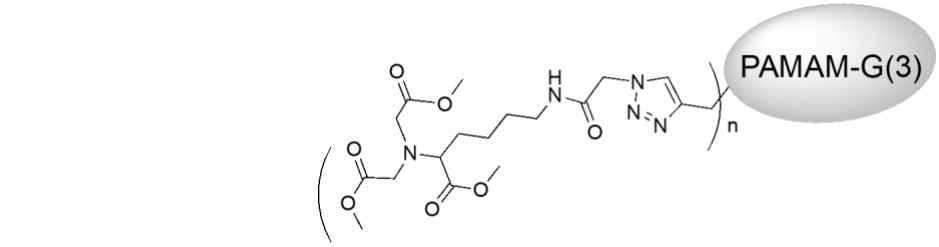

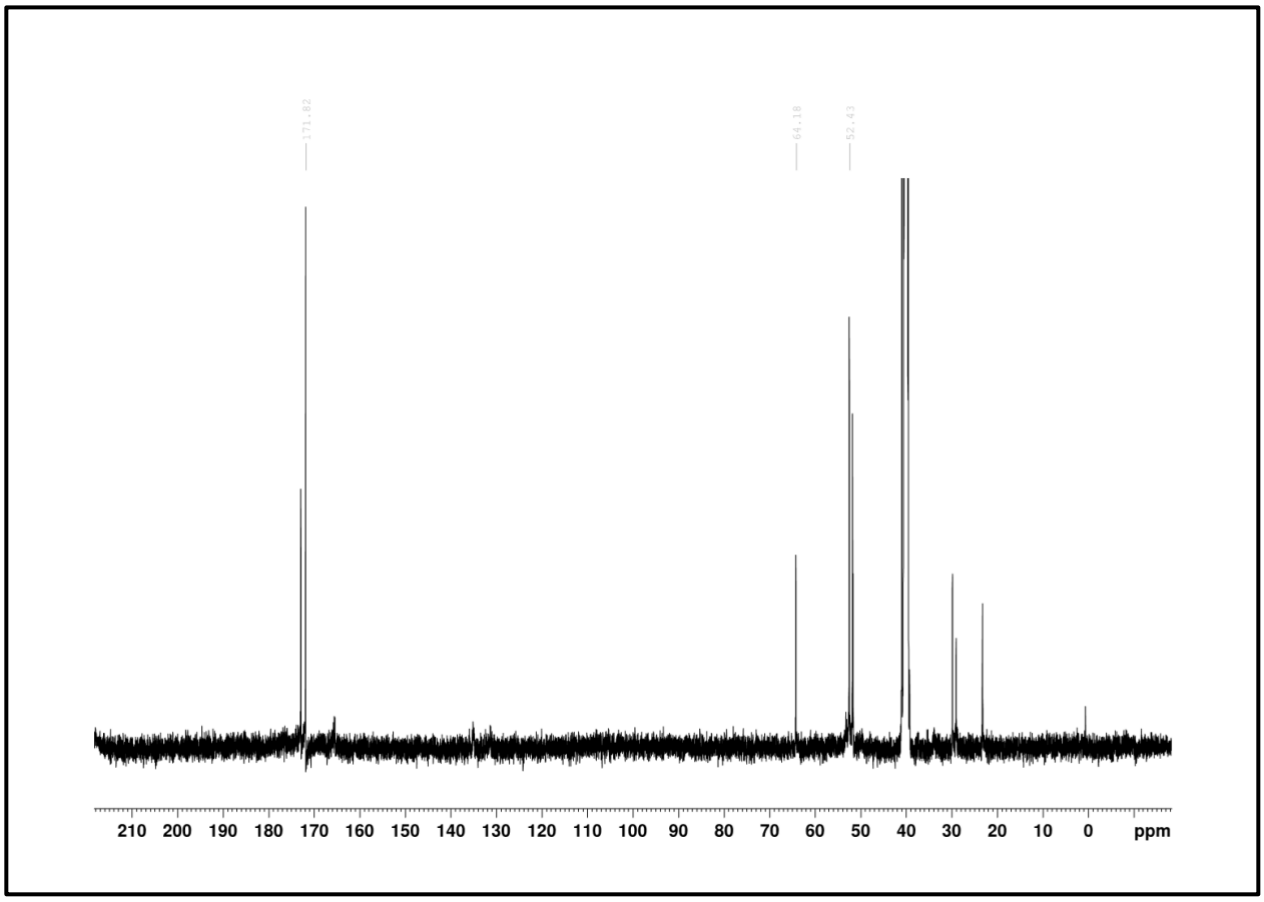

Figure S25: G (3) clicked-C-13 of 9b

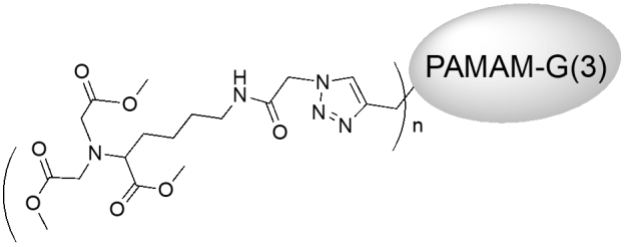

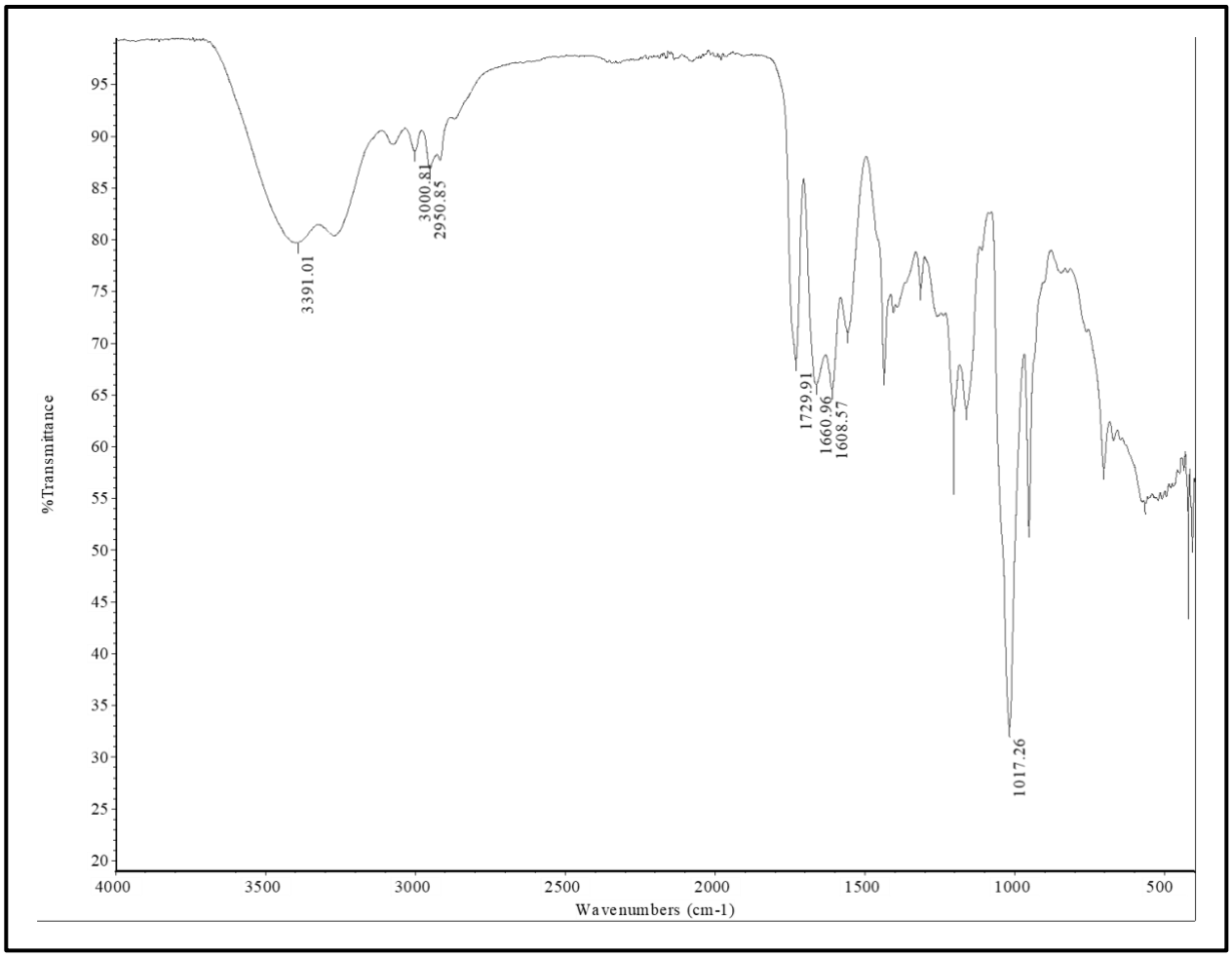

Figure S26: G (3) clicked IR of 9b

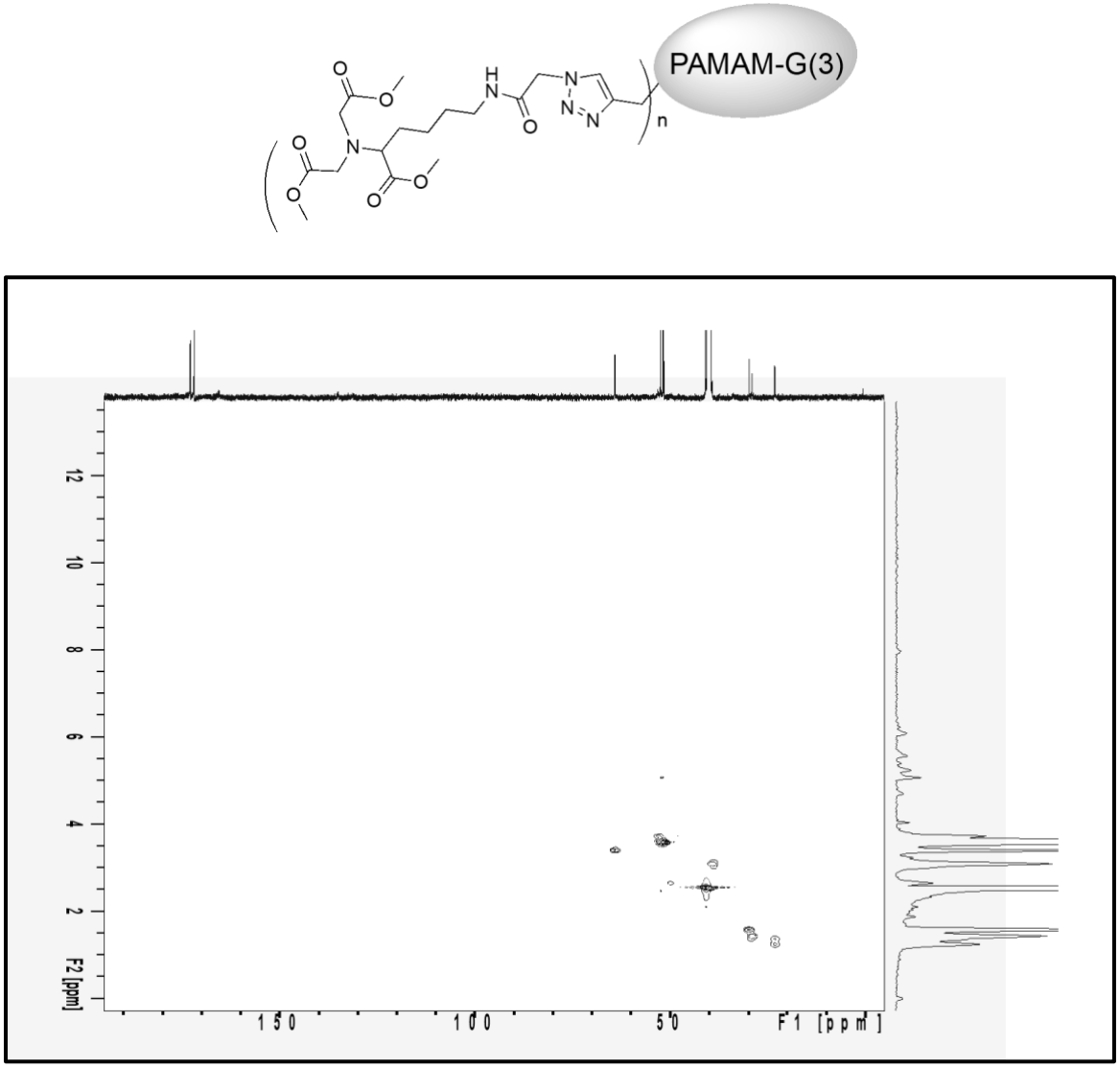

Figure S27: G (3) clicked HSQC of 9b

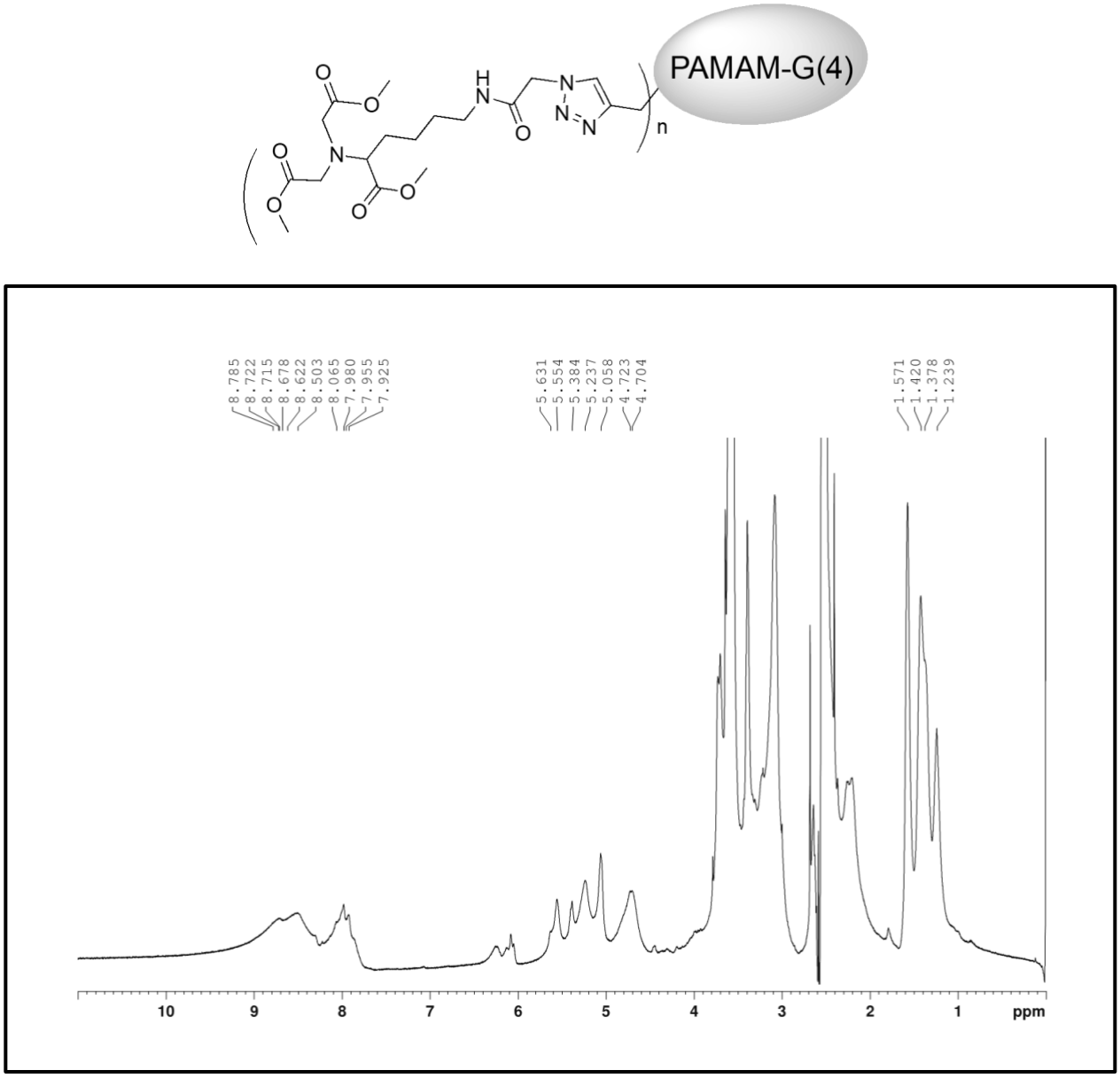

Figure S28: G (4)-clicked: H NMR of 9c

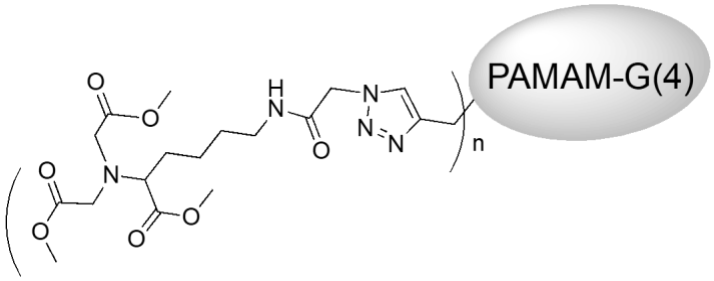

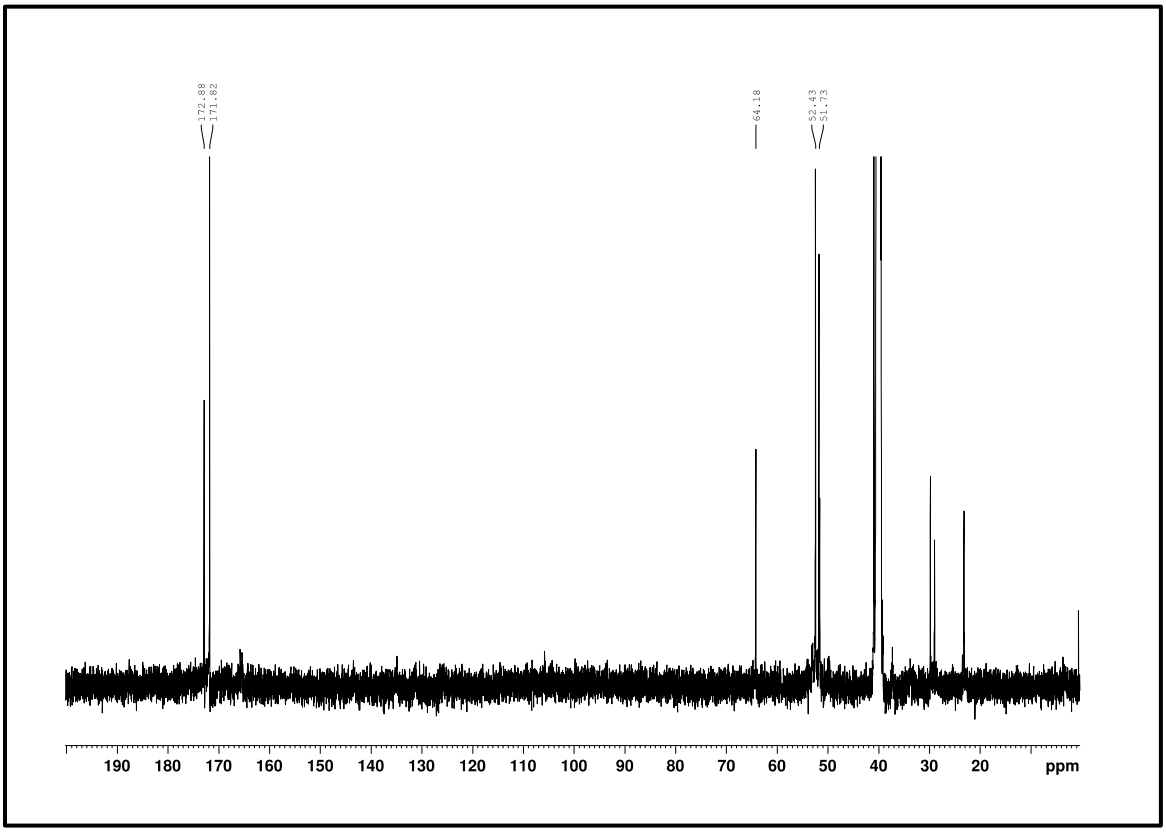

Figure S29: G (4) clicked-C-13 of 9c

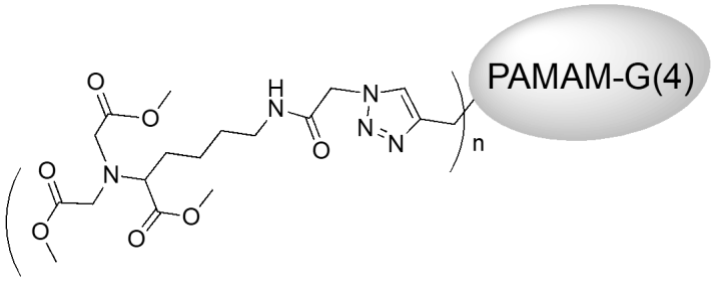

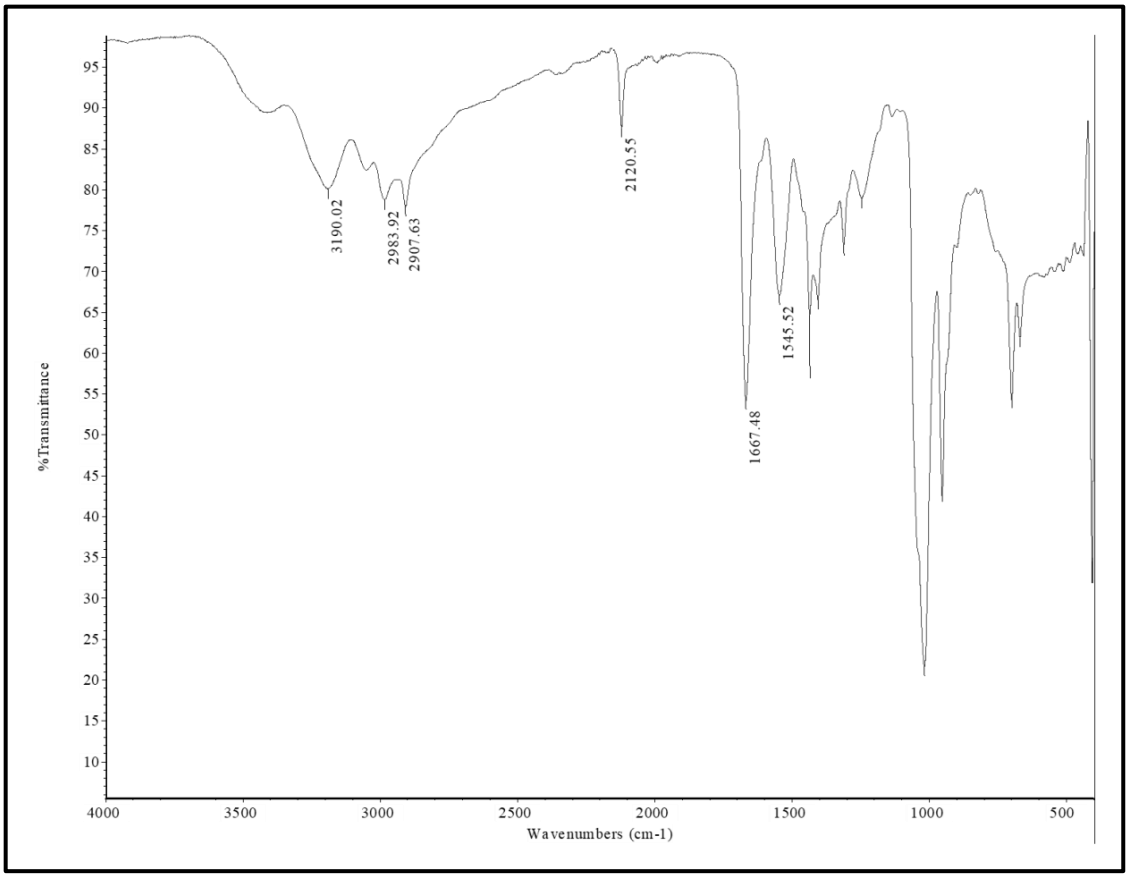

Figure S30: G (4) clicked IR of 9c

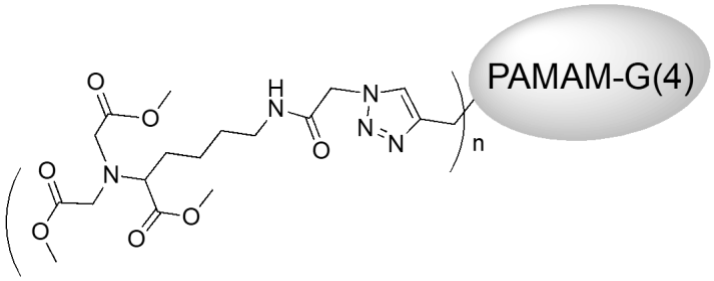

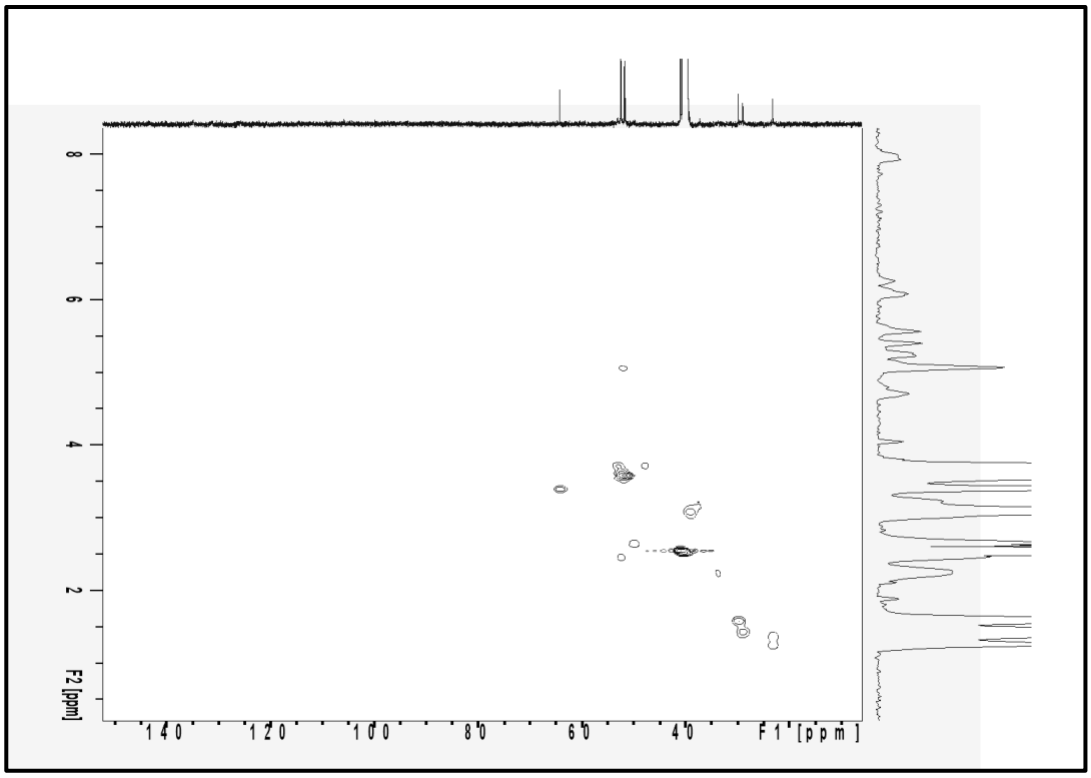

Figure S31: G (4) clicked HSQC of 9c

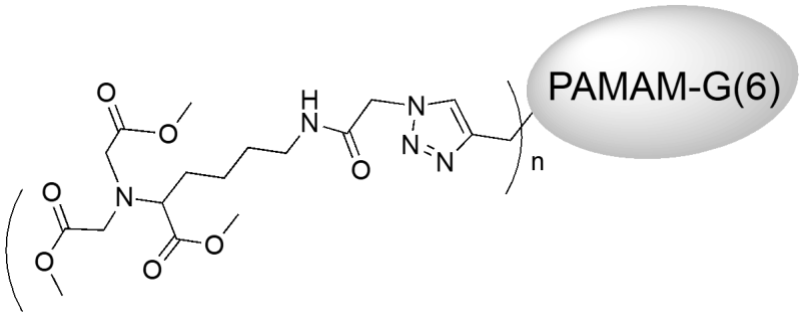

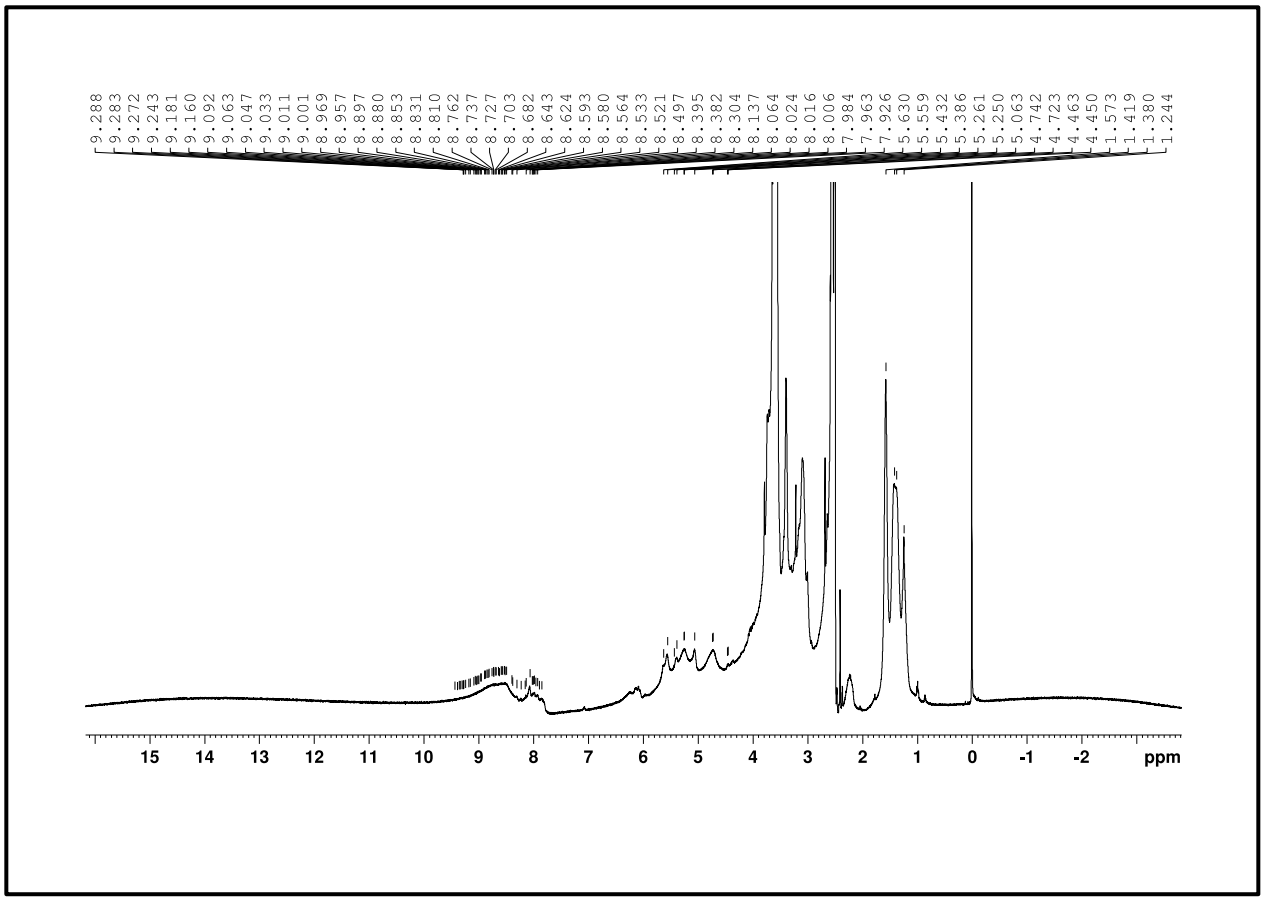

Figure S32: G (6)-clicked: H NMR of 9d

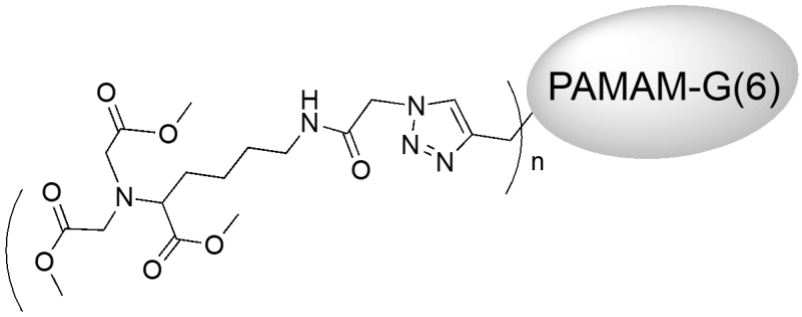

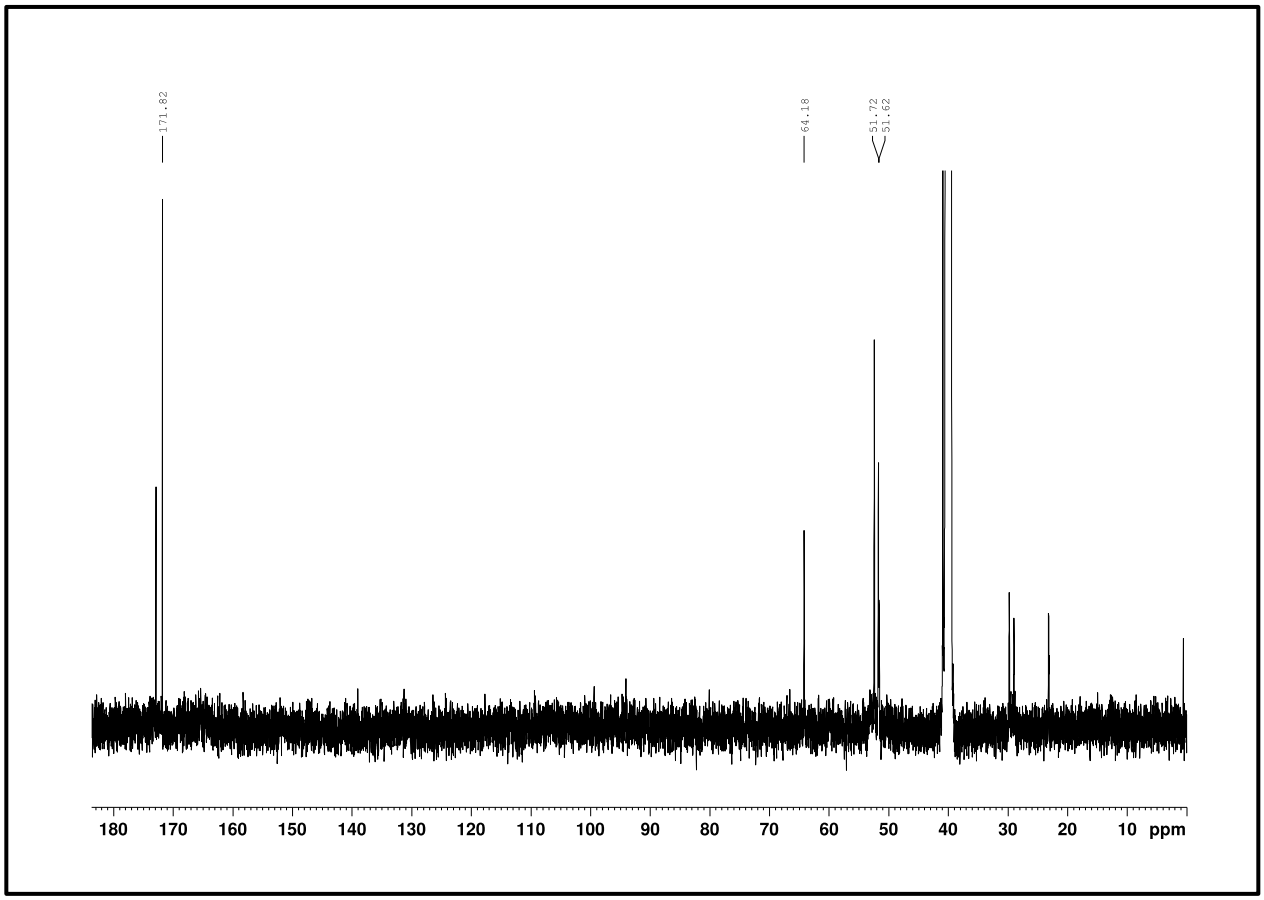

Figure S33: G (6)-clicked-C13 of 9d

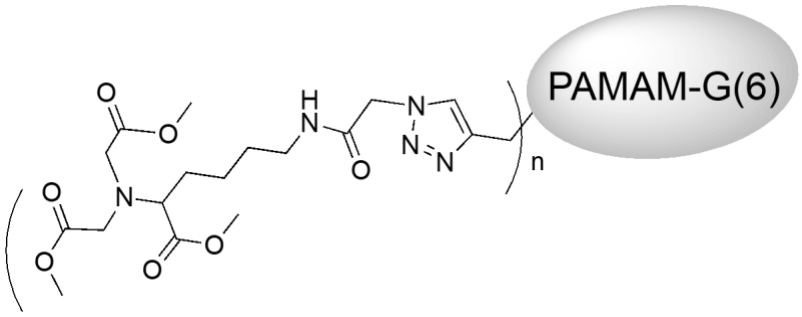

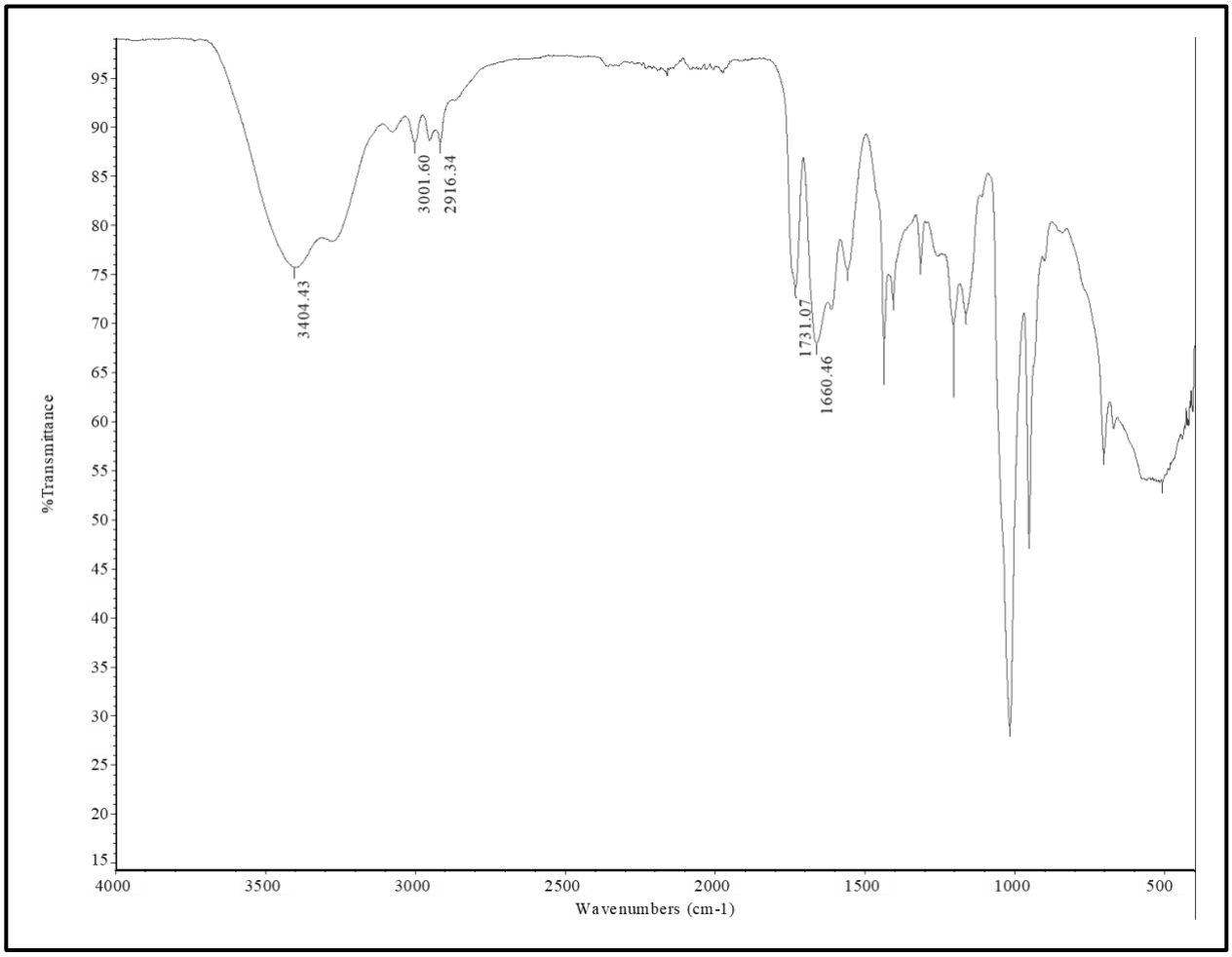

Figure S34: G (6) clicked IR of 9d

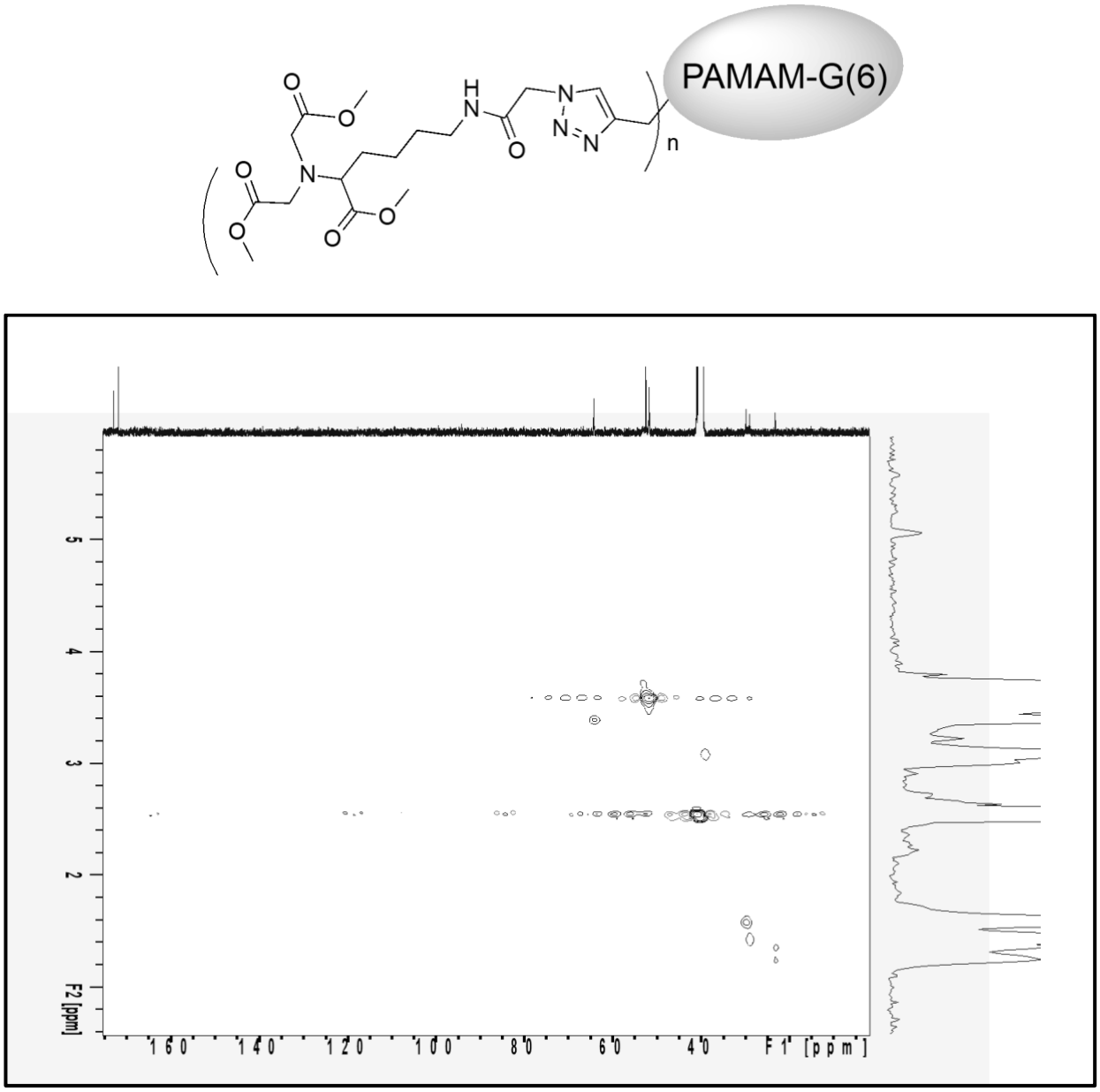

Figure S35: G (6) clicked HSQC of 9d

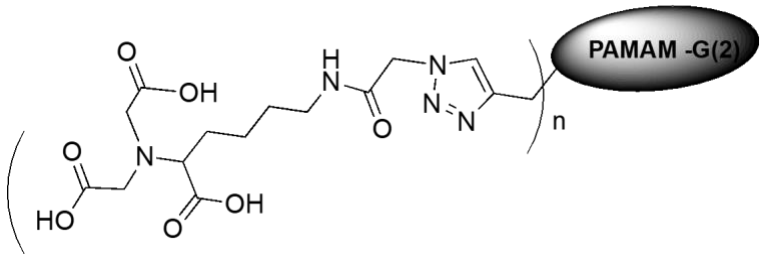

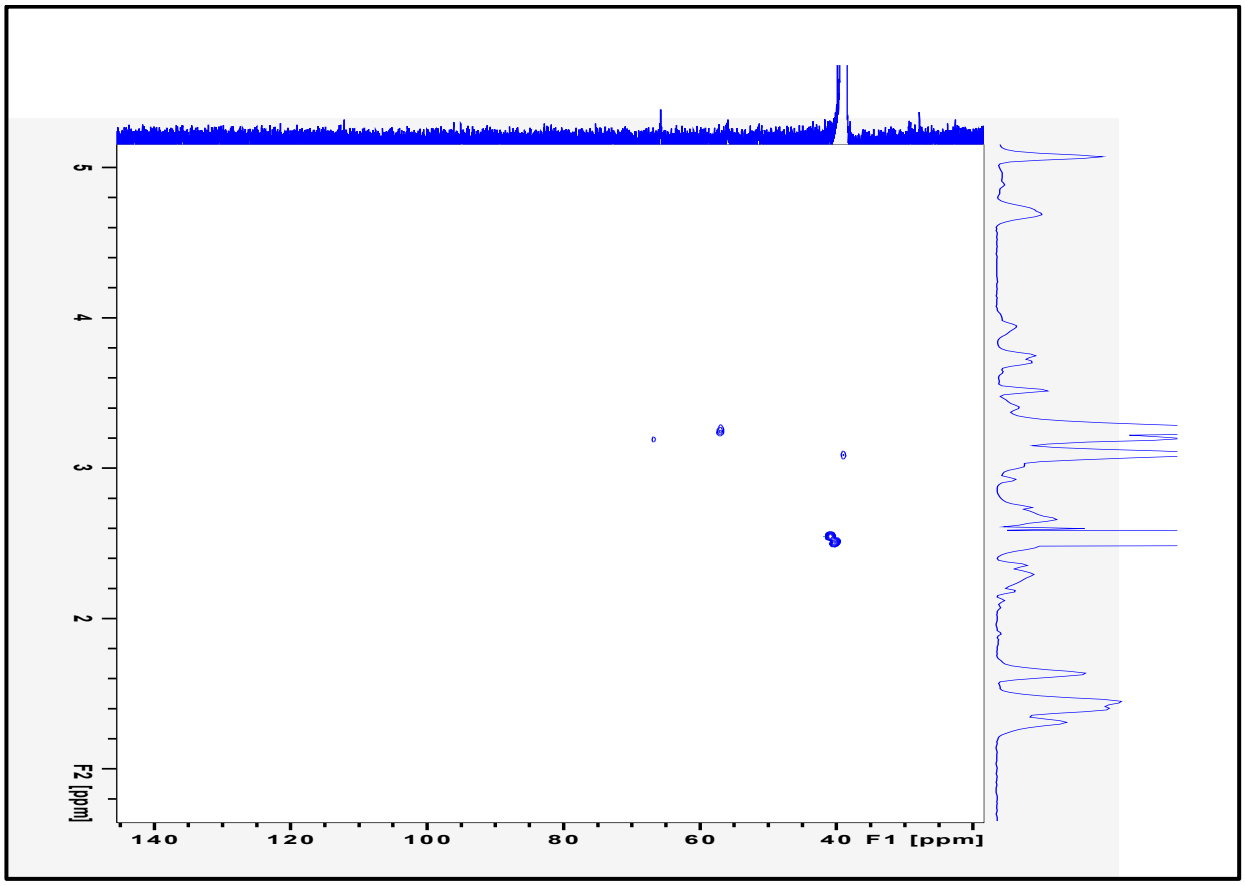

Figure S36: G (2)-deprotected-HSQC

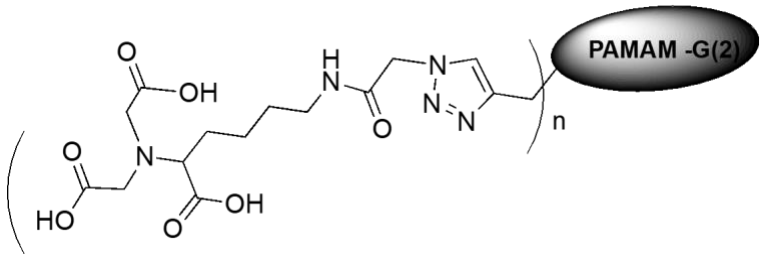
PAMAM -G(2)
n
OH
HO
OH
H
N
N
N
N
O
O
O
O
O

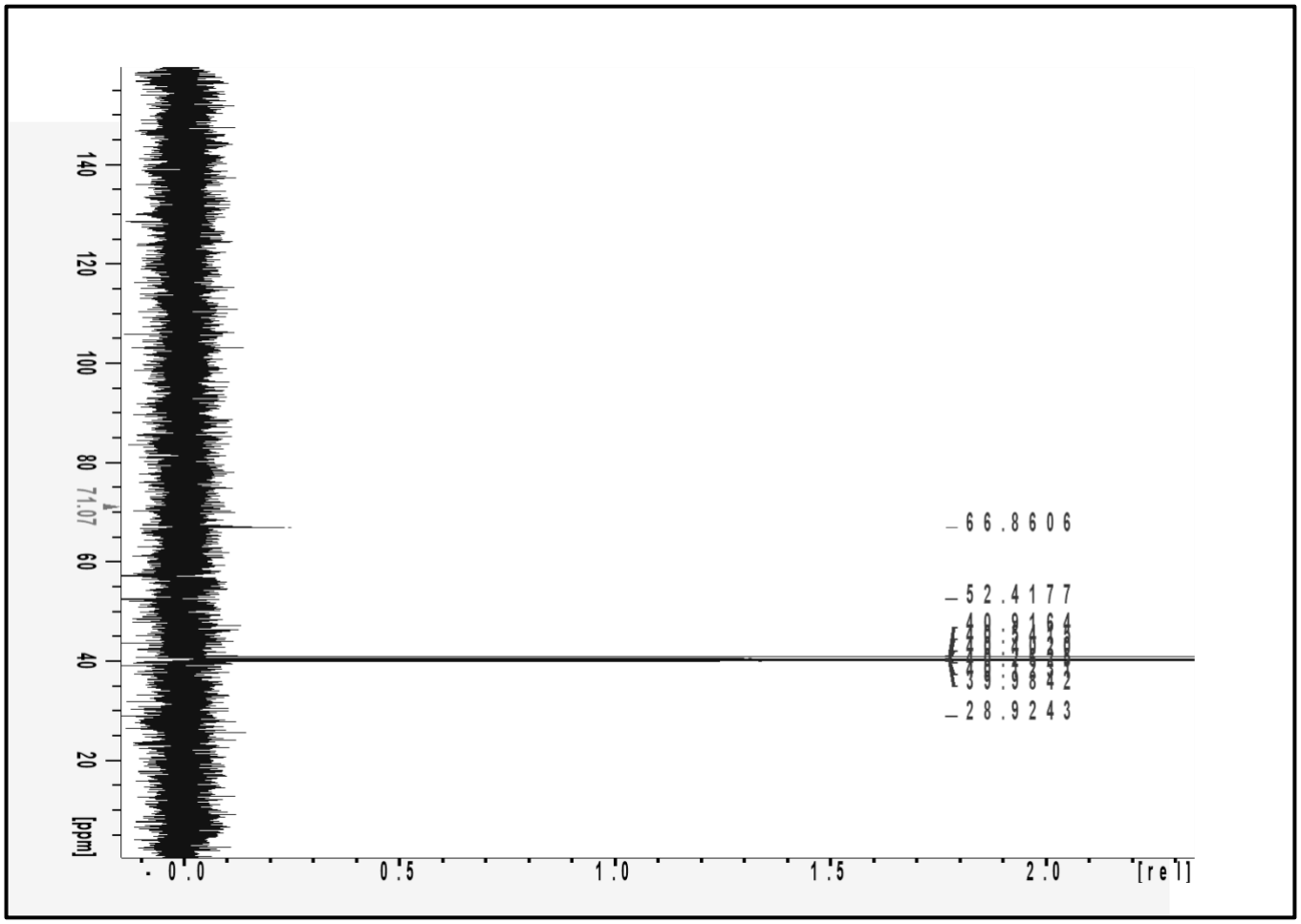
66.8606
52.4177
40.9164
39.9842
28.9243
71.07
140
120
100
80
60
40
20
[ppm]
0.0
0.5
1.0
1.5
2.0
[rel]

Figure S37: G (2)-deprotected-DEPT-135

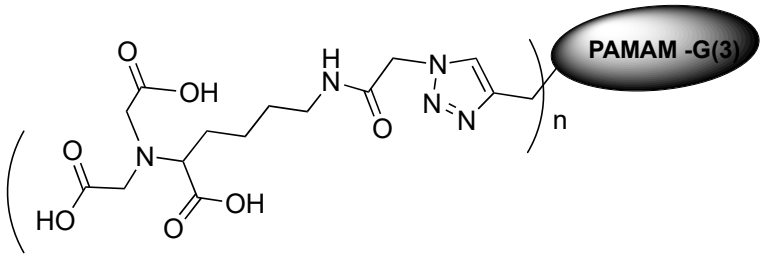

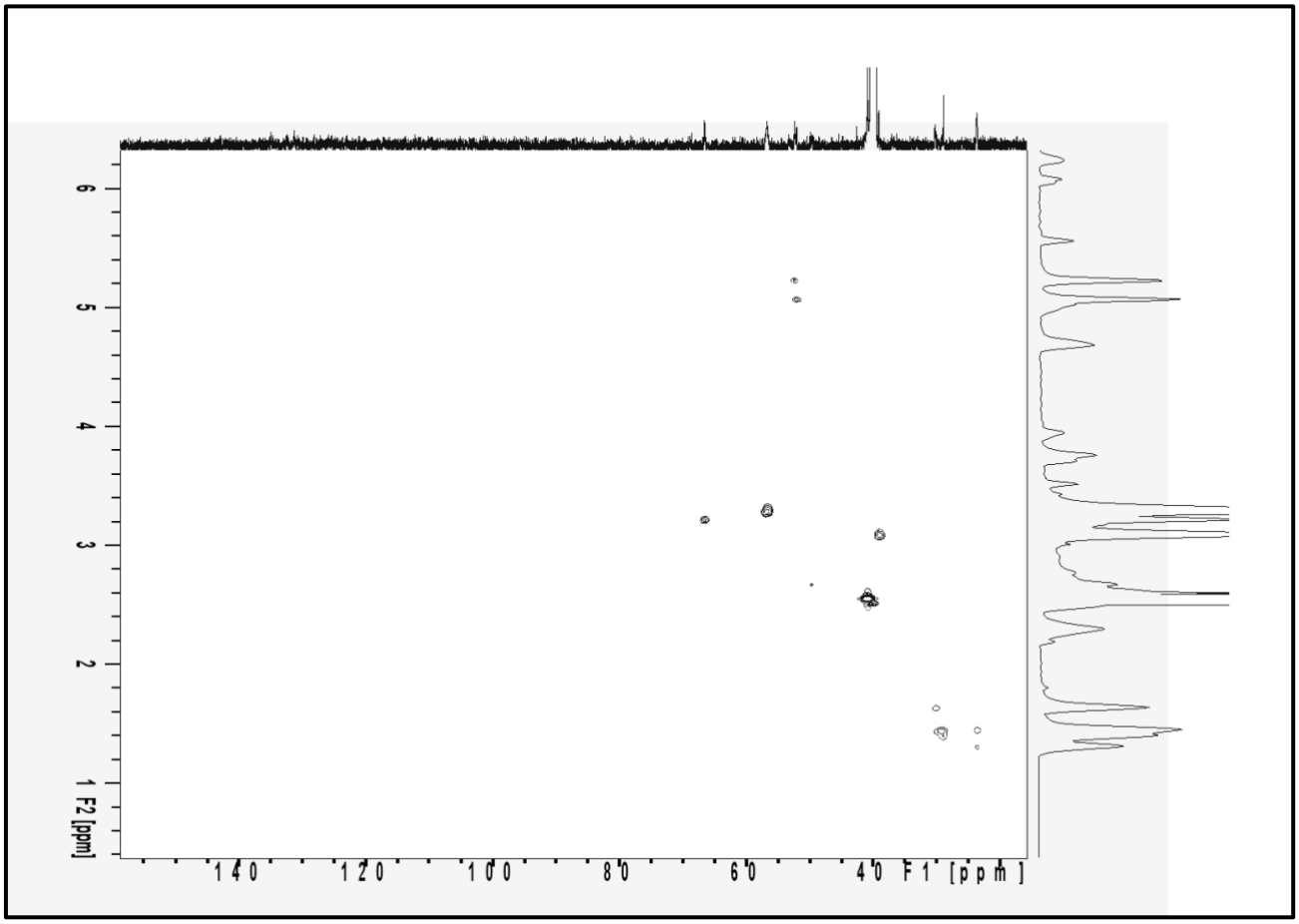

Figure S38: G (3)-deprotected-HSQC of 10b

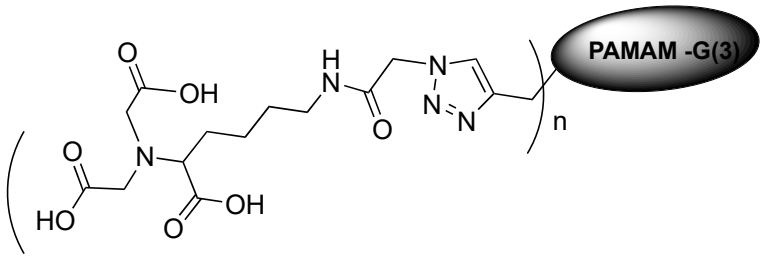

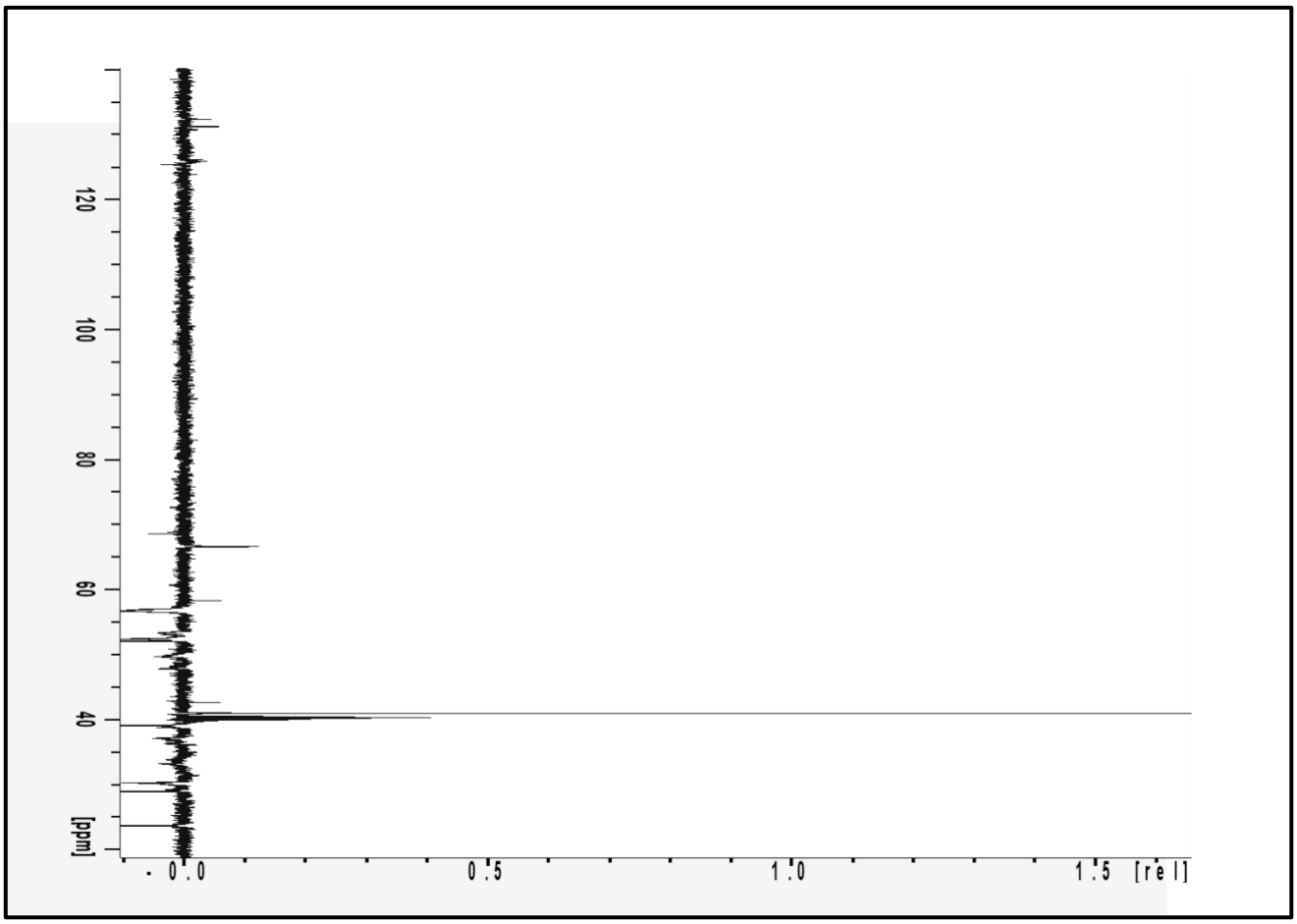

Figure S39: G (3)-deprotected-DEPT-135 of 10b

G (4)-DEPROTECTED-HSQC

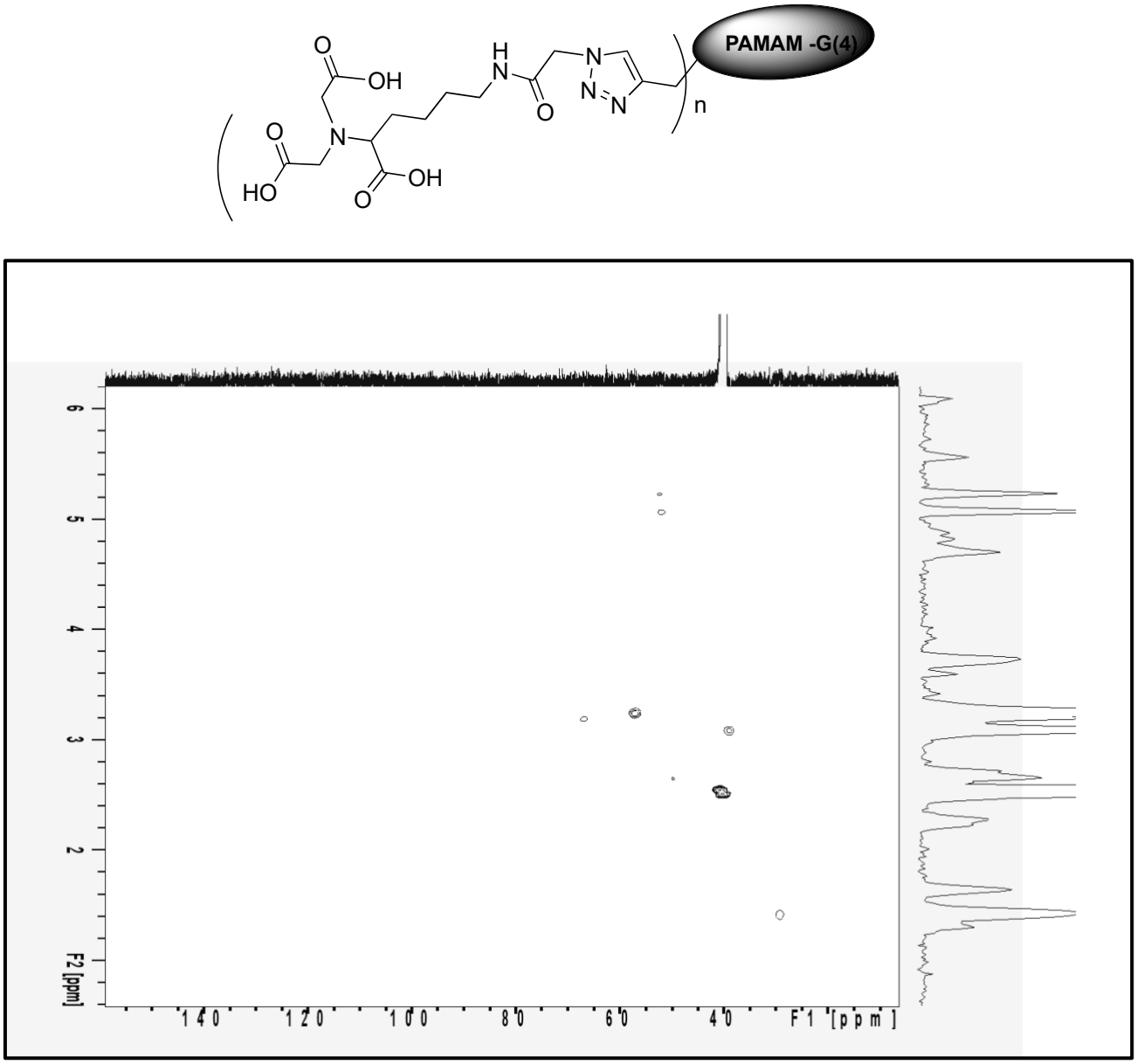

Figure S40: G (3)-deprotected-HSQC of 10c

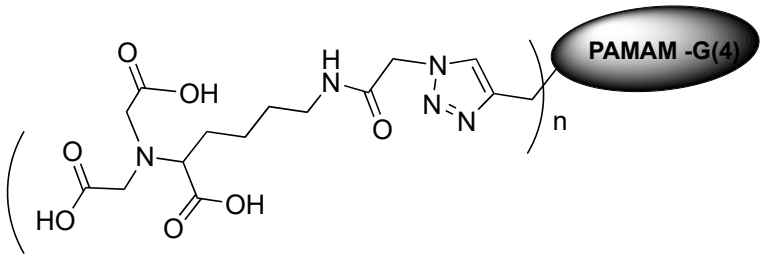

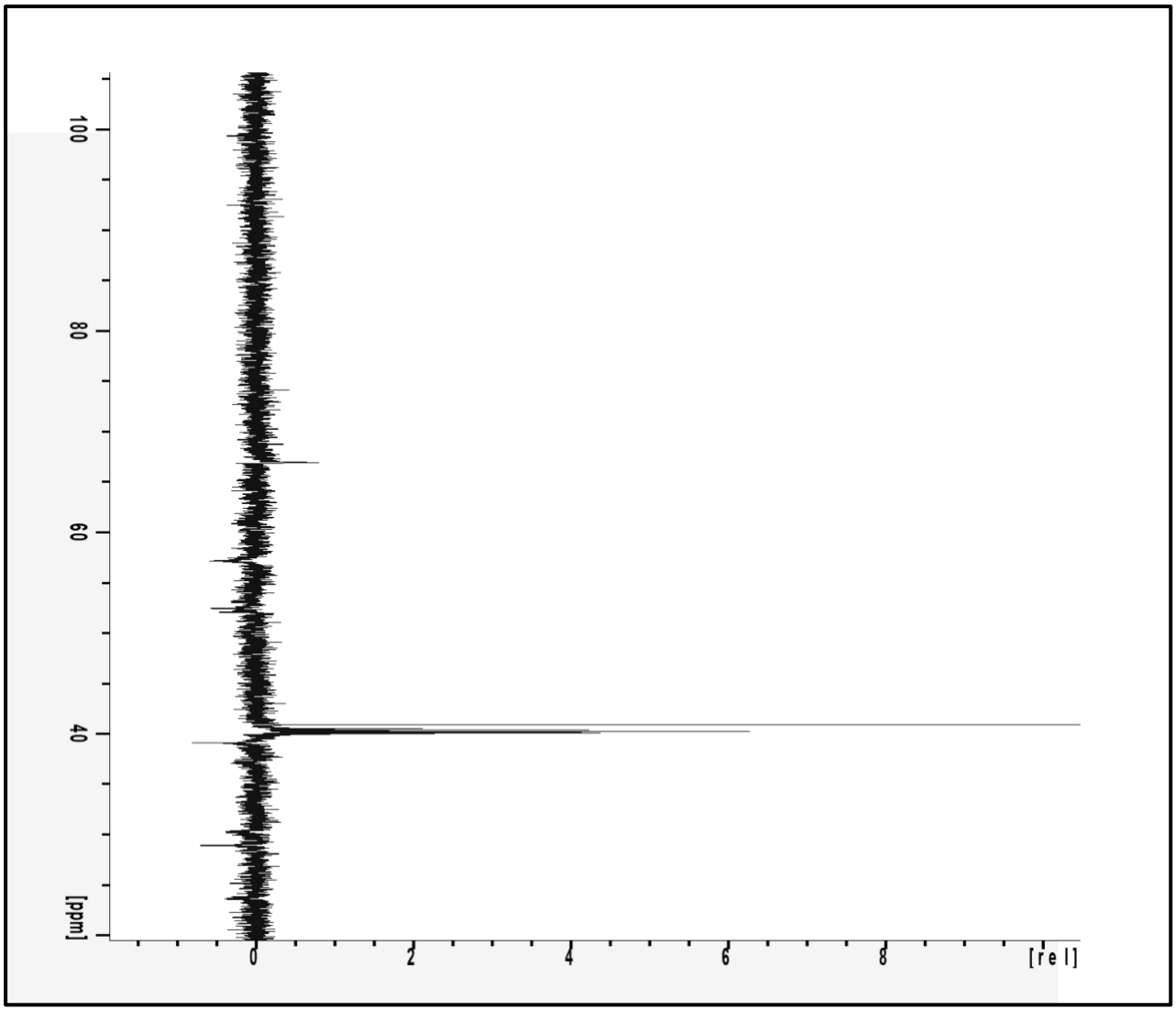

Figure S41: G (4)-deprotected-DEPT-135 of 10c

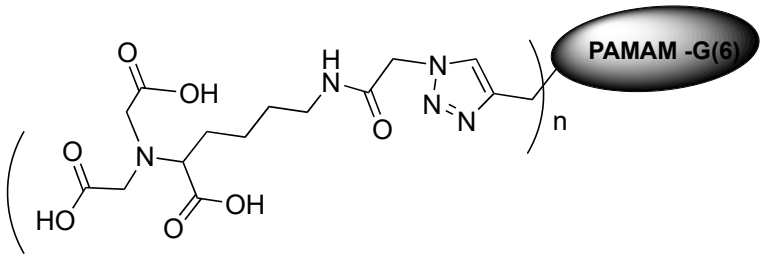

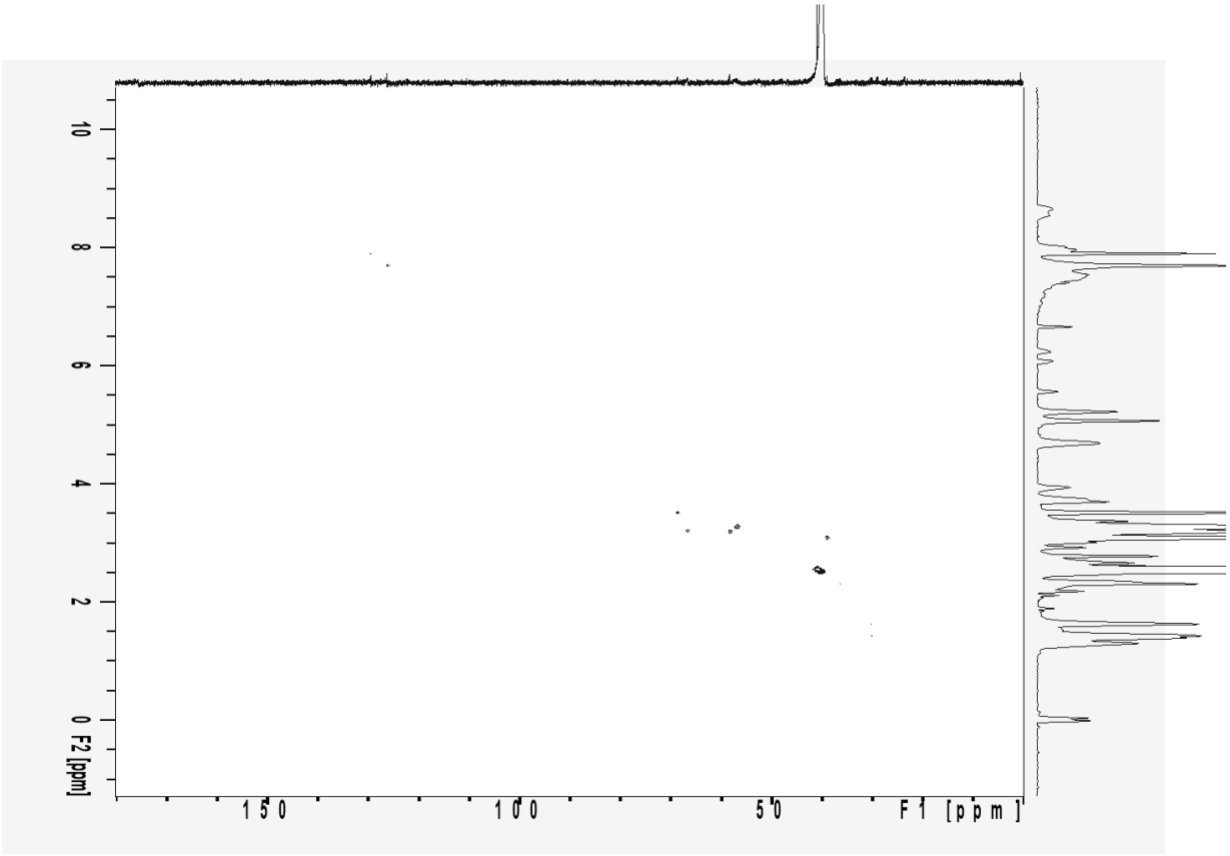

Figure S42: G (6)-deprotected-HSQC 10d

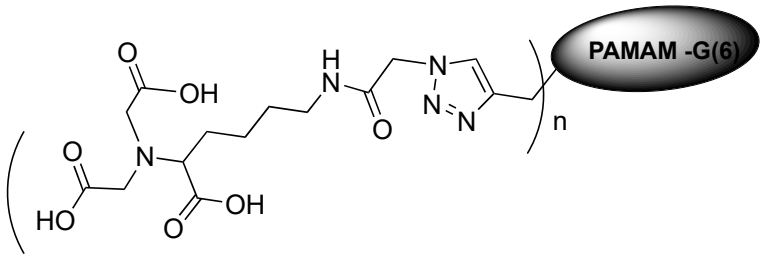

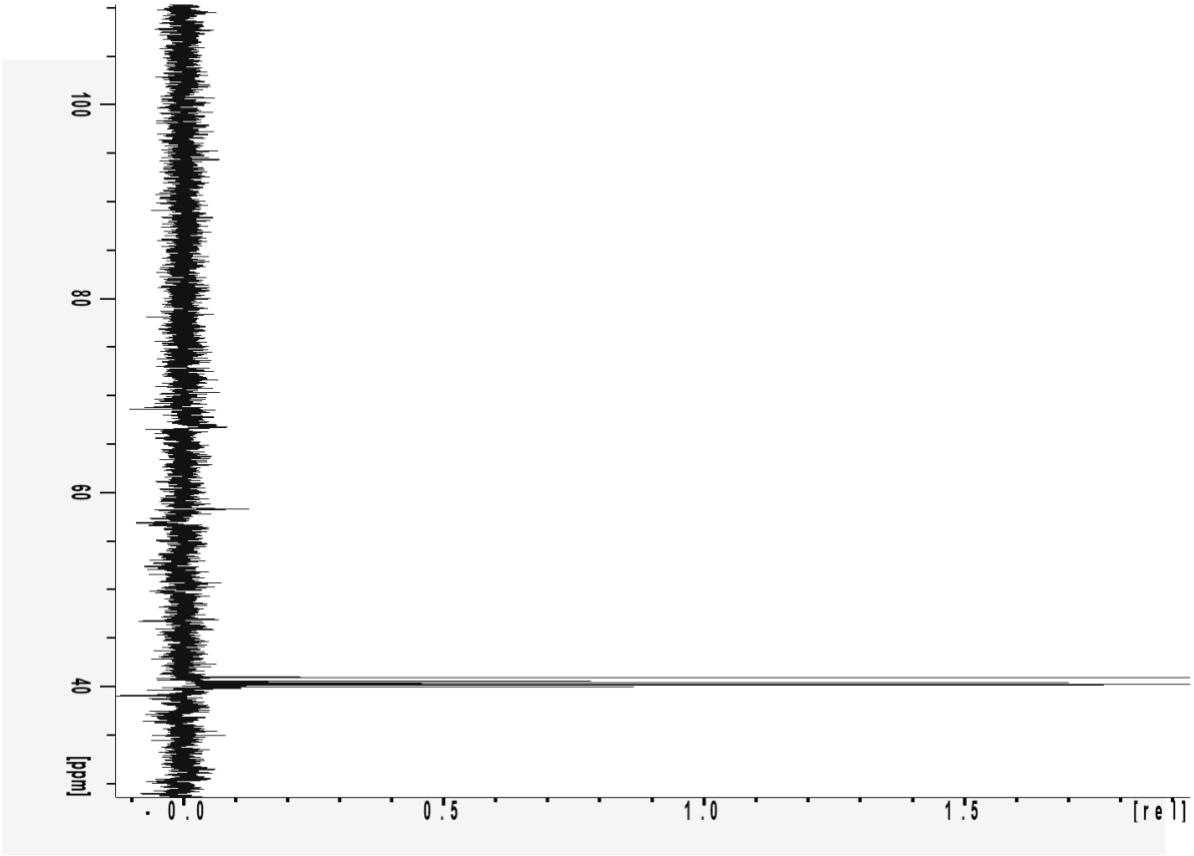

Figure S43: G (6)-deprotected-DEPT-135 of 10

APPENDIX B

MICROGRAPHS AND CIRCULAR DICHROISM SPECTRA FOR THE SYNTHESIZED MOLECULES

Transmission Electron Microscopy

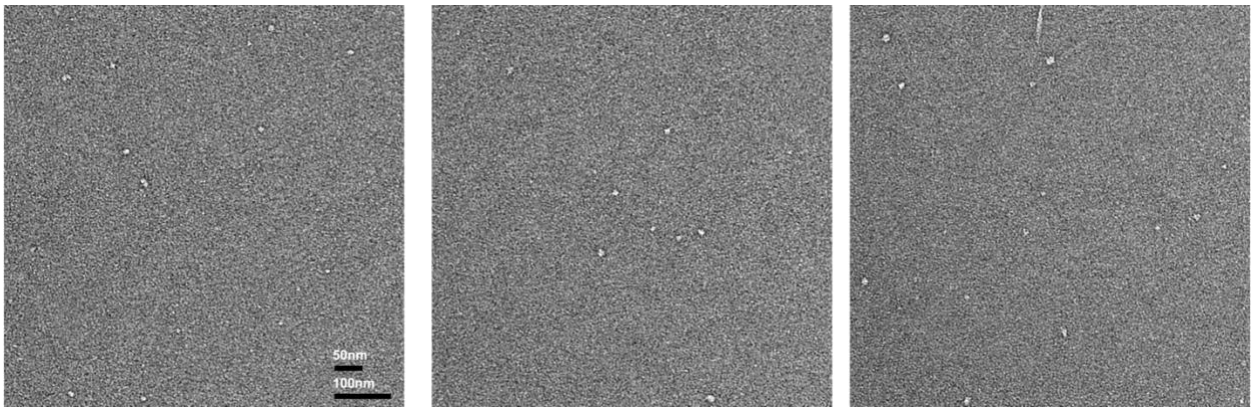

Figure S43: TEM for protein-G(6)-NI-NTA complex

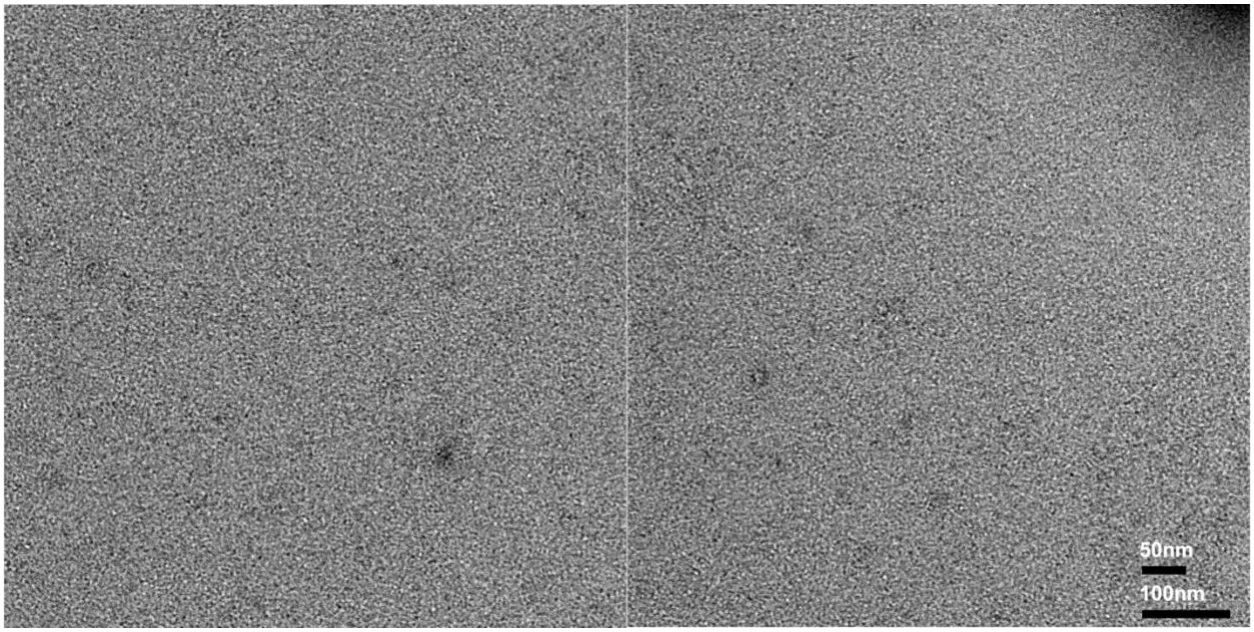

Figure S44: TEM for protein-alone

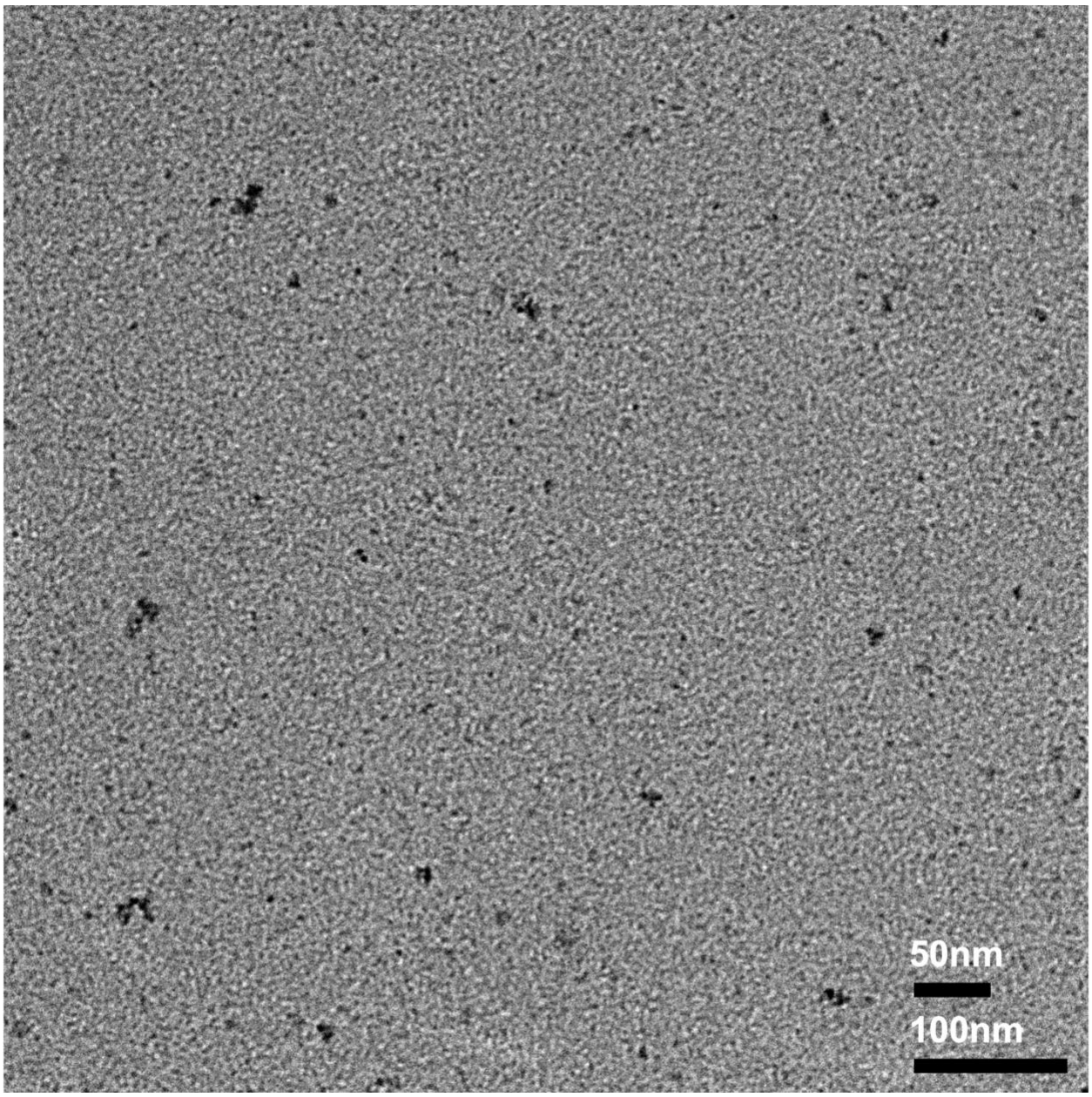

Figure S43: TEM for G(6)-NI-NTA complex, no stains.

Circular Dichroism Spectra

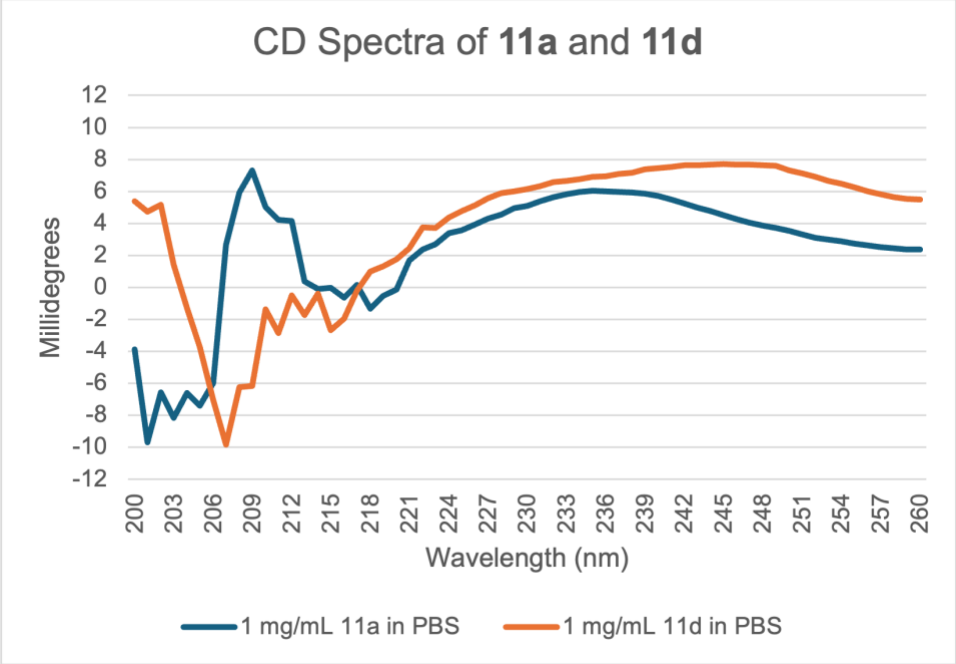

S44: Circular dichroism of synthesized complex for G(2) and G(6)

S45: Circular dichroism for Galectin-3, and complex with Galectin-3